The role of the CtIP gene as a genetic susceptibility factor for radiation leukaemogenesis

Agata Nasilowska
St Catherines College, University of Oxford



Submission for the degree of Doctor of Philosophy

Trinity Term, 2014

Abstract

Exposure to ionising radiation increases the risk of cancer, including acute myeloid leukemia (AML), which is the most common myeloid leukaemia. The C-terminal binding protein (CtBP)-interacting protein (CtIP), which is essential for embryonic development and possibly functions as a tumour suppressor, has been identified as a strong candidate for susceptibility to radiation-induced AML (rAML).

The 129Sv mouse strain carries nonsynonymous single nucleotide polymorphism (nsSNP) within the CtIP gene. The tumour incidence in this strain is low, however its sensitivity to rAML is as yet unknown. This thesis investigates if the nsSNP present in the CtIP mouse gene of 129Sv mouse strain affects post-irradiation survival, carcinogenesis (with a focus on rAML development), CtIP functionality and DNA damage repair by homologous recombination (HR).

The Q418P nsSNP, present in the CtIP mouse gene of 129Sv mouse was identified by several algorithms as disease-causing. After exposure to 3 Gy X-rays, the decrease in life span of 129Sv (30 %) mice was similar to that of CBA/H (25 %) mice, a strain sensitive to rAML, and much higher than that of C57BL/6 (1 %) mice, a stain resistant to rAML. Nine out of 78 (11 %) irradiated 129Sv mice were diagnosed with possible rAML, which is less than irradiated CBA/H (28 %) but greater than C57BL/6 (0%) mice.

The CtIP gene is essential for double-strand break (DSB) resection in HR repair. A lower level of recruitment of HR markers Rad51 and replication protein A (RPA) was observed in 129Sv cells post 10 Gy γ-irradiation, in comparison to CBA/H and C57BL/6 cell lines. Similarly, hydroxyurea (HU) treatment induced phosphorylation of RPA32 in CBA/H and C57BL/6 cells but not in 129Sv. These findings indicate that the nsSNP causes reduced activity of CtIP in the 129Sv cell line. This was further confirmed by CtIP shRNA knock down in the three mouse embryonic fibroblast (MEF) cell lines where there was a decrease in Rad51 and RPA levels in irradiated CBA/H and C57BL/6 cells by about 2 fold, when compared to CtIP proficient controls. The number of Rad51 and RPA positive cells observed in response to irradiation were lower in 129Sv cells compared with CBA/H and C57BL/6 and were unaffected by CtIP knock down. This phenotype was reversed by overexpression of CtIP in 129Sv cells, which confirms the hypothesis that the HR impairment observed in 129Sv cells is due to the nsSNP present in the CtIP gene. Sister chromatid exchanges (SCEs) are a direct effect of HR. Reduced levels of spontaneous, mitomycin C (MMC) and α-particle induced SCEs were observed in 129Sv cells compared to CBA/H and C57BL/6, supporting the suggestion of a defect in HR in 129Sv cells.

The results presented here strongly indicate that the Q418P nsSNP influences the efficiency of CtIP function in HR repair of DSBs. This appears to contribute to shortening of the life span of the mouse strain carrying this variant, and to increasing radiation-induced carcinogenesis, including rAML. These results contribute towards improving understanding of how a mutation in a protein essential for HR results in impairment of this repair pathway and potentially predisposes to cancer in mice.

Acknowledgements

I would like to thank my supervisors Peter O'Neill, Christophe Badie and Jennifer Anderson for sharing their knowledge and experience with me, as well as for guidance and new ideas throughout the project.

I would like to thank several people from Cancer Genetics and Cytogenetics group, Public Health England, Harwell for contribution towards my project: Paul and Rosie Finnon for animal work, Sylwia Kabacik and Grainne Manning for designing the primers, help with RT-PCR and fun lunch breaks, as well as Ken Raj for long, inspiring discussions.

I would like to acknowledge many people from Radiation Oncology and Biology Institute, the whole DNA damage group, especially Siobhan Cunniffe for the help with bacterial work, taking care of my well-being and a lot of teasing; Pamela Reynolds for help with confocal microscope; Daniel Martins for brain storming and complains about a life of a Dphil student; Martine Lomax for a lot of good advice; Sarah Cooper and Alanna Maguire for a great time during work and after hours, as well as Lisa Folkes, Danielle Liddle and Luca Mariotti.

I would like to express my gratitude to Madalena Tarsounas for providing me with a few transfection constructs and Sophie Badie for taking her time to teach me the technique. James Thompson, Mark Hill and Luke Bird for gamma and alpha irradiation; Mick Woodcock for a lot of help with FACS and fun conversation during the experiments; Andy Ryan for advice and discussions, and my dear friends from his group: Sivan, Aoife, Anika, Neele for their help and scientific as well as private intriguing conversations, what made my time in the lab pleasurable, and scientific failures less painful.

I owe a big thank you to my dear friends: Fabiola, Verena, Shena, Nazanin and Alex who contributed to my amazing Oxford experience.

Lastly, I would like to thank my family, my parents, brother and grandma in Poland, who supported me in everything I've been doing; my parents in the UK, who took very good care of me, especially during thesis writing; my best friend Alex who listened to my complaints every day, and every time managed to make me laugh, and my husband who calmed me down, supported me, bravely bore my crazy mood swings and who was my main incentive to move forward.

Table of Contents

Abstract 1
Acknowledgements 3
Table of Contents 4
List of Figures 9
List of Tables 15
Abbreviations 17
1 Introduction 20
1.1 Overview 20
1.2 Types of ionising radiation 21
1.3 DNA damage 23
1.3.1 Non-radiation sources of DNA damage 24
1.4 DNA repair 25
1.4.1 DNA double strand break repair 25
1.4.1.1 NHEJ and SSA 25
1.4.1.2 HR 27
1.4.1.3 DNA damage measurement 34
1.4.2 DNA single strand breaks and base lesions repair 35
1.4.3 Biological effectiveness 37
1.4.4 Euchromatin and heterochromatin 40
1.4.5 Deficiency in DNA repair pathways 41
1.4.6 Chromosomal aberrations 43
1.5 Ionising radiation and AML 45
1.5.1.1 The subtypes of AML 48
1.5.2 The CBA/H mouse strain as a model for radiation-induced acute myeloid leukaemia (rAML) 49
1.5.3 Possible link between CtIP and rAML 49
1.6 Aims 51
2 Materials and Methods 52
2.1 *In vivo* studies 52
2.1.1 Mouse strains 52
2.1.2 X-ray irradiation of mice 52
2.1.3 AML diagnosis 52
2.1.3.1 Flow cytometry phenotyping of 129Sv rAML cases 54

2.2 Cell culture 56
2.2.1 Cell culture reagents 56
2.2.2 Isolation of Mouse Embryonic Fibroblasts (MEFs) from pregnant mice 56
2.2.3 Immortalisation of MEFs-retroviral transfection 57
2.2.4 Culture conditions 59
2.2.4.1 Primary MEFs 59
2.2.4.2 Immortal MEFs 60
2.2.5 Cell counting 60
2.2.5.1 Comparison of the cell growth in low (3 %) and normal (21 %) O_2 conditions between primary and immortal cell lines. 61
2.2.6 Cell cryo-storage 62
2.3 Amplification and purification of plasmid DNA 62
2.3.1 Preparation of electrocompetent bacteria 62
2.3.2 Transformation of electro-competent bacteria 63
2.3.3 Amplification and purification of plasmid DNA 63
2.3.4 Transfection of immortal MEF cells with plasmid for CtIP knock down 65
2.3.5 Transfection of 129Sv cells with plasmid overexpressing CtIP gene 65
2.4 Bioinformatics- algorithms used for CtIP nsSNP prediction 66
2.5 Semi-quantitative PCR 67
2.5.1 DNA isolation 67
2.5.2 Semi-quantitative PCR 67
2.5.3 Agarose gel electrophoresis 68
2.5.4 Sequencing of CtIP and PU.1 gene for the presence of nsSNP 68
2.5.4.1 Sequencing 69
2.6 Multiplex Quantitative Real-Time-PCR (MQ-RT-PCR) 70
2.6.1 RNA isolation 70
2.6.1.1 RNA isolation from solid tissues 70
2.6.1.2 RNA isolation from bone marrow 71
2.6.2 Reverse Transcription (RT) 71
2.6.3 Multiplex Quantitative Real-Time-PCR 72
2.7 Induction and detection of DNA double strand breaks 74
2.7.1 Ionising radiation 74
2.7.1.1 γ-radiation 74
2.7.1.2 α-particle irradiation 74
2.7.2 Immunofluorescent staining for γH2AX, 53BP1, Rad51 and RPA32 75
2.8 Sister chromatid exchange 76
2.8.1 Mitomycin C (MMC) treatment 76

2.8.1.1 Fluorescence plus Giemsa (FPG) staining 77
2.8.2 α-particle irradiation 77
2.9 Western blotting 78
2.9.1 Preparation of whole cell lysates 78
2.9.2 Preparation of nuclear and cytoplasmic cell lysates 78
2.9.3 Determination of a protein concentration 79
2.9.4 Western blotting 80
2.9.4.1 Reagents 80
2.9.4.2 Western blotting 80
2.9.5 Survival assay 84
2.9.5.2 Proliferation assay 85
2.9.5.3 Clonogenic assay – colony formation 85
2.9.6 Detection of S-phase cells using EdU 88
2.9.7 Determination of the cell cycle distribution using flow cytometry 89
2.10 Statistics 90
3 Association between CtIP nsSNP and the onset of radiation-induced AML 91
3.1 Introduction 91
3.1.1 Mouse models 91
3.1.2 Single nucleotide polymorphism in CtIP gene of 129Sv strain 93
3.1.3 Prediction of an effect on a protein caused by an amino acid substitution 94
3.2 Aim 95
3.3 Results 96
3.3.1 Evaluation of disease-causing potential of nsSNP within CtIP gene. 96
3.3.2 Identification of the presence of nsSNP in CtIP gene in the mouse strains CBA/H, C57BL/6 and 129Sv 98
3.3.3 The survival rate of CBA/H, C57/BL6 and 129Sv mice post-irradiation with 3Gy X-rays 100
3.3.4 Post-radiation development of AML 103
3.3.4.1 The diagnosis of rAML in 129Sv stain 103
3.3.4.2 The rate of AML in CBA/H, C57/BL6 and 129Sv mice post 3 Gy X-rays radiation 108
3.3.5 Confirmation of the Q418P nsSNP in CtIP gene and evaluation of a potential nsSNP in the PU.1 gene of 129Sv rAMLs 110
3.3.6 Post-irradiation expression of the CtIP gene in the different CBA/H, C57BL/6 and 129Sv mouse strain tissues 111
3.3.7 Expression of CtIP and PU.1 gene in 129Sv mice diagnosed with rAML 114
3.4 Discussion 115

4 The influence of the Q418P nsSNP on the role of CtIP in the repair of radiation-induced DSBs 116
4.1 Introduction 116
4.2 Aim 117
4.3 Results 118
4.3.1 The influence of oxidative stress on the growth of CBA/H, C57BL/6 and 129Sv primary and immortal MEFs 118
4.3.2 Efficiency of DSB repair assessed from the dynamics of formation and loss of γH2AX and 53BP1 foci induced in primary MEFs by γ-radiation and α-particles 120
4.3.3 Homologous recombination repair of DSBs assessed by formation and loss of Rad51 and RPA foci induced in primary and immortal MEFs by γ-radiation 123
4.3.4 Levels of CtIP and phospho-RPA32 in primary and immortal MEFs post-radiation or HU treatment 126
4.3.4.1 shRNA knock down of CtIP protein expression 130
4.3.4.2 The effect of CtIP knockdown on radiation-induced formation and loss of Rad51 and RPA foci in immortal MEFs 132
4.3.4.3 The effect of CtIP overexpression on the formation and loss of Rad51 and RPA foci post-irradiation in immortal MEFs 134
4.3.5 CtIP and cell cycle 136
4.4 Discussion 143
5 The influence of the Q418P nsSNP in CtIP on homologous recombination and survival 146
5.1 Introduction 146
5.2 Aim 147
5.3 Results 148
5.3.1 The differences between cell lines in spontaneous and induced SCE levels 148
5.3.2 Sensitivity to radiation and HU in MEF cell lines 153
5.4 Discussion 159
6 Discussion 161
6.1.1 The CtIP gene of 129Sv mouse strain contains disease-causing nsSNP 161
6.1.2 The CtIP nsSNP Q418P reduces the life span of 129Sv mice but not the survival of 129Sv MEF cell line following radiation and increases rAML development 162
6.1.3 The Q418P nsSNP impairs CtIP function 165
6.2 Conclusion 167
7 Future Plans 169
Appendix A: References 171

Appendix B.....183

Sequencing of DNA from three mouse strains for the presence of H388Y, Q418P, A498T, A882V nsSNPs found in the CtIP gene.....183

Tumours (other than rAML) found in irradiated and non-irradiated 129Sv mice.....186

List of Figures

FIGURE 1.1 Comparison of the distribution of ionising radiation in the cell by low and high LET radiation. 22

FIGURE 1.2 Model of the key steps required for NHEJ and SSA.. 26

FIGURE 1.3 A possible model of DSB resection with focus on CtIP function. 29

FIGURE 1.4 Homologous recombination- repair of two-ended DSBs. 32

FIGURE 1.5 HR: repair of one-ended DSB. 33

FIGURE 1.6 The scheme of short and long patch of base excision repair pathway. 36

FIGURE 1.7 Schematic illustration of chromosomal aberrations. 44

FIGURE 2.1 Blood smears from a non-irradiated 129Sv mouse (A) and 3 Gy X-ray irradiated 129Sv diagnosed with AML (B). 54

FIGURE 2.2 Haemocytometer 61

FIGURE 2.3 The illustration of a probe specific to the amplified sequence.....73

FIGURE 2.4 The standard curve prepared using: 2, 4, 6 and 8 µg/µl of BSA protein, used to determine concentration of the protein lysates. 80

FIGURE 3.1 The sequence of DNA from C57BL/6 (A) and 129Sv (B) mice without (A) or with (B) a Q418P nsSNP, respectively.....99

FIGURE 3.2 The survival percentage of controls versus 3 Gy X-ray irradiated mouse strains: CBA/H (A), and 129Sv (B).. 101

FIGURE 3.3 The comparison of CBA/H, C57BL/6* and 129Sv mouse strains survival post 3 Gy X-ray radiation. 102

FIGURE 3.4 Representative FACS images of the spleen cells from 129Sv 3 Gy X-ray irradiated mouse diagnosed with rAML (AN 59) (A), and cells from 129Sv non-irradiated control (B) 106

FIGURE 3.5 The percentage of rAML cases in CBA/H (28 %), 129Sv (11 %) and C57BL/6 (0 %) mouse strains post 3 Gy X-rays 109

FIGURE 3.6 Comparison of survival rate in the whole population after acute 3 Gy X-ray irradiation of CBA/H and 129Sv mice and those irradiated mice diagnosed with rAML.109

FIGURE 3.7 The expression of CtIP gene in CBA/H and C57BL/6 mouse tissues irradiated with 3 Gy X-rays. 112

FIGURE 3.8 The expression of CtIP gene in bone marrow and spleen of 129Sv mouse strain irradiated with 3 Gy X-rays. 113

FIGURE 3.9 The expression of CtIP (A) and PU.1 (B) gene in the spleen of 129Sv rAML mice. 114

FIGURE 4.1 Comparison of cell growth of CBA/H, C57BL/6 and 129Sv primary MEFs under low (3 %) and normal (21 %) oxygen tensions. 119

FIGURE 4.2 Comparison of cell growth of CBA/H, C57BL/6 and 129Sv immortal MEFs under low (3 %) and normal (21 %) oxygen tensions 119

FIGURE 4.3 Representative images of γH2AX (A-C) and 53BP1 (D-F) foci in C57BL/6 MEF cell line after 1 Gy γ-ray radiation.....121

FIGURE 4.4 Representative images of γH2AX (A-C) and 53BP1 (D-F) foci in C57BL/6 MEF cell line after 1 Gy α-particles radiation. 121

FIGURE 4.5 γH2AX and 53BP1 foci formation and loss in CBA/H, C57BL/6 and 129Sv MEFs after irradiation with 1 Gy γ-rays (A,B) and 1Gy α-particles (C,D).....122

FIGURE 4.6 Representative images of Rad51 and RPA positive (Rad51+, RPA+) and Rad51and RPA negative (Rad51-, RPA-) C57BL/6 cells 4 h post 10 Gy γ-ray radiation 124

FIGURE 4.7 The effect of radiation dose on percentage of Rad51 (A) and RPA (B) positive cells in 129Sv and RPA positive cells (B) in CBA/H, C57BL/6 and 129Sv primary MEFs 2 h after exposure γ-radiation 124

FIGURE 4.8 The percentage of Rad51 (A) and RPA (B) positive cells in CBA/H, C57BL/6 and 129Sv primary MEFs after irradiation with 10 Gy γ-rays 124

FIGURE 4.9 The number of Rad51 foci formation and loss in CBA/H, C57BL/6 and 129Sv primary MEFs after irradiation with 10 Gy γ-rays 125

FIGURE 4.10 The percentage of Rad51 (A) or RPA (B) positive cells (>5 foci/cell) in CBA/H, C57BL/6 and 129Sv immortal MEFs after irradiation with 10 Gy γ-rays. 125

FIGURE 4.11 CtIP protein levels in cytoplasm and nuclear extracts of CBA/H, C57BL/6 and 129Sv MEF cell lines.....126

FIGURE 4.12 RPA32 protein expression in primary CBA/H, C57BL/6 and 129Sv MEFs post 10 Gy γ-radiation 128

FIGURE 4.13 RPA32 protein expression in immortal CBA/H, C57BL/6 and 129Sv MEFs post 10 and 50 Gy γ-radiation.....128

FIGURE 4.14 CtIP, RPA32 and pRPA32 protein expression in primary CBA/H, C57BL/6 and 129Sv MEFs post treatment with 1 mM HU 128

FIGURE 4.15 RPA32 and pRPA32 protein expression in immortal CBA/H, C57BL/6 and 129Sv MEFs post treatment with 1 mM HU 129

FIGURE 4.16 The level of ATR expression in CBA/H, C57BL/6 and 129Sv immortal MEFs 129

FIGURE 4.17 The level of CtIP protein in CBA/H, C57BL/6 and 129Sv transfected with shRNA for CtIP knock down (shCtIP), shRNA for GFP protein (shGFP) as a control, or untransfected (controls).. 131

FIGURE 4.18 The level of CtIP and RPA32 pS4/S8 expression in CBA/H, C57BL/6 and 129Sv immortalised MEFs, control (shGFP) and CtIP knock down (shCtIP), determined 6 and 24 h post 10 Gy γ-radiation or 1 mM HU treatment.....131

FIGURE 4.19 The percentage of Rad51 and RPA positive cells in CBA/H, C57BL/6 and 129Sv controls (A,B) and corresponding CtIP knock down cells (C,D) after irradiation with 10 Gy γ-rays 133

FIGURE 4.20 The level of CtIP in the 129Sv cell line with CtIP knock down (shCtIP), CtIP overexpression or control.....134

FIGURE 4.21 The percentage of Rad51 (A) and RPA (B) positive cells in CBA/H, C57BL/6, 129Sv and 129Sv + CtIP (129Sv overexpressing CtIP) post 10 Gy γ-ray radiation.....135

FIGURE 4.22 Representative data of the cell cycle distribution, showing diploid and tetraploid populations in passage 2 and passage 7 with C57BL/6 primary MEFs.. 137

FIGURE 4.23 Representative data of cell cycle distribution of primary MEFs: CBA/H, C57BL/6 and 129Sv; Cells were irradiated with 0, 1, 5 or 10 Gy γ-rays and cell cycle distribution determined at 0, 6 or 24 h post-irradiation. 138

FIGURE 4.24 Percentage of S phase cells in primary CBA/H, C57BL/6 and 129Sv MEFs 0, 1, 5 and 10 Gy post γ-radiation at 0, 6 and 24 h time points. 139

FIGURE 4.25 The percentage of S phase cells with CBA/H, C57BL/6 and 129Sv controls (A) and CtIP knock-down (B) immortal MEFs.....140

FIGURE 4.26 Representative images of EdU, DAPI and 53BP1 in C57BL/6 post 1 Gy γ-radiation.....141

FIGURE 4.27 The number of 53BP1 foci per EdU positive cell in CBA/H, C57BL/6 and 129Sv immortal controls (A) and CtIP knockdown (B) MEFs after irradiation with 10 Gy γ-rays. 142

FIGURE 4.28 The number of 53BP1 foci per cell in the whole population in CBA/H, C57BL/6 and 129Sv immortal control (A) and CtIP knockdown (B) MEFs after irradiation with 10 Gy γ-rays. 142

FIGURE 5.1 Representative images of SCEs in control (A) and MMC treated (B) C57BL/6 MEF cell line 149

FIGURE 5.2 The frequency of SCEs in control and MMC treated (0.5 μg/ml) immortal MEF cell lines, CBA/H (A), C57BL/6 (B) and 129Sv (C). 150

FIGURE 5.3 Comparison of spontaneous (A), and MMC induced (B) SCEs in CBA/H, C57BL/6 and 129Sv MEF cell lines.....150

FIGURE 5.4 The frequency of SCEs in control and α-particles irradiated (0.5 and 1 Gy) immortal MEF cell lines, CBA/H (A), C57BL/6 (B) and 129Sv (C).....152

FIGURE 5.5 Comparison of the frequency of spontaneous (A), 0.5 Gy (B) and 1 Gy (C) α-particles induced SCEs in CBA/H, C57BL/6 and 129Sv immortal MEF cell lines.....152

FIGURE 5.6 Dilution assay to determine dose dependence for cell survival with control (shGFP) (A) and CtIP KD (B) immortal MEFs: CBA/H, C57BL/6 and 129Sv, irradiated with γ-radiation.....153

FIGURE 5.7 Clonogenic assay with immortal MEF cell lines: CBA/H, C57BL/6, 129Sv and 129Sv shCtIP, exposed to the stated doses of X-rays.....155

FIGURE 5.8 Clonogenic assay with immortal MEF cell lines: CBA/H, C57BL/6, 129Sv exposed to the stated doses of γ-radiation 156

FIGURE 5.9 Clonogenic assay with immortal MEF cell lines: CBA/H, C57BL/6, 129Sv and 129Sv shCtIP, treated with the stated doses of HU for 24 h 156

FIGURE 5.10 Resazurin proliferation assay with primary (A) and immortal (B) MEF cell lines: CBA/H, C57BL/6 and 129Sv. Cells were treated with stated doses of γ-radiation.158

FIGURE 5.11 Resazurin proliferation assay with primary (A) and immortal (B) MEF cell lines: CBA/H, C57BL/6 and 129Sv. Cells were treated with stated doses of HU for 6 h 158

List of Tables

TABLE 1.1 A quantitative summary of the typical effects of 1 Gy of low and high LET radiation to a mammalian cell 39

TABLE 1.2 AML subtypes according to WHO classification from 2001 with some modifications made during revision in 2008 48

TABLE 2.1 The antibodies used for phenotyping of possible rAML cases in 129Sv mouse strain. 55

TABLE 2.2 The cell culture reagents used for primary and immortal mouse embryonic fibroblasts (MEFs).. 56

TABLE 2.3 Plasmids used for immortalisation of MEFs. 57

TABLE 2.4 Reagents used for the retroviral transfection of MEFs. 57

TABLE 2.5 The PCR reagents The volume is given per one PCR reaction. 68

TABLE 2.6 Primers used for genotyping CBA/H, C57/BL6 and 129Sv mice. 69

TABLE 2.7 Reagents used for preparation of RT master mix 72

TABLE 2.8 Primers and probes used for MQ-RT-PCR. 73

TABLE 2.9 Antibodies used for immunofluorescent staining. 75

TABLE 2.10 Reagents used for western blot technique. 80

TABLE 2.11 Antibodies and conditions used during western blot technique. 83

TABLE 2.12 Seeding densities for each dose of X-ray radiation and cell line used in the clonogenic survival assay. 87

TABLE 2.13 Seeding densities for each dose of γ-ray radiation and cell line used in the clonogenic survival assay. 87

TABLE 2.14 Seeding densities for each dose of HU treatment and cell line used in the clonogenic survival assay. 87

TABLE 3.1 The predictions of disease-causing status of nsSNPs by five algorithms: Panther, PhD-SNP, SIFT, SNAP and Meta-SNP using Meta-predictor website. 97

TABLE 3.2 The presence of: H338Y, Q418P, A498T and A882V CtIP nsSNPs in spleen DNA of mouse strains CBA/H, C57BL/6, and 129Sv.. 98

TABLE 3.3 The number of CBA/H, C57BL/6 and 129Sv control mice and 3 Gy X-ray irradiated used in this study and their mean life span.....101

TABLE 3.4 Assessment of total white blood cell count, neutrophils count and the weight of spleen in 9 potential rAML cases and controls 104

TABLE 3.5 Spleen cells from seven 129Sv potential AML mice stained with antibodies for immature forms/blasts as well as with isotope control. 107

TABLE 5.1 The mean number of SCEs per metaphase in control and MMC treated CBA/H, C57BL/6 and 129Sv cell lines. 149

TABLE 5.2 The mean number of SCEs per metaphase in control and α-particles irradiated CBA/H, C57BL/6 and 129Sv cell lines. 152

TABLE B.1 Tumours found in irradiated 129Sv mice. 186

TABLE B.2 Tumours found in non-irradiated 129Sv mice 186

Abbreviations

A	adenine
A16V	Alanine16Valine
A498T	Alanine498Threonine
A882V	Alanine822Valine
ADP	adenosine diphosphate
Alt-NHEJ	alternative NHEJ
AML	acute myeloid leukaemia
AP	apurinic/apyrimidinic
APE1	AP endonuclease 1
ATM	ataxia telangiectasia mutated
ATR	ataxia telangiectasia and Rad3-related
BD	base damage
BER	base excision repair
BLM	Bloom syndrome helicase
Bp	base pair
BRCA	breast cancer
BrdU	bromodeoxyuridine
BSA	bovine serum albumin
C	cytosine
CDK2	cyclin dependent kinase 2
CER	cytoplasmic extraction reagent
CGH	comparative genome hybridisation
CHO	Chinese hamster ovary
CtBP	C-terminal binding protein
CtIP	CtBP interacting protein
c-NHEJ	classical NHEJ
DAPI	2-(4-amidinophenyl)-1H -indole-6-carboxamidine
dH_20	distilled water
DMEM	Dulbecco's modified Eagle's medium
DMSO	dimethyl sulfoxide
DNA	deoxyribonucleic acid
DNA-PKcs	DNA-dependent protein kinase catalytic subunit
dNTP	deoxyribonucleotide
DSB	double strand break
EDTA	Ethylenediaminetetraacetic acid
EdU	5-ethynyl-2´-deoxyuridine
EGTA	ethylene glycol tetraacetic acid
ERCC	excision repair cross complementation group
FAB	French-American-British
FACS	fluorescence-activated cell sorting
FBS	foetal bovine serum
FEN	Flap endonuclease
FPG	fluorescence plus Giemsa
FSC/SSC	forward scatter/side scatter
G	guanine

G7S	Glycine7Serine
GFP	green fluorescent protein
GST	glutathione S-transferase
H388Y	Histidine388Tyrosine
HBS	HEPES buffered saline
HEPA	High-efficiency particulate absorption
HEPES	2-[4-(2-hydroxyethyl)piperazin-1-yl]ethanesulfonic acid
HPRT	hypoxanthine–guanine phosphoribosyltransferase
HR	homologous recombination
HU	hydroxyurea
I366T	Isoleucine366Threonine
ICL	inter-strand crosslink
IR	ionising radiation
KAP	Kruppel-associated box-associated protein
LB	Luria-Bertani
LD_{50}	median lethal dose
LET	linear energy transfer
LP	long patch
MDS	myelodysplastic syndrome
MEF	mouse embryonic fibroblasts
M-FISH	Multicolour-fluorescence *in situ* hybridization
MGI	mouse genome informatics
MLL	myeloid/lymphoid leukaemia
MMC	mitomycin C
MMEJ	microhomology-mediated end joining
MRC	Medical Research Council
MRN	Mre11-Rad50-Nbs1
NBS	Nijmegen break syndrome
NER	nuclear extraction reagent
NHEJ	non-homologous end joining
Ns	not significant
nsSNP	non-synonymous SNP
PANTHER	protein analysis through evolutionary relationships
PARP	poly(ADP-ribose) polymerase
PBS	phosphate buffered saline
PCNA	proliferating cell nuclear antigen
PCR	polymerase chain reaction
PE	plating efficiency
PFGE	pulse field gel electrophoresis
PhD-SNP	Predictor of human Deleterious Single Nucleotide Polymorphism
PolyPhen	polymorphism phenotyping
Q418P	Glutamine418Proline
rAML	radiation-induced AML
R3	region 3
RB	retinoblastoma
RBE	relative biological effectiveness
Rbbp8	retinoblastoma binding protein 8
RFC	replication factor C
RNA	ribonucleic acid
RPA	replication protein A
S4	serine 4

S8	serine 8
SCE	sister chromatid exchange
SDS	sodium dodecyl sulphate
SF	surviving fraction
SIFT	sorting intolerant from tolerant
SNAP	single nucleotide polymorphism annotation platform
SNP	single nucleotide polymorphism
SOB	super optimal broth
SP	short patch
SSA	single strand annealing
SSB	single strand breaks
ssDNA	single-stranded DNA
SVMs	Support Vector Machines
T	thymine
TALEN	transcription activator-like effector nuclease
t-AML	therapy-related AML
TBE	Tris/borate
t-MDS	therapy-related MDS
Tris	2-Amino-2-hydroxymethyl-propane-1,3-diol
WHO	World Health Organization
WRN	Werner syndrome helicase
Wt	wild-type
XLF	XRCC4 like factor
XPF	xeroderma pigmentosum complementation group F
XRCC	X-ray cross complementing protein

1 Introduction

1.1 Overview

Cancer is a disease which results from genomic instability [11]. Genomic instability occurs after activation of oncogenes or inactivation of tumour suppressor genes [12]. This can be caused by exposure of DNA to various damaging agents, including ionising radiation (IR) [13, 14]. IR induces different types of DNA damage [15, 16], including double strand breaks (DSBs), which are considered to be the most critical DNA lesions [17]. Non-homologous end joining (NHEJ) and homologous recombination (HR) are the main DSB repair mechanisms [6,18,19]. Impairment of HR, which is highly accurate, and consequent failure to repair DSBs can lead to genome instability and tumour development [20, 21]. C-terminal binding protein (CtBP) interacting protein (CtIP) has been identified as a potential tumour suppressor [22, 23] and a strong candidate for susceptibility to radiation-induced AML (rAML) [2]. The focus of this project was to examine whether a non-synonymous single nucleotide polymorphism (nsSNP), identified within the CtIP gene, could influence CtIP function upon irradiation (and therefore HR), leading to the development of cancer, in particular rAML.

1.2 Types of ionising radiation

Electromagnetic radiation is composed of photons, and is characterised by the frequency or wavelength of its wave. X-rays, γ-rays, ultraviolet, visible light, microwaves and radio waves are types of electromagnetic radiation which differ in the wavelength and frequency and therefore in photon energy. X-rays and γ-rays have short wavelengths with high frequency, and therefore the energy per photon is large. In contrast radio waves have a long wavelength and low frequency resulting in less energy per photon [24, 25].

Ionising radiation (IR) is a form of radiation that possesses sufficient energy to remove electrons from the atoms or molecules as opposed to non-ionising radiation, which can be characterised by an increase in energy level of an electron without its ejection. Ionising radiation can be classified as electromagnetic or particulate, depending on the radioactive source. X-rays and γ-rays are electromagnetic types of ionising radiation, whilst α-particles, neutrons, protons or heavy charged ions are particulate types. X-rays and γ-rays have the same properties but differ in the way they are produced. X-rays are produced extra-nuclearly by an X-ray tube, where electrons are accelerated to a high velocity and stopped with a target (usually tungsten or gold). In contrast, γ-rays are produced intra-nuclearly and emitted by radioactive isotopes (for example ^{137}Caesium) through nuclear rearrangement. Examples of particulate radiation include positively charged (α-particles), negatively charged (β-particles) or electrically neutral (neutrons) particles. α-particles are positively charged, naturally occurring and biologically relevant particles, which consist of two protons and two neutrons, forming a particle identical to a helium nucleus. α-particles are emitted by larger radioactive nuclei like plutonium or uranium in the α-decay process [1].

Ionising radiation causes direct or indirect biological effects. The severity of these effects is related to the linear energy transfer (LET) of the radiation [26, 27], which is a measure of energy deposited along a unit length of a radiation track. The higher the density of the deposited energy, the more likely that severe damage is caused to the structures near or within the track. **FIGURE 1.1** illustrates the distribution of energy deposition events in the cell by ionising radiation such as X-rays and γ-rays (A) or α-particles radiation (B) [3]. X-rays and γ-rays are types of low LET radiation and the energy is homogenously distributed through the cell, therefore a small amount of energy is present along the tracks length. The damage to deoxyribonucleic acid (DNA) induced by X- or γ-rays is produced mainly via indirect effects through ionisation of surrounding molecules liberating diffusible water radical species, (mainly the hydroxyl radical) [26],[28]. α-particles have high LET and cause damage by direct deposition of energy onto DNA with a small contribution from indirect effects [28]. Their positive charge and relatively large mass cause strong interactions with the material they traverse. The high energy is distributed in a small volume of the cell creating severe damage along a narrow track. α-particles are much less penetrative than X- or γ-rays and are generally hazardous to tissue only when exposure occurs internally [1, 29].

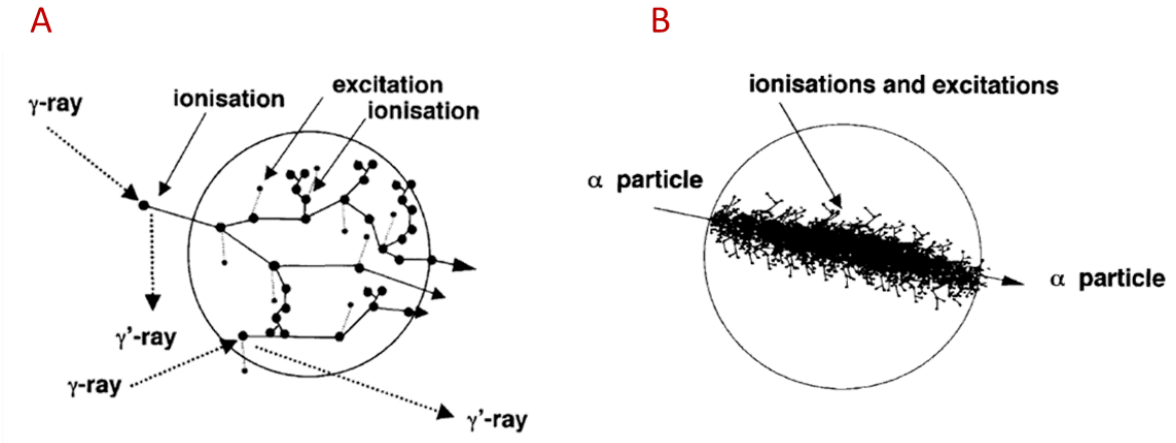


FIGURE 1.1 Comparison of the distribution of ionising radiation in the cell by low LET radiation- γ-rays (A) and high LET radiation- α-particles (B). Figure reproduced with permission from reference [3].

1.3 DNA damage

Ionising irradiation induces different types of DNA damage: base damage (BD), single strand breaks (SSBs), DSBs, clustered DNA damage as well as DNA inter-strand crosslinks (ICLs) [15,16,30]. DSBs can be classified as direct, with two free DNA ends, and indirect/secondary DSBs, generally one-ended DSBs [21, 31]. The indirect DSBs can be formed as a result of collision between a replication fork and unrepaired SSBs, leading to stalled and subsequently collapsed replication fork [17, 21]. DSBs are considered to be the most critical DNA lesions, as failure to repair or misrepair of DSBs can lead to chromosomal rearrangements and therefore genome instability, cancer or cell death [17, 21]. SSBs are relatively common and occur, either after spontaneous DNA damage caused by, for example reactive oxygen species [32 ,30], or post high or low LET irradiation [33, 16] (**FIGURE 1.1**). A SSB does not cause critical damage [27], provided it does not form a secondary DSB. Clustered DNA damage, which is a key feature of ionising radiation, is defined as two or more lesions within 1-2 helical turns of DNA produced by a single radiation track [23], and can be classified as either DSB or non-DSB clusters. Non-DSB clusters consist of SSBs, base lesions and apurinic/apyrimidinic (AP) sites. AP sites arise when DNA undergoes hydrolytic attack on the N-glycosyl bond [17,27,34]. Clustered DNA damage can be induced by low and high LET radiation with the complexity of the damage proportionate to increasing LET [35]. Complex DSBs are predicted to be the most severe DNA lesions with significant biological importance [27, 36], and are thought to be less reparable by DNA repair processes [37-43]; in other words the more complex the damage the lower the reparability of the breaks.

1.3.1 Non-radiation sources of DNA damage

DNA damage is also caused by exposure to various cytotoxic agents such as hydroxyurea (HU) or mitomycin C (MMC). HU is an agent which affects DNA synthesis by reversibly inhibiting ribonucleotide reductase and preventing reduction of ribonucleotides to deoxyribonucleotides (dNTPs). Preventing accumulation of dNTPs, that normally occur as cells enter S-phase, impedes S-phase progression leading to stalled and possibly collapsed replication forks [44-46]. MMC causes DNA inter-strand crosslinking, which is extremely toxic to cells because it blocks DNA replication, transcription, and other processes which require strand separation. The separation of two strands is prevented by coordinated chemical reactions between bases on opposing strands [47-49]. Both of these cytotoxic agents can therefore cause replication induced DSBs [13, 14].

1.4 DNA repair

Maintaining the stability of DNA is crucial to a cell's survival therefore numerous mechanisms, such as DNA repair pathways and cell cycle checkpoints, exist to protect it [15, 27].

1.4.1 DNA double strand break repair

DSBs are repaired either by NHEJ or HR [6, 18, 50, 51,19] with replication induced DSBs repaired mainly by HR [13, 17].

1.4.1.1 NHEJ and SSA

NHEJ is the major DNA repair pathway, in which the broken ends are ligated without or with minimal homology, which makes this pathway potentially error prone [20, 52, 53]. NHEJ is active in all the phases of cell cycle and can be divided into classical and alternative NHEJ (c-NHEJ, alt-NHEJ, respectively) [18,52,54], also referred to as microhomology-mediated end joining (MMEJ) or back-up NHEJ [51,55,56]. The major difference between the two pathways is processing of DSBs. Alt-NHEJ requires short resection of broken ends and alignment of 5–25 base pair (bp) microhomologous sequences before the ligation of the DNA ends, while c-NHEJ seals the break without any homology [57, 58]. The first protein in c-NHEJ pathway to bind DNA broken ends is the Ku70/80 heterodimer (Ku) which then recruits the DNA-dependent protein kinase catalytic subunit (DNA-PKcs)–Artemis complex, which is able to cleave damaged overhangs. Polymerases μ and λ process the broken ends in preparation for ligation by DNA ligase IV–X-ray repair cross complementing protein (XRCC) 4 complex [19, 53, 57] (**FIGURE 1.2**). Alt-NHEJ pathway is Ku-independent [59], however it has been reported that alt-NHEJ might be also active in the presence of c-NHEJ [57]. Alt-NHEJ shares the initial end resection step with HR and single strand annealing (SSA) which is cyclin dependent kinase

2 (CDK2), Mre11-Rad50-Nbs1 (MRN), and CtIP dependent [51, 53]. The regions of homology are annealed post resection with shorter fragments (5- 25 bp) in alt-NHEJ and longer regions (>30 bp) in SSA. In SSA Rad52 protein and nonhomologous tails are trimmed off by xeroderma pigmentosum complementation group F (XPF; also known as ERCC4)–excision repair cross complementation group 1 (ERCC1) [18, 60].

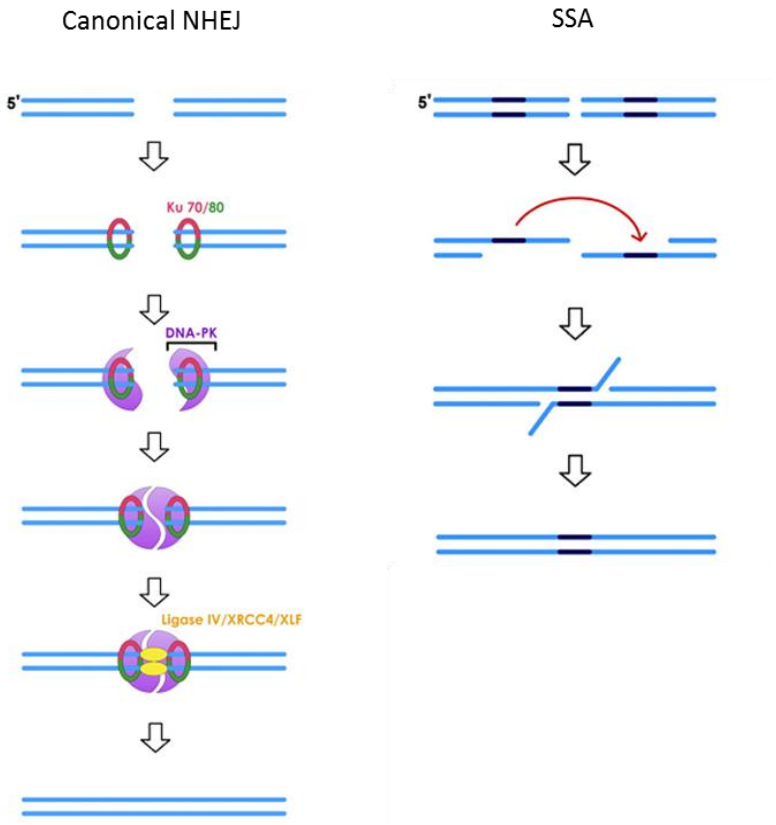


FIGURE 1.2 Model of the key steps required for NHEJ and SSA.
In canonical NHEJ DNA ends are first bound by the Ku70/80 heterodimer, which recruits DNA-PKcs-Artemis complex. This complex then attracts the ligase IV complex (comprised of ligase IV, XRCC4 and XRCC4 like factor (XLF)), which together seal the DNA ends. SSA, similar to alternative-NHEJ pathway (not shown), relies on MRN complex and CtIP for DSB resection. In SSA the regions of homology are annealed post resection by RAD52 and the nonhomologous tails are trimmed off by XPF-ERCC1 complex. Figure reproduced with permission from Helleday et al 2007 [9].

1.4.1.2 HR

In contrast to NHEJ and SSA, HR is restricted to the S and G2 phases of the cell cycle as it requires the presence of sister chromatids [4,61,62]. Moreover, NHEJ and SSA can be error prone whereas HR is generally accurate in preserving genetic information as it employs a homologous template to repair DSBs [20, 57], unless a repair defect is present which may lead to crossovers. HR requires DSB resection in order to generate single stranded DNA (ssDNA) necessary for homology searching and strand invasion [63]. The initial resection is shared with alt-NHEJ and SSA repair pathways, however in the case of HR much longer ssDNA tracks are generated when compared to the other two pathways [53, 64].

1.4.1.2.1 DSB resection and involvement of CtIP

When a DSB occurs, the MRN complex binds to both sides of the DSB and stabilises it [6]. Mre11, which possesses nuclease activity, initiates DSB resection. Nbs1 interacts with checkpoint kinase- ataxia telangiectasia mutated (ATM), facilitating its activation [6,65,66]. In response to DSBs, ATM undergoes autophosphorylation as well as phosphorylating numerous repair and cell cycle checkpoint proteins including: CtIP, Chk2, histone H2AX, p53, 53 binding protein 1 (53BP1) and breast cancer 1 (BRCA1) [20,61,67]. Mre11 is required but not solely for DSB resection; CtIP and BRCA1, which are both bound to the MRN complex, are also required [8, 61]. CtIP binds to the MRN complex through Nbs1 prior to its phosphorylation by CDK2 and ATM as well as its ubiquitination by BRCA1 [4, 20]. It has been reported that phosphorylation of CtIP at Thr859 by ATM is essential for promoting end resection [20]. In addition, other data shows that CtIP is phosphorylated by ataxia telangiectasia and Rad3-related (ATR) checkpoint kinase at Thr859, promoting association of CtIP with damaged chromatin, and this phosphorylation is preceded by ATM activation [5]. CDK2 phosphorylation of CtIP at

Ser327 mediates its interaction with BRCA1 and the CtIP-BRCA1 complex is required for the G2/M transition and Chk1 activation [68]. The phosphorylation of CtIP at Thr847 by CDK2 is essential for localisation of CtIP at DSBs [69]. Thus phosphorylation of both sites by CDK2 results in assembly of the MRN-CtIP-BRCA1 complex [6].

FIGURE 1.3 shows a possible model of DSB resection with focus on CtIP function. CtIP together with MRN complex initiates DSB resection by endonucleolytic cleavage of 5' DNA termini. Werner syndrome helicase (WRN) promotes this initial step by unwinding the DNA ends. The resection is continued by endonuclease EXO1 and DNA2 with the help of bloom syndrome helicase (BLM) [4, 51]. The ssDNA is subsequently bound by replication protein A (RPA), which is then replaced by Rad51 in order to form a ssDNA-Rad51 nucleofilament with the help of BRCA2, RAD52 and RAD54. The nucleofilament is essential for homology searching and invasion of sister chromatids to create a "D-loop" [61,64,70]. RPA, mainly activated by DNA-PKcs upon DNA damage, can recruit ATR, which in response phosphorylates Chk1 to promote a G2/M or intra-S phase checkpoint activation [10,71,72].

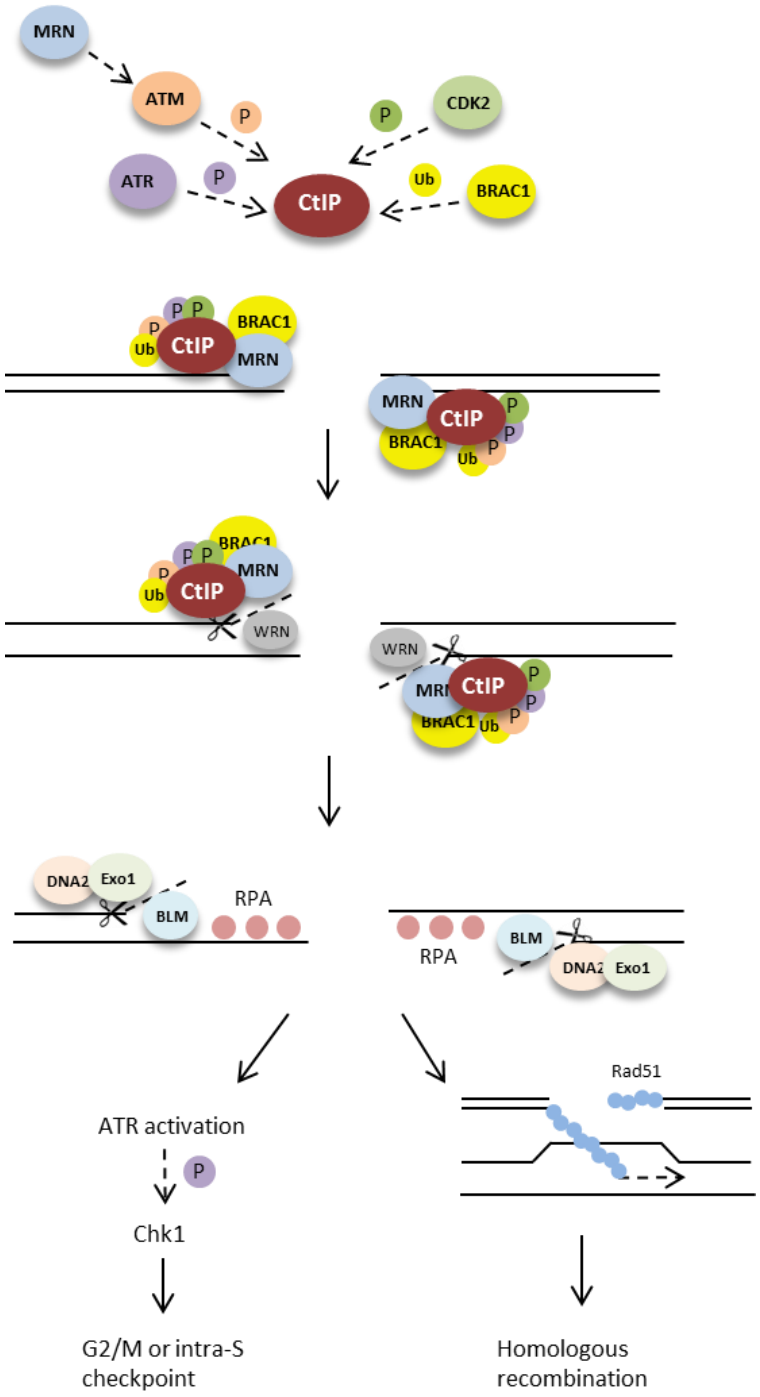


FIGURE 1.3 A possible model of DSB resection with focus on CtIP function based on You and Bailis' 2010 proposed model [4] and modified using data from several publications [5-8].
Upon DSB, CtIP is recruited to the DNA ends prior to its phosphorylation by CDK2, ATM and ATR, and ubiquitination by BRCA1. DSB resection is initiated by CtIP and MRN which together promote cleavage of the 5'-DNA termini. The WRN helicase unwinds the DNA ends. Further resection of 5' termini is done by Exo1, DNA2 and BLM nuclease/helicase complex. The ssDNA is bound by RPA, which is then replaced by Rad51 to initiate strand invasion, leading to DNA repair by HR. Alternatively ATR is activated which can result in cell cycle arrest after G2/M or intra-S checkpoint activation.

1.4.1.2.2 CtIP

CtIP, also called retinoblastoma binding protein 8 (Rbbp8) [73], is a large nuclear protein (897 amino acids), localised on chromosome 18, conserved among vertebrates and discovered as a cofactor for transcriptional repressor CtBP [23]. CtIP is a binding partner for transcription and cell cycle regulators, including retinoblastoma protein (RB), and BRCA1 [74,75]. CtIP associates with RB during the G1 phase of the cell cycle. This association releases RB-mediated transcriptional repression and increases expression of genes required for S phase entry [76]. Cells depleted of CtIP arrest in G1 phase, therefore a direct interaction between CtIP and RB is needed to facilitate G1 to S phase transition [22, 23]. Homozygous inactivation of the CtIP gene causes very early embryonic lethality during mouse development [23] and CtIP heterozygote mice develop tumours, principally lymphomas, suggesting that CtIP functions as a tumour suppressor [23, 77].

Upon DNA damage, CtIP is required for DSB resection particularly in HR [22, 61] but also in SSA and alt-NHEJ for minor resection of broken ends [51, 52]. Cells depleted of CtIP exhibit sensitivity to ionising radiation in S, G2 and also in G1 phase indicating that CtIP also plays a role in NHEJ [8]. Additionally, CtIP knock down results in impairment of cyclin-dependent kinase inhibitor- p21 induction upon DNA damage [78]. The interaction between CtIP and BRCA1 is essential for G2/M transition and Chk1 activation, moreover CtIP is involved in intra-S phase checkpoint [10,68,71,72]. The CtIP protein level varies with the cell cycle progression and the pattern is identical to that of BRCA1. The levels of these proteins are very low in G0 and G1 cells but drastically increase when cells traverse the G1/S boundary, peaking in S and G2 phases [74].

CtIP is a crucial protein for embryonic development, DNA repair, and cell cycle progression, therefore impairment of its functions could result in serious disorder. So far two syndromes have been described as a consequence of nsSNPs present in the human

CtIP gene. Seckel and Jawad syndrome are recessively inherited dwarfism disorders, characterised by microcephaly and growth impairment [79]. A few cancers have been reported in these patients, however these syndromes are mainly characterised by neurological impairments [79]. Cells derived from Seckel patients are impaired in ATR signalling and therefore in G2/M cell-cycle checkpoint arrest when treated with UV light or replication stalling agents such as HU [80].

1.4.1.2.3 HR: synthesis-dependent strand annealing pathway (repair of two-ended DSBs)

There are two primary models for HR repair of two-ended DSBs: double Holliday junction and synthesis-dependent strand annealing. The former is an X shaped structure made of ssDNA arising from homologous chromosomes. The latter is believed to be the main HR repair mechanism and in contrast to the double Holliday junction pathway results in a non-crossover product [9] (**FIGURE 1.4**).

After the formation of a D-loop and Holliday junction, the annealed 3' end is extended into the region that is homologous to the opposite DNA end [9]. DNA polymerase η is responsible for performing 3' end extension at a D-loop [81]. After completion of repair synthesis the newly synthesized end is released by the Holliday junction sliding towards the 3' end. This so called 'branch migration' is facilitated by RAD54, WRN and BLM proteins [82, 83]. In case of a flap formation following an annealing step, endonucleases like XPF/ERCC1 cut the long non-homologous tails [84]. Polymerase δ and ε fill the remaining gaps and DNA ligase I seals the nicks [9, 85].

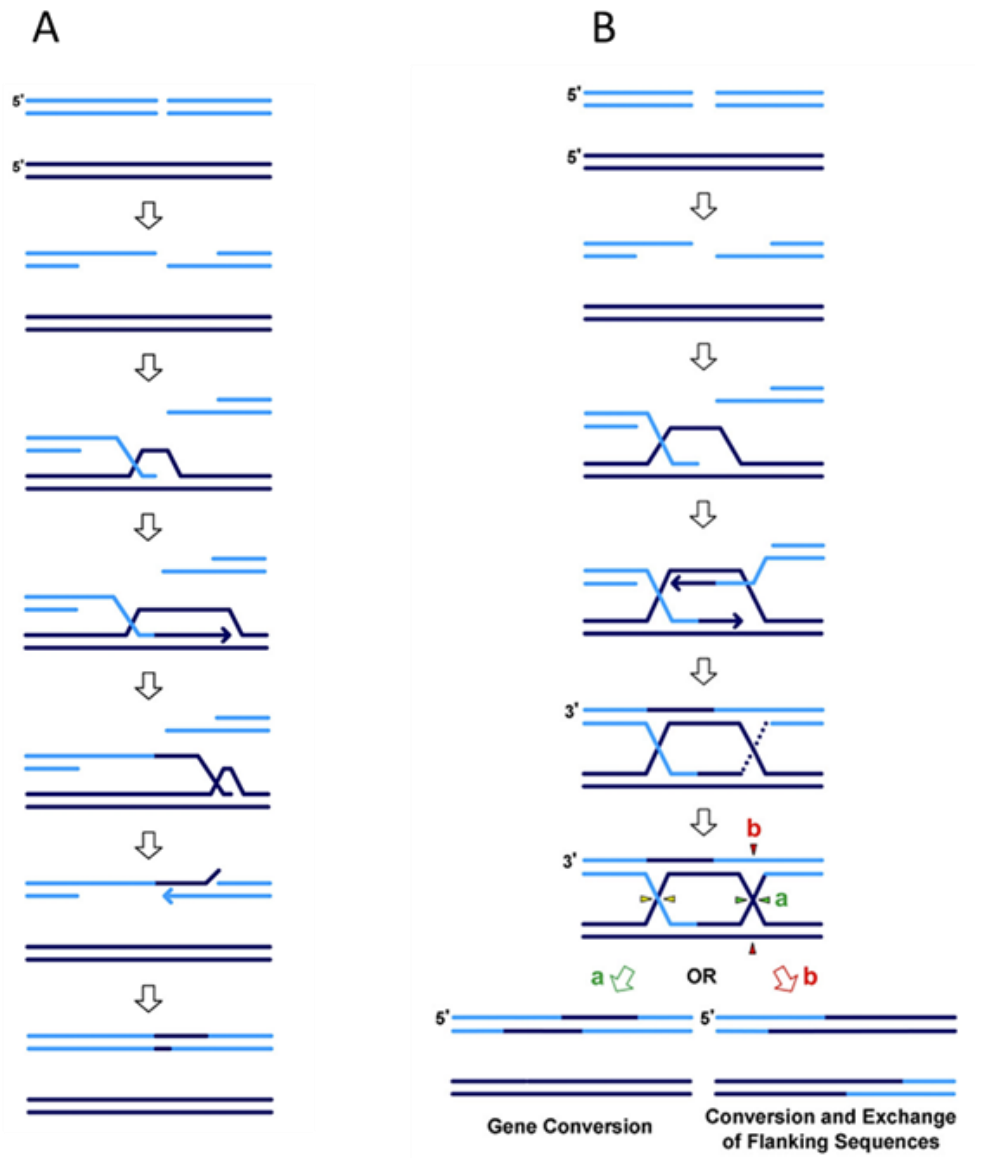


FIGURE 1.4 Homologous recombination- repair of two-ended DSBs.
A: Synthesis dependent strand annealing. Post DSB resection, which relies on the MRN complex and CtIP, D-loop and Holliday Junctions are formed. Once repair is completed, branch migration takes place, where the Holliday junction slides towards the 3' end, and is facilitated by RAD54, WRN and BLM proteins. B: Double Holliday Junction. This pathway is very similar to synthesis dependent strand annealing with the difference that a double Holliday junction is formed and depending on the orientation of the cleavage, resolution of the Holliday Junctions either preserves flanking sequence continuity or results in a crossover event. Figure reproduced with permission from Helleday et al 2007 [9].

1.4.1.2.4 HR: repair of one-ended DSBs

A one-ended DSB is formed when a replication fork collapses, which can be caused by cytotoxic agents such as HU [45] and MMC [47] or can happen upon a replication fork encountering a SSB [86]. One-ended DSBs are processed in a very similar way to two-ended DSBs with the difference that only one DNA end is resected [9] (FIGURE 1.5). Furthermore, Rad51-dependent homologous recombination of one-ended DSBs can result in sister chromatid exchanges (SCE) [87], which is defined as symmetrical exchange between homologous portions of a chromosome [88].

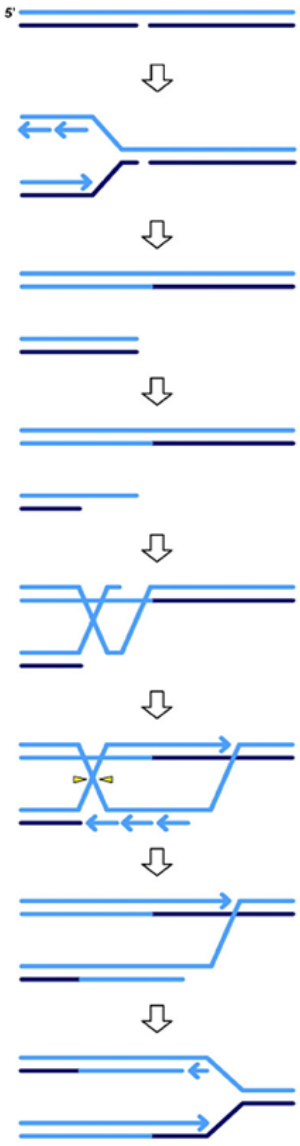


FIGURE 1.5 HR: repair of one-ended DSB.
Upon encounter with a DNA single-strand break, the replication fork can breakdown to create a one-ended DNA double-strand break. Rad51-dependent homologous recombination of one-ended DSB creates a D-loop. Cleavage of the resulting Holliday Junction (shown in the scheme as X-shaped structure) restores the replication fork. Figure reproduced with permission from Helleday et al 2007 [9].

1.4.1.3 DNA damage measurement

Different methods are used to determine levels of DSB, including pulse field gel electrophoresis (PFGE), comet assay and determination of foci levels following phosphorylation of H2AX or accumulation of 53BP1 at DNA damage sites.

PFGE quantifies the amount of DSB damage in a cell population, before and after exposure to an insult, by separation of the DNA fragments in the gel according to their size. DSBs result in high molecular weight DNA fragments, which can be resolved by electrophoresis. DNA repair can be measured by a reduction in the levels of migrating DNA [89]. The advantage of this assay is the analysis of multiple samples on the same gel and a greater separation of DNA sizes, leading to a better understanding of the nature of the DNA damage [89].

The comet assay is a similar technique to PFGE but based on a single cell assay. Only one sample can be analysed at a time. A comet is a pattern that the DNA creates while migrating through the electrophoresis gel and out of the cell. The intensity of the comet tail relative to the head reflects the number of DNA breaks [90]. These two assays are characterised by their different sensitivity and specificity [90]. Where low doses of around a few Gy are used in the comet assay, the limitation of PFGE is the requirement of irradiation doses $\geq$ 1 Gy, typically very high (10-80 Gy) [91], to determine DSB levels [92]. Furthermore, the high doses required with PFGE can lead to apoptosis at later times [91].

In contrast, phosphorylation of the histone protein H2AX (γH2AX), relatively recently used as a DSB marker [93, 94], detects DSBs induced at physiological doses, as low as 1 mGy of low LET radiation [95]. In response to DSB histone H2AX is one of the first substrates to be phosphorylated, which is visualised through immunohistochemistry in the

form of antibody-labelled foci [96]. H2AX phosphorylation is carried out by ATM, ATR and DNA-PKcs kinases [97]. The size and number of γH2AX foci has been shown to increase with radiation dose [96,98,91,92], although for low LET a significant proportion of DSBs will have been repaired within the time required for complete formation of γH2AX [91,92,96,98,99]. DSB repair is also commonly assessed using another DSB marker- 53BP1 [50, 100]. 53BP1 is phosphorylated by ATM and ATR in response to DSBs, it accumulates into discrete foci which co-localise with γH2AX foci [101]. H2AX is however essential to facilitate the recruitment of 53PB1 onto damaged DNA [102]. 53BP1 has been shown to be required not only for NHEJ but also for HR at heterochromatin during DSB repair in G2 phase [103].

γH2AX and 53BP1, are now widely used markers of DSBs [50, 100], however it has been reported that γH2AX foci can be also found in senescing, non-irradiated cells [104, 105]. Moreover γH2AX can form at ssDNA regions during replication, therefore it does not purely reflect two-ended DSB formation [91].

In order to compare different DNA DSB repair methods, MRC-5 (human fibroblasts) cells were irradiated with 80 and 3 Gy X-rays and the repair of DSB was evaluated by PFGE and by γH2AX foci loss, respectively. The results showed a strong correlation between the two methods [91].

1.4.2 DNA single strand breaks and base lesions repair

Base damage and SSBs are mainly repaired by the base excision repair (BER) pathway [106, 107]. BER proceeds via two sub-pathways, short patch (SP) and long patch (LP) (**FIGURE 1.6**). The main difference between the two pathways is the number of nucleotides excised (1 nucleotide for SP and 2-10 nucleotides for LP) [108]. The BER pathway is initiated by DNA glycosylase that releases a target base to form an AP site, and

in SP repair cleaves a phosphodiester bond 3' to the AP site. AP endonuclease 1 (APE1) then cleaves the 5' bond to the site and recruits polymerase β to add in 1 nucleotide with subsequent ligation by Ligase 3/XRCC1. In LP repair, after the AP site has been generated by DNA glycosylase, APE1 cleaves the 5' phosphodiester bond and the complex consisting of replication factor C (RFC), proliferating cell nuclear antigen (PCNA) and polymerase δ/ε, carries out repair through addition of several nucleotides. Flap endonuclease 1 (FEN1) cleaves off the flap structure and then ligation by Ligase 1 occurs. When SSB occurs, it is rapidly bound by poly(adenosine diphosphate (ADP)-ribose) polymerase 1 (PARP1), and the end processing may need additional proteins to the ones mentioned above. However, the repair process by BER SP or LP is exactly the same for the initial step of damage recognition and base removal by DNA glycosylase [10, 109].

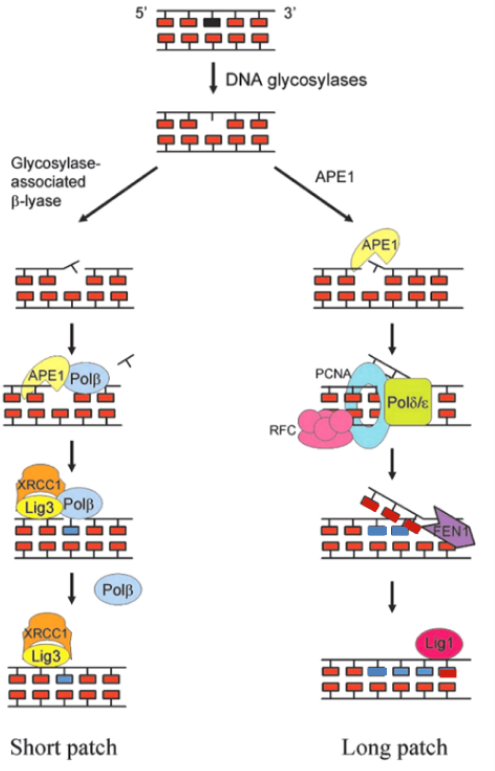


FIGURE 1.6 The scheme of short (1 nucleotide) and long patch (2-10 nucleotides) of base excision repair pathway.
Short patch: After formation of AP site, APE1 endonuclease recruits polymerase β to fill in 1 nucleotide that is ligated by the Ligase 3/XRCC1 complex. Long patch: RFC-PCNA- polymerase δ/ε complex carries out the synthesis of several nucleotides post AP site formation. FEN1 then cleaves off the flap structure and the nucleotides are ligated by Ligase 1. Figure reproduced with permission from Sancar et al 2004 [10]

1.4.3 Biological effectiveness

The quality, commonly defined as LET, dose and dose rate of radiation are the main factors in determining the level of DNA damage and therefore the severity of biological effects [110,37,111]. The relative biological effectiveness (RBE) is defined as the ratio of biological effectiveness of one type of ionising radiation relative to another, given the same amount of absorbed energy [112].

Localised DNA damage caused by dense ionisations from high LET radiation is more difficult to repair and therefore results in greater biological effect (higher RBE) than the diffuse DNA damage caused by sparse ionisations from low LET radiation [27]. Techniques, which have been developed for relatively quick assessment of cell damage to provide information on radiosensitivity, include clonogenic survival assay, measurement of chromosomal aberrations and quantification of ionising radiation-induced foci of DNA repair proteins (e.g. γH2AX) at DSBs [113]. The clonogenic assay is a cell survival assay based on the ability of a single cell to form a colony, defined as containing at least 50 cells [114]. Cell killing is proportionate to increasing radiation or drug dose. The higher the dose the more damage is delivered to the cell, and as a consequence cells lose their ability to form colonies [113, 115]. The clonogenic assay has been used for over 40 years as the most relevant end-point as cell survival is generally significantly lower following irradiation with high LET compared to the same dose of low LET radiation. This can be seen in **TABLE 1.1** [36,110,113,1,113,115].

The relative biological effects of high and low LET have been investigated in several studies. One study used SW-1573 (human squamous cell lung carcinoma) cells and irradiated them with γ-rays and α-particles to determine dose-effect relationships for survival, chromosomal aberrations and DNA DSBs. The doses of γ-rays used to determine

cell reproductive death (clonogenic assay), chromosomal aberrations (quantification of chromosome translocations and fragments) and DNA DSBs (γH2AX foci quantification) were 8.0, 4.0, and 1.4 Gy respectively. The doses of α-particles used to determine these effects (in the same order) were 1.6 Gy, 0.8 Gy and 1.4 Gy, respectively. The results showed similar induction of DSBs after α-particle and γ-ray irradiation, as measured by the number of γH2AX foci at the DSB sites. However, cell reproductive death was much more frequently induced after α-particle irradiation than after γ-ray irradiation for the same dose. Similarly, induction of chromosomal aberrations was much higher when cells were exposed to the same dose of α-particle irradiation when compared with γ-ray irradiation. The RBE values for induction of cell death and chromosome translocations, 14.7 ± 5.1 and 15.3 ± 5.9, respectively, were much higher than the RBE value for induction of γH2AX foci- 1.0 ± 0.3. It was therefore concluded, in agreement with other reports [116], that the number of induced γH2AX foci in the irradiated cells does not correlate with radiosensitivity. However, the RBE values for induction of cell reproductive death are quite similar to the values for chromosome aberrations, making these assays the most relevant end-points when assessing cell damage [113].

The RBE value is quite similar between cell survival and chromosome aberrations (depending on the cell line - RBE for high LET ranges from 5-20 in comparison to γ-rays, which is around 1) [117, 118]. Due to the high energy deposition in just a few tracks by α-particles, the number of DNA repair foci is lower than in cells exposed to low LET radiation (X- or γ-rays), sometimes reflecting the geometry of whether the radiation is delivered perpendicular or horizontally to the plane of detection. However, the complexity of damage is higher and therefore leads to greater biological effects (cell kill or chromosomal aberrations) [36, 113]. The RBE for induction of DNA DSBs does not differ between X- or γ-rays and α-particles irradiation and therefore there is no correlation with

radiosensitivity [119], suggesting that the survival and chromosomal aberration assays might be more appropriate end-points to assess biological effectiveness of high-LET than radiation-induced foci [116] (TABLE 1.1).

TABLE 1.1 A quantitative summary of the typical effects of 1 Gy of low and high LET radiation to a mammalian cell [36, 110, 113].

	Ionizing radiation	
	Low LET	High LET
Tracks in nucleus	1000	2
SSBs	850	450
DSBs	40	40
Complex DSBs % (out of total DSBs)	30%	70%
RBE for DSB	~1	~1
RBE for survival	~1	~14.7
RBE for chromosomal aberrations	~1	~15.3

1.4.4 Euchromatin and heterochromatin

It has been shown that structural organisation of DNA influences the dynamics of processing of radiation-induced DNA damage [120-123,124-126]. DNA is packaged into chromatin which consists of nucleosomes, composed of 146 base pairs of DNA wrapped around a histone octamer. The octamer is made out of two copies of the four core histones: H2A, H2B, H3 and H4. The nucleosome core, together with DNA and linker histone- H1 assembles into chromatin [127]. Histones, particularly their tails, are subject to post-translational modifications, which include: acetylation, methylation, ubiquitylation and phosphorylation [128].

There are two types of chromatin: eu- and hetero-chromatin. Euchromatin is defined as open, gene rich, transcriptionally active regions, whereas heterochromatin is a region of condensed and low gene density, with high levels of repetitive sequences [124],[125, 126]. It has been proposed that euchromatin is much more susceptible to DSB induction by X- or γ-rays than heterochromatin, which is transcriptionally inactive. The lower sensitivity of heterochromatin to repair of DSB induced by ionising radiation is thought to be related to chromatin condensation as well as the presence of higher number of proteins compared to euchromatin [120].

Clustered damage induction is influenced more by chromatin state than induction of simple DSBs, with euchromatin showing much more clustered damage in comparison to heterochromatin [121]. DSBs are known to be repaired by two component kinetics. For low LET radiation, the majority of DSBs (~85%) are repaired with fast kinetics (t(50): 5-30 min) in an ATM-independent manner whereas 15% are repaired with slow kinetics (t(50): 1-20 h) [125,126,129]. The DSBs repaired with slow kinetics are predominantly localised within heterochromatin and require ATM to phosphorylate Kruppel-associated

box-associated protein-1 (KAP-1), a heterochromatin-building protein [122]. This stimulates chromatin relaxation and thereby facilitates DSB repair [39, 125]. DSBs within euchromatin are mainly repaired by NHEJ in G0/G1 and G2 phase. DSBs in heterochromatin however, are also repaired by HR in G2 phase, with ATM phosphorylating CtIP thus enabling DNA resection and DSB repair [39, 103].

Although chromatin compaction may influence the reparability of some DNA damage sites, the complexity of damage has been argued to be an additional factor contributing to slowly repairing DSBs [130, 131]. In addition, proteins involved in DNA damage repair are recruited to and form foci at similar rates in euchromatin and heterochromatin [132-134].

1.4.5 Deficiency in DNA repair pathways

Cell lines carrying mutations in the proteins important for one of the DNA repair pathways have been engineered in order to study the importance of individual DSB pathway in different cell cycle phases.

An experiment measuring cell survival in G1 or S phase cells post X-ray or α-particle irradiation was performed in Chinese hamster ovary (CHO) wild type cell line and its derivatives, SSA-deficient (carrying ERCC4 mutation), HR-deficient (mutation in XRCC3) and NHEJ deficient (mutation in DNA-PKcs) [135]. SSA-deficient cells exhibited similar sensitivity to X-rays and α-particles as wild type cells when irradiated in G1 phase. However enhanced radiosensitivity of SSA-deficient cells in comparison to wild type cells was observed when simple or complex DNA damage, caused by X-rays or α-particles, respectively, was induced in S phase of the cell cycle. This suggests that SSA increases the survival of cells in S phase, but not in G1, following low (X-rays) or high (α-particles) LET radiation. CHO cells defective in either HR, NHEJ or SSA pathway showed

greater sensitivity to X-rays and α-particles as measured by colonogenic assays in G1 phase of the cell cycle compared to CHO wild type cells [135]. It was also shown that NHEJ and SSA contribute to repair but HR is the most important mechanism for repair of DSBs in S phase cells [135]. Irradiation in G1 phase with X-rays or α-particles suggested that simple DSBs in G1 phase are mainly repaired by NHEJ but not by SSA [135]. It has also been reported that α-particles are more effective per unit of absorbed dose than X-rays at inducing cell death in HR or NHEJ deficient exponentially growing cell lines [136]. Other studies have also shown very similar cell viability between HR defective and HR proficient cells exposed to low LET radiation [14, 137]. MCF-7 cells with impaired RPA32 phosphorylation sites exhibit higher sensitivity to HU (a replication inhibitor) than MCF-7 wild type cells, although no difference is seen between the cell lines post 1-6 Gy of X-ray exposure [14].

Higher frequencies of chromosome breaks have been observed in MCF-7 cells with mutated RPA32 after exposure to HU compared with cells expressing wild type RPA32 [14]. BRCA2 deficient HeLa cells irradiated with 2 Gy X-rays exhibit elevated levels of chromatid breaks and gaps in G2 phase, compared to irradiated wild type cells [138]. Moreover, cells depleted of BRCA2 or Ku80 showed increased chromosomal deletions post 2 Gy X-rays when compared with wild type cells [39]. In contrast, the level of deletions per cell in irradiated cells with a CtIP knock down is similar to that seen in CtIP proficient cells post-irradiation, suggesting that DSBs are repaired by the NHEJ pathway [39]. The SCE levels (spontaneous, mitomycin C and radiation-induced), which are a direct effect of HR, have been reported to be reduced in cells [137-140] deficient in either BRCA2 or CtIP, both of which are involved in HR [39]. In contrast, cells defective in NHEJ show similar SCE yield to that of NHEJ proficient cells [140].

1.4.6 Chromosomal aberrations

Chromosomal aberrations caused by ionising radiation occur if a cell is irradiated early in interphase, before the DNA has been replicated. This is in contrast to chromatid aberrations, which result if a cell has been irradiated in late interphase, after the chromosome material has been duplicated [1].

Chromosomal aberrations include rings and dicentrics, which may be lethal (**FIGURE 1.7**). The formation of rings is induced by radiation in each arm of a single chromatid early in the cell cycle. The 'sticky ends' (any two complementary DNA ends) then rejoin incorrectly to form a ring and a fragment lacking the centromere (acentric). Dicentrics are formed when a break is produced in two chromosomes early in the interphase, and the sticky ends are sufficiently close to one another leading to an interchange between these chromosomes. The interchange then replicates during S phase, resulting in a distorted chromosome with two centromeres (dicentric) and an acentric fragment [1].

Chromosomal aberrations are associated with many cancers [141], including therapy-related acute myeloid leukaemia (t-AML) [142]. Chromosomal rearrangements include: deletions, duplications, translocations, inversions or insertions, as well as ploidy change (aneuploidy, monosomy, trisomy, tetrasomy etc.). Deletions and translocations (**FIGURE 1.7**) are considered to play a very important role in carcinogenesis [1, 141]. Translocation occurs when the portions of two chromosomes are exchanged, or when an entire chromosome has attached to another at the centromere. Translocations between chromosomes 8 and 21, and 8 and 16 have been reported in t-AML after chemo- and radiotherapy [142]. Translocation between chromosomes 8 and 14 has also been observed in patients with Burkitt lymphoma [143]. Deletions result from two breaks on one arm of the chromosome and loss of genetic information between these breaks. Examples of

cancers with reported deletions include t-AML and retinoblastoma. Deletion of the long arm of chromosome 5 and/or chromosome 7 has been reported in t-AML [144] and deletion of the long arm of chromosome 13 has been seen in retinoblastoma [145].

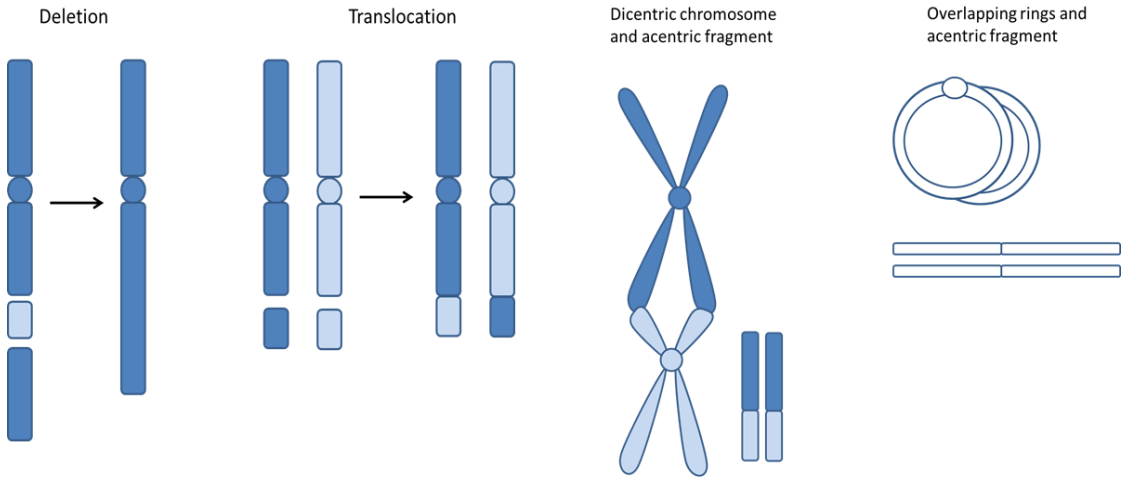


FIGURE 1.7 Schematic illustration of chromosomal aberrations: deletion, translocation, dicentric, ring. Adapted from Hall, E.J 1994 [1].

1.5 Ionising radiation and AML

It is estimated that the average exposure to background ionising radiation in the UK is 2.7 mSv per year [146]. The sources of exposure can be natural, from medical treatment or nuclear accidents (e.g. Chernobyl 1986, Fukushima 2011). Natural sources account for about 84 % of the average radiation exposure in the UK, include radiation from space, the sun and from the earth (radon, found within the earth's crust). Artificial radiation sources, like radiation therapy, make up about 16 % of overall exposure [146].

Epidemiological studies have shown an increased risk of cancer, including leukaemias, lung cancer and skin cancer, from medical radiation exposure, in atomic bomb survivors, and in workers at nuclear sites [147, 148]. An approximately 5-fold increase in leukaemias, including acute myeloid leukaemia (AML), was observed in Hiroshima and Nagasaki atomic bomb survivors [149]. Furthermore, deletions on chromosomes 5, 7, and 13 were seen at a higher rate in atomic bomb survivors who developed AML, compared to AML patients not exposed to IR [150, 151].

Leukaemia is a cancer of blood or bone marrow characterised, amongst other features, by an abnormal increase in immature forms of white blood cells (also known as blasts). Leukaemia can be acute or chronic, dependent on the speed of progression of the disease. Chronic leukaemia usually takes months or years to progress while acute leukaemia is characterised by a rapid accumulation of blasts. Based on the blood cells which are affected, leukaemia can be classified as lymphoid or non-lymphoid. Lymphoid involves T-, B- or natural killer cells, whereas leukaemias of other lineages arising from hematopoietic stem cells are termed non-lymphoid. Myeloid, erythroid and megakaryocytic leukaemias are subtypes of non-lymphoid leukaemias [152]. Biphenotypic leukaemia is also a non-lymphoid leukaemia where the lineage is of both lymphoid and myeloid origin [153]. Myeloid leukaemia is further divided into granulocytic and

monocytic leukaemia, depending on whether proliferation of mature granulocytes (neutrophils, eosinophils, basophils) or monocytes, and their precursors, is found.

AML is a type of non-lymphoid leukaemia, a cancer of haematopoietic stem cells and/or myeloid progenitor cells which are not able to differentiate normally and are not responsive to regulators of proliferation [154]. This leads to the accumulation of undifferentiated myeloid cells in the bone marrow which outgrow the normal white cell population. AML is the most common myeloid leukaemia (~2,000 cases/year in the UK), with increased incidence in males and elderly people [154]. General clinical features, similar for human and mice, are related to bone marrow failure or organ infiltration, and include: dizziness, shortness of breath, fever, anaemia, neutropenia, thrombocytopenia, splenomegaly, elevated total white blood cell count, presence of immature forms/blasts (minimum 20%) [152, 155], and rapid presentation of the disease [156]. One of the main criteria of leukaemia in mice is the presence of the abnormal hematopoietic cells/blasts in the spleen, detected by several antibodies which are recommended by the Mouse Models of Human Cancers Consortium [152]. A high level of Gr-1 and Mac-1 antibodies indicates granulocytic leukaemia, whereas low or negative Gr-1 and positive Mac-1 is classified as monocytic leukaemia [152]. CD31 and Ly6C are known as markers for myeloid progenitors [157], Sca-1 together with c-Kit indicates the presence of haematopoietic stem cells [158], and a high level of c-Kit alone is usually present in myeloid progenitors [159]. T- and B-cells markers such as CD3 [160] and B220 [161], respectively are expressed in lymphoid leukaemias but not (or at a very low level) in non-lymphoid leukaemias [152]. Co-expression of B220 with both Gr-1 and Mac-1, possibly indicates a presence of biphenotypic leukaemia [152].

Therapy-related acute myeloid leukaemia (t-AML) and myelodysplastic syndrome (t-MDS), formally known as preleukaemia (in about 40 % of cases of MDS the disease can

progress to AML), are believed to be serious long-term consequences of radiotherapy or chemotherapy and account for 10-20% of all AML cases [148, 162]. Therapy-related leukaemias (including AML), resulting from the use of cytotoxic drugs, can be divided into two groups, depending on whether patients were treated with alkylating agents (e.g. melphalan or MMC) or DNA-topoisomerase II inhibitors (e.g. etoposide) [163-165]. Patients from the first group commonly develop t-AML 5-10 years post treatment, a second type of t-AML however is seen after 1-5 years and is less common [154]. A higher rate of chromosome aberrations are observed in t-AML. A common feature of t-AML, caused by a treatment of prior lymphoma with alkylating agents, is the deletion of the long arm of chromosome 5 and/or chromosome 7 [144]. Translocations (t(8,21) and t(8,16)), as well as inversions (inv(16)) are also reported in t-AML after chemo- and radiotherapy [142]. Exposure to topoisomerase II inhibitors is often associated with abnormalities of the Myeloid/Lymphoid Leukaemia (*MLL*) gene (11q23), a critical transcriptional regulator [162, 164].

Numerous different factors, such as environment (e.g. pollution), life style (e.g. smoking), genetic diseases (e.g. Fanconi anaemia and Down syndrome) and enzymatic or DNA repair polymorphisms can result in predisposition to t-AML [162]. An example of enzymatic polymorphism is variation in glutathione S-transferase (GST), an enzyme which inactivates cytostatic drugs, like etoposide, melphalan or MMC [162]. Polymorphism, as well as homozygote deletion of some of the *GST* genes decreases the activity of the enzyme leading to increased risk of t-AML [166, 167]. Defects in DNA repair can also contribute to the development of t-AML: It has been shown that the frequency of Rad51 polymorphism, one of the main proteins in HR, is increased in t-AML when compared to healthy individuals [168]. Haematologic (Hodgkin's lymphoma, acute lymphoid

leukaemia) [169, 170] as well as non-haematologic malignancies (breast cancer, osterosarcoma) [171] have also been shown to influence t-AML development.

1.5.1.1 The subtypes of AML

There are several subtypes of AML, which were historically classified by the French-American-British (FAB) criteria, based on the stage where the leukaemic blasts have stopped differentiating [172]. Since 2001, AMLs are classified according to the World Health Organization (WHO), which uses genetic abnormalities or clinical features in its classification (**TABLE 1.2**) [173, 174].

TABLE 1.2 AML subtypes according to WHO classification from 2001 with some modifications made during revision in 2008 [173, 174].

Subtype	Description
AML with genetic abnormalities	Translocations: t(8,21), t(15,17), inversion-inv(16), MLL gene abnormalities (11q23)
AML with myelodysplasia-related changes	Derived from MDS
AML therapy related	Developed after chemotherapy (with alkylating agents or topoisomerase II inhibitors) with or without radiation
AML Down syndrome related	Developed in patients with Down syndrome (trisomy of chromosome 21)
AML not otherwise categorized	Do not fit into above categories

1.5.2 The CBA/H mouse strain as a model for radiation-induced acute myeloid leukaemia (rAML)

The CBA/H mouse model was first developed about 3 decades ago by exposing mice to a whole body single dose of 3 Gy X-rays. Approximately 25% of mice developed rAML 12-18 months post-irradiation [175]. Spontaneous incidence of AML in CBA/H strain is very low (0.1%), which makes CBA/H a very good model for rAML studies [176]. Indeed, this model has been used to predict the RBE value for AML. In comparison to X-ray-induced AML, the RBE for neutrons and ^{56}Fe ions is 3 and 1 respectively [177, 178].

It has been shown that the key feature of the CBA/H mouse strain is the partial deletion of one copy of chromosome 2 following exposure to X-rays [175]. The transcription factor gene PU.1/Sfpil, essential for the development of myeloid and lymphoid lineage, has been identified in this deleted region of chromosome 2 [179].

Another mouse strain, C57BL/6, is known to be susceptible to radiation-induced thymic lymphoma, and resistant to rAML [176]. The tumour incidence in the 129Sv mouse strain (which is the focus of this thesis) is overall low and its sensitivity to rAML is as yet unknown [180, 181]. There is no published information on chromosome 2 aberrations in the 129Sv mice, however this strain is reported to carry nsSNPs within the CtIP gene (Mouse Genome Informatics website).

1.5.3 Possible link between CtIP and rAML

Chromosome 2 deletion is a feature of CBA/H mice but not the rAML resistant C57BL/6 strain [182]. Using a surrogate assay, based on chromosome 2 radiosensitivity, the susceptibility to rAML has been investigated by a group at Public Heath England [2]. Firstly, aberrations (translocations, insertions, dicentrics, multi-coloured fragments and chromatid exchanges) for chromosomes 1, 2, and 3 in bone marrow cells from 12 inbred

mouse strains (including CBA/H and C57BL/6), were scored 24 h post 3 Gy X-ray exposure. The number of aberrations in chromosome 1, 2 and 3 were similar between five mice strains (including C57BL/6). However, in the seven remaining strains (including CBA/H) there were increased chromosome 2 aberrations in comparison to chromosome 1 and 3. CBA/H, together with a few other strains with high number of chromosome 2 aberrations, are known to be sensitive to rAML. In contrast, there is no known increased rAML incidence in C57BL/6 mice and the 4 other mouse strains with low number of chromosome 2 aberrations. Subsequently, microsatellite association mapping was performed, in order to identify candidate regions associated with chromosome 2 aberrations and rAML sensitivity. It was predicted that the chromosome 2/rAML sensitive mouse strains would share common microsatellite alleles, while mouse strains of a different phenotype would show divergent microsatellite alleles at the particular location. The microsatellite allele comparisons were carried out by computer based analysis of mouse microsatellite data. Chromosomal regions associated with chromosome 2 radiation sensitivity were identified and the most significant difference in microsatellite alleles between chromosome 2/rAML sensitive and resistant mouse strains was found on chromosome 18. The candidate genes were identified in this particular region of chromosome 18 by using NCBI and Ensembl mouse map viewers. Out of several genes in this region predicted to be associated with cancer susceptibility the Rbbp8/CtIP gene was the strongest candidate, as it interacts with tumour suppressors- Rb and BRCA1 [74,75,183]. CtIP, which was later found to be essential for embryonic development and to possibly function as a tumour suppressor [23,22,184], was therefore identified as a strong candidate for an rAML susceptibility gene [2].

1.6 Aims

The aims of this project were to:

- To evaluate the disease-causing potential of nsSNPs present in the CtIP mouse gene of the 129Sv mouse strain and examine the influence of this variant on carcinogenesis, mainly rAML development, and mice survival following exposure to an acute dose of 3 Gy of X-rays.
- To investigate whether the nsSNP identified within the CtIP gene impairs its function and consequently affects the activity of proteins downstream of CtIP in the HR pathway, which could lead to impaired repair of radiation-induced DSBs.
- To examine differences in cell survival between a cell line carrying a SNP within the CtIP gene and those with no mutation in this gene, following radiation or HU treatment.

2 Materials and Methods

2.1 *In vivo* studies

2.1.1 Mouse strains

CBA/H, a mouse strain sensitive to radiation-induced AML [175] was obtained from Medical Research Council (MRC), Harwell, UK. C57BL/6, resistant to radiation-induced AML [176], as well as 129Sv [180, 181] mouse strains were received from Harlan SeraLab, Loughborough, UK.

All animals were bred and housed according to the UK Home Office (Animals Scientific Procedures) Act 1986, with guidance from the local ethical review committee on animal experiments.

The Mouse Genome Informatics (MGI) website provided information about polymorphisms in various strains of mice: http://www.informatics.jax.org/

2.1.2 X-ray irradiation of mice

CBA/H, C57BL/6 and 129Sv mice were given a whole body dose of 3 Gy X-ray radiation at 12-15 weeks of age, at a dose rate 0.7 Gy min^{-1} (250 kV,14 mA, LET=2 keV/µm,) using an AGO HS X-ray system at Public Health England, Harwell.

2.1.3 AML diagnosis

AML diagnosis was based on Bethesda proposals for classification of non-lymphoid hematopoietic neoplasms in mice [152]. The animal work, including monitoring of the animals, schedule one procedures, total and differential white cell counting and

fluorescence-activated cell sorting (FACS) was performed by Dr. Rosemary Finnon and Paul Finnon, Public Health England.

Mice were administered one dose of 3 Gy X-rays to the whole body (section 2.1.2) and were monitored daily post-irradiation for signs of lethargy, poor grooming, hunched posture and rapid breathing. Any mouse showing any three of these signs was euthanised with a rising concentration of CO_2.

Post mortem blood samples were taken from the heart and placed in a heparinised blood tube. Blood samples were used for total white blood cell count and preparation of blood smears for differential counts. For total white blood cell counts, red blood cells were lysed with 1 % acetic acid and counted on a haemocytometer (section 2.2.5). For differential counts, 5 µl of blood were smeared onto a microscope slide, dried for 24 to 48 h, fixed with 100 % methanol for 2 min and stained with leukocyte staining buffer (Gibco) mixed with May-Grunwald Giemsa (Sigma-Aldrich) (ratio 1:3) for 5 min, leukocyte staining buffer mixed with May-Grunwald Giemsa (ratio 1:40) for 30 min, followed by rinsing twice with leukocyte staining buffer. Once the slides were dry, they were mounted with xylene. Different types of leukocytes were identified under the microscope, but the emphasis was put on counting neutrophils. The number of neutrophils per 200 leucocytes was counted per slide. Immature forms/blasts were distinguished from mature white blood cells by their high granularity and abnormally big nucleus (**FIGURE 2.1**). The spleen was also weighed and frozen in liquid nitrogen in RNA later solution (Ambion®, Life Technologies) for DNA/RNA extraction. Signs of AML, which can be observed post mortem, include neutropenia (lower than normal numbers of neutrophils), splenomegaly (enlarged spleen), elevated total white blood cell count and presence of immature forms/blasts. The last criterion was examined thoroughly by flow cytometry.

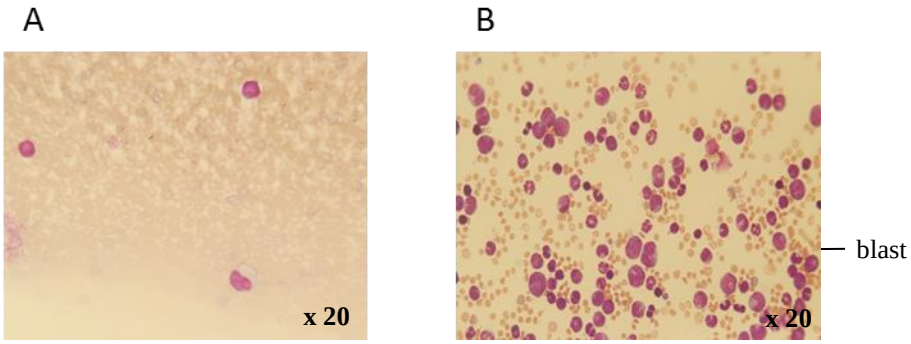


FIGURE 2.1 Blood smears from a non-irradiated 129Sv mouse (A) and 3 Gy X-ray irradiated 129Sv diagnosed with rAML (B). Much higher number of white blood cells can be observed in panel B, as well as the presence of immature forms/blasts.

2.1.3.1 Flow cytometry phenotyping of 129Sv rAML cases

Tissue samples from spleens were homogenised and stored in liquid nitrogen. Spleen cells were defrosted by placing the cryovials in a water bath (37 °C) for 2 min and prepared for flow cytometry by staining samples of 3 x 10^6 cells in FACS tubes (VWR ltd). Cells were first washed twice in 5 ml of 1 % foetal bovine serum (FBS) in phosphate buffered saline (PBS) and spun at 1200 rpm for 5 min at 4 °C (Sorvall Heraeus, 75006445). Cells were then resuspended in 5 ml of 3 % FBS in PBS. 2 µl of Fc block (BD Biosciences) was added into each sample for 5 min, whilst on ice. Diluted antibodies (**TABLE 2.1**), one per each sample, were added to 10 µl of cells diluted in 3 % FBS in PBS to a final volume of 25 µl and incubated for 45-60 min on ice. Cells were washed in 1 % FBS in PBS, spun at 1200 rpm for 5 min at 4 °C and resuspended in 300 µl of 1 % FBS in PBS. Cells were left on ice until they were analysed on a FACS Calibur flow cytometer (BD Bioscience).

Regions were drawn around major populations of the cells on a forward scatter/side scatter (FSC/SSC) dot plot using BD CellQuestPro software. Events with low FSC/SSC were assumed to be dead cells and debris and were excluded from analysis. In leukaemic samples, the analysis was performed on a region with high FSC/SSC, which is not normally present in control spleen.

TABLE 2.1 The antibodies used for phenotyping of possible rAML cases in 129Sv mouse strain.

Antibody	Cell type expression	Fluorochrome	Dilution in 3% FBS in PBS; volume used	Company
Gr-1	Granulocytes	Phycoerythrin (PE)	1/10; 3 µl	BD Biosciences
Mac-1	Monocytes/macrophages	PE	1/5; 3 µl	BD Biosciences
Ly6c	Myeloid progenitors, dendritic cell precursors and macrophages	PE	1/10; 2 µl	Abcam
c-Kit	HSCs in combination with Sca-1, myeloid progenitors	PE	Undiluted; 1 µl	Abcam
Sca-1	HSCs in combination with c-Kit	PE	Undiluted; 1 µl	BD Biosciences
CD31	Myeloid progenitors, dendritic cell precursors and macrophages	PE	1/10; 5 µl	BD Biosciences
B220	B-cells	PE	1/5; 2 µl	BD Biosciences
CD3	T-cells	PE	1/10; 5 µl	BD Biosciences
Isotope control	Nonspecific binding	PE	1/10; 5 µl	BD Biosciences

2.2 Cell culture

2.2.1 Cell culture reagents

TABLE 2.2 The cell culture reagents used for primary and immortal mouse embryonic fibroblasts (MEFs). DMEM= Dulbecco's Modified Eagle's medium, EDTA= Ethylenediaminetetraacetic acid.

Reagent	Company
DMEM + GlutaMAX™	Invitrogen, Life Technologies
Foetal Bovine Serum (FBS)	Invitrogen, Life Technologies
100 units/ml Penicillin, 100 µg/ml Streptomycin	Invitrogen, Life Technologies
Phosphate buffered saline (PBS)	Invitrogen, Life Technologies
Trypsin-EDTA (0.05 % Trypsin-EDTA)	Gibco, Life Technologies

2.2.2 Isolation of Mouse Embryonic Fibroblasts (MEFs) from pregnant mice

Embryos were isolated from female mice of the mouse strains CBA/H, C57BL/6 and 129Sv on day 13 of pregnancy. They were placed onto 6 cm petri dishes (Sterilin ltd) with PBS containing 1 % Amphoterin B (Sigma-Aldrich). Subsequently embryos were removed from the sack, their heads were separated from the rest of the body and discarded. The remaining parts of the embryos were disaggregated with scissors and syringe in order to get a homogenous mix of cells. The mix was then transferred into 15 ml falcon tubes (Sarstedt) filled with PBS and centrifuged at 1200 rpm (Sorvall Heraeus 75006445) for 5 min at 4 ºC. Supernatants were discarded and pellets were resuspended in 10 ml of culture medium supplemented with 50 ml of FBS and 5 ml of penicillin/streptomycin (**TABLE 2.2**), and transferred into T_{25} flasks (Sarstedt). Cells were maintained in a low oxygen incubator (3 % O_2, 5 % CO_2, 37 ºC; Thermo Scientific, Forma Steri-Cycle, high-efficiency particulate absorption (HEPA) Class 100) for 48 h. Cultures were expanded (section 2.2.4) until sufficient cells were obtained for cryogenic preservation (section 2.2.6)

2.2.3 Immortalisation of MEFs-retroviral transfection

For amplification of plasmids see section 2.3.

TABLE 2.3 Plasmids used for immortalisation of MEFs. MEFs were immortalised in two ways, either by SV40 immortalisation, using the pZip-LT plasmid or by knock down of p53 protein, using a pRS-p53shRNA plasmid.

Plasmid	Description	Received from
pZip(Neo)-LT	Carries the SV40 large T antigene, which inhibits p53 and Rb tumour suppressors; carries neomycin resistance gene.	Maria Blasco, Spanish National Cancer Research Centre
pRS(Puro)-p53shRNA	Retroviral short hairpin expression vector carrying sequences that target p53 transcripts; carries puromycin resistance gene.	Rene Bernards [185], Netherlands Cancer Institute
pCl-ECO	Packaging vector; a mammalian cell expression vector carrying the retroviral gag, pol and env genes.	Maria Blasco, Spanish National Cancer Research Centre
pEGFP-N1	Transfection control; a mammalian expression vector carrying the enhanced green fluorescent protein (GFP).	Purchased from Addgene

TABLE 2.4 Reagents used for the retroviral transfection of MEFs.

Reagents	Description / Concentration	Company
Polybrene	8 mg/ml	Sigma-Aldrich
$CaCl_2$	2.5 M, diluted in dH_2O	Sigma-Aldrich
2x 2-[4-(2-hydroxyethyl)piperazin-1-yl]ethanesulfonic acid (HEPES) buffered saline (HBS)	280.6 mM NaCl, 50 mM HEPES (no Na salt), 1.48 mM Na_2HPO_4, pH 7.00-7.15	Sigma-Aldrich
G-418 disulphate	500 mg/ml	Apollo Scientific
Puromycin dihydrochloride	3 mg/ml	Apollo Scientific

Day 1

Early in the morning, 293T cells were trypsinised (293T cells were cultured in the same way as immortal MEFs, section 2.2.4) and seeded at a concentration of 3.5-4 x 10^6 into a 10 cm cell culture dish using culture medium (**TABLE 2.2**). 7 h later, 293Ts were transfected by mixing 10 µg of pZip(Neo)-LT or pRS(Puro)-p53sh plasmid DNA with 10 µg of pCl-ECO, 1-2 µg of pEGFP-N1, 2.5 M $CaCl_2$ and topped up to 1 ml with distilled water (dH_2O). While bubbling, 1 ml of 2 x HBS buffer was added to the mix and left at room temperature for 1 min. The resulting solution was added to 293T cells drop wise and plates were swirled to mix.

Day 2

Medium was removed from 293T cells and replaced with 7 ml fresh medium. CBA/H, C57BL/6 and 129Sv MEFs were seeded at a density of 6 x 10^5 per 10 cm cell culture dish to ensure exponential growth. Two additional dishes with C57BL/6 cells were seeded to serve as negative controls.

Day 3

After making sure 293T cells were successfully transfected, seen as 80 % of 293T cells expressing green fluorescent protein (GFP) as a result of the pEGFP-N1 plasmid uptake, retrovirus containing media was collected and replaced with fresh medium (7 ml) and cells were incubated at 21 % O_2, 5 % CO_2, 37 ºC . To collect only retroviral particles, retrovirus containing media was filtered using 0.45 µm mounted on a syringe. The filtered supernatant was divided 1:3 in growth medium and polybrene was added at a concentration of 1:1000. Old medium from MEFs was replaced by the diluted viral supernatant, 7 ml per 10 cm dish.

Day 4

In the morning and afternoon, the infection was repeated as described above.

Day 5

MEF cells, including dishes set up for negative control, were refed with fresh medium containing either selecting agent G-418, an equivalent to neomycin, or puromycin antibiotic. The initial concentration of G-418 used was 1 mg/ml and after approximately 2 weeks (medium was changed every 3 days) it was reduced, firstly to 0.5 mg/ml and then to 0.25 mg/ml for maintenance. The concentration of puromycin used was 2 μg/ml and remained the same for the entire selection period (approximately 2 weeks), with medium being changed every 3 days. Cells were grown in 1 μg/ml puromycin containing medium thereafter. After approximately 2 weeks of treatment with G-418 or puromycin, all untransfected cells in the 2 negative controls died.

MEFs immortalised using pRS(Puro)-p53shRNA were used only for the transfection with the Rbbp8-pCMV6 plasmid, carrying a neomycin resistance gene, for CtIP overexpression. The different antibiotic resistance genes allowed for selection of co-transfected cells. The remaining experiments were performed on MEFs immortalised using pZip(Neo)-LT plasmid.

2.2.4 Culture conditions

2.2.4.1 Primary MEFs

Primary MEFs were cultured in growth medium (**TABLE 2.2**) in a low oxygen incubator (3 % O_2, 5 % CO_2, 37 ºC). Cells were grown to 80 % confluence, medium removed and cells washed with PBS to remove residual FBS which would inhibit the action of trypsin. Cells were covered with trypsin-EDTA (1 ml for T_{25}, 2ml for T_{75} and 3 ml for T_{175} flask) and left in an incubator for 10 min. Trypsin cleaves the proteins bonding the cells to the flask. In order to inactive trypsin, growth medium was added (2x the amount of trypsin) as the serum present in the growth medium inhibits trypsin activity. Cells were then split and

plated or centrifuged (1200 rpm, Sorvall Heraeus 75006445, for 5 min) and cryogenically frozen (section 2.2.6). Primary MEFs were maintained in a low oxygen incubator except for the cell growth experiments when they were grown under low (3 % O_2, 5 % CO_2, 37 ºC) and normal (21 % O_2, 5 % CO_2, 37 ºC) (Thermo Scientific, Forma Steri-Cycle HEPA Class 100) oxygen levels for comparison.

2.2.4.2 Immortal MEFs

Immortal MEFs were cultured in growth medium (TABLE 2.2) in a normal oxygen level cell culture incubator (21 % O_2, 5 % CO_2, 37 ºC). Cells were grown to 80 % confluence, they were then washed with PBS, covered with trypsin-EDTA and left in the incubator for 3-5 min. In order to inactivate trypsin growth medium was added (2x the amount of trypsin) and cells were then split and plated or centrifuged (1200 rpm, Sorvall Heraeus 75006445, for 5 min) and cryogenically frozen (section 2.2.6). Immortal MEFs were maintained in a normal oxygen incubator except for the cell growth experiments when they were grown under low and normal oxygen levels for comparison.

2.2.5 Cell counting

Cells were counted with an automated cell counter ‘Adam’ (Digital Bio), cell counter Countess (Invitrogen) or using a hemocytometer.

Adam cell counter: 20 µl of T reagent (containing propidium iodide - a fluorescent, nucleus dye and a detergent) was added to 20µl of cell suspension in order to count the total number of cells. The number of dead cells was measured by addition of 20 µl N reagent (containing propidium iodide) to the 20 µl cell suspension. In order to calculate the number of viable cells, the number of dead cells (N) was subtracted from the total cell number (T).

Cell counter Countess: 10 µl of cell suspension was mixed with 10 µl of Trypan Blue Stain (0.4 %), in order to identify dead cells. The number of total, alive or dead cells was given by the cell counter.

Haemocytometer: cells in 4 squares of haemocytometer were counted and the mean value was calculated. Each square is 1 mm^2 and the number of cells is equivalent to the value x 10^4/ml.

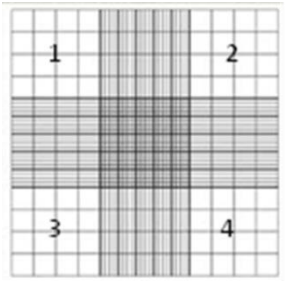


FIGURE 2.2
Haemocytometer, cells in squares, labelled 1-4, were counted and the mean value was calculated.

It was ensured that the same method was used for all the repeats within an experiment.

2.2.5.1 Comparison of the cell growth in low (3 %) and normal (21 %) O_2 conditions between primary and immortal cell lines.

The cell number of primary and immortal MEF cell lines: CBA/H, C57BL/6 and 129Sv was calculated by automated cell counter 'Adam'. 4 x 10^4 cells was plated into each T_{25} flask (30 flasks per each cell line) and cultured in low (3 %) or normal (21 %) oxygen incubator. Three flasks per cell line, from 3 % and 21 % O_2 incubator, were counted (using 'Adam' cell counter) for each time point, starting 72 h (1^{st} time point) after plating and every 48 h thereafter for 12 days.

2.2.6 Cell cryo-storage

Exponential growing cells were harvested as described in section 2.2.4. The number of cells in suspension was counted using a haemocytometer (section 2.2.5). Cells were cryogenically frozen at 1 x 10^6 cells per vial. Cells were centrifuged for 5 min at 1200 rpm at room temperature (Sorvall Heraeus 75006445). The culture medium was aspirated and the cell pellet was re-suspended in 1 ml per vial of freezing mix containing 90 % of FBS and 10 % Dimethyl sulfoxide (DMSO, a cryoprotectant which stops ice forming). The cryogenic tubes were placed in a freezing container (Thermo Scientific) with a 1 °C / min cooling rate for successful cryopreservation of cells. The cells were maintained at -80 °C for 24 h and transferred into liquid nitrogen for long-term storage.

2.3 Amplification and purification of plasmid DNA

2.3.1 Preparation of electrocompetent bacteria

5 ml Luria-Bertani (LB) broth (10 g/l peptone, 5 g/l yeast extract, 10 g/l NaCl, Merck) was inoculated with the DH5α strain of *E.coli* and incubated at 37 °C overnight in a shaking incubator (220 rpm, New Brunswick Scientific model innova 4230). 1 ml of bacterial culture was then added to two flasks each containing 100 ml LB broth and incubated at 37 °C in a shaking incubator at 220 rpm for approximately 2 h. The OD_{595nm} should be between 0.5 and 0.7 to ensure exponential growth of bacteria and therefore efficient transformation. The culture was divided into four 50 ml centrifuge tubes and spun at 5000 x g, 4 °C for 10 min. The supernatant was removed and each pellet was resuspended in 50 ml ice cold distilled H_2O followed by centrifugation at 5000 x g, 4 °C for 10 min. This wash step was repeated four times. Each pellet was then resuspended in 200-300 µl of 10% glycerol, flash frozen on dry ice in 60 µl aliquots and stored at -80 °C.

2.3.2 Transformation of electro-competent bacteria

1 µl of plasmid DNA (pZip(Neo)-LT, pRS(Puro)-p53shRNA, pCl-ECO, pEGFP-N1, pRS(Puro)-shCtIP or pRS(Puro)-shGFP or Rbbp8-pCMV6 (section 2.2.3, 2.3.4 and 2.3.5) was incubated with a 60 µl aliquot of DH5α electro-competent *E.coli* on ice for 10 min. The sample was transferred to a 0.1 cm electroporation cuvette (BioRad) and the bacteria were transformed by electroporation (1.8 kV) using an *E.coli* pulser with time constraints of approximately 5 ms, followed by immediate addition of 500 µl super optimal broth (SOB - 2% w/v tryptone, 0.5% w/v yeast extract, 10 mM NaCl, 2.5 mM KCl). The sample was transferred to a 15 ml centrifuge tube and incubated in a shaking incubator for 1 h at 37 °C. The pZip(Neo)-LT, pRS(Puro)-p53shRNA, pCl-ECO, pRS(Puro)-shCtIP and pRS(Puro)-shGFP plasmids contain an ampicillin resistance cassette and the pEGFP-N1 and pCMV6 plasmid contain a kanamycin resistance cassette. Transformants were selected by plating 100 µl and 50 µl of the SOB containing electroporated bacteria on to LB agar (Sigma-Aldrich) containing either 50 µg/ml kanamycin or 100 µg/ml ampicillin and incubated overnight at 37 °C.

2.3.3 Amplification and purification of plasmid DNA

From the transformants left to grow on the agar plates overnight, a single colony was used to inoculate an aliquot of 2 ml LB broth containing either kanamycin or ampicillin and incubated at 37 °C in a shaking incubator for 8 h. 1 ml of bacterial culture was added to two conical flasks each containing 200 ml LB broth containing either kanamycin or ampicillin and incubated at 37 °C in a shaking incubator overnight at 37 °C. The bacteria were harvested by centrifugation at 6000 x g for 15 min at 4 °C. The plasmid DNA was then purified using a QIAfilter Plasmid Maxi Kit (Qiagen). Each bacterial pellet was resuspended in 10 ml Buffer P1. Subsequently, 10 ml Buffer P2 was added and mixed by vigorously inverting 6 times, in order to lyse the bacterial cells. The suspension was then

incubated at room temperature for 5 min. In order to enhance precipitation, chilled Buffer P3 (10 ml) was added to each lysate and mixed by vigorously inverting 6 times. The solution was then poured into the barrel of the QIAfilter cartridge (prepared by screwing the cap onto the outlet nozzle of the QIAfilter cartridge, which was then placed in the QIArack) and incubated at room temperature for 10 min. In the meantime, a QIAGEN-tip column was equilibrated by adding 10 ml Buffer QBT and allowing the column to empty by gravity flow. After 10 min incubation, the cap was removed from the QIAfilter Cartridge outlet nozzle and the plunger gently inserted into the cartridge. The cell lysate was filtered into the equilibrated QIAGEN-tip column. The cleared lysate was then allowed to enter the resin by gravity flow. The QIAGEN-tip column was then washed twice with 30 ml Buffer QC. The DNA was eluted with 15 ml Buffer QF and collected in a 50 ml centrifuge tube.

The DNA was precipitated by adding 10.5 ml (0.7 volumes) room temperature isopropanol (Fisher Scientific) to the eluted DNA. The solution was mixed and centrifuged at 15,000 x g for 30 min at 4 °C. The supernatant was carefully removed and discarded. The DNA pellet was then washed with 5 ml room temperature 70 % ethanol (Fisher Scientific), to allow for easier redissolvement of DNA, and centrifuged at 15,000 x g for 10 min, followed by careful removal of supernatant. The DNA pellet was air-dried for 30 min and then dissolved in 200 µl of tris-EDTA buffer, pH 8.0 (Sigma-Aldrich). The concentration of the plasmid DNA was measured using a spectrophotometer (GeneQuant, Amersham Biosciences) at 260 nm and the DNA was stored at -20 °C.

2.3.4 Transfection of immortal MEF cells with plasmid for CtIP knock down

The CtIP knock down in immortal MEF cell lines was performed with short hairpin RNA (shRNA) containing the following sequence:

TGCTGTTGACAGTGAGCGAGCTCTCTATGTACAAATGAATTAGTGAAGCCACA
GATGTAATTCATTTGTACATAGAGAGCGTGCCTACTGCCTCGGA

targeting exon 7 and 8 of CtIP gene [186] and cloned into the Retro-Super plasmid, carrying a puromycin resistance gene. The construct was a gift from Andre Nussenzweig, National Cancer Institute, Maryland, USA.

MEFs immortalised using pZip(Neo)-LT plasmid (section 2.2.3) were transfected with the plasmid carrying shRNA for CtIP knock down pRS(Puro)-shCtIP or control plasmid with shRNA for GFP knock down: pRS(Puro)-shGFP (OriGene). Transfection was performed as described in section 2.2.3 by mixing 10 µg of pRS(Puro)-shCtIP or pRS(Puro)-shGFP plasmid DNA with 10 µg of pCl-ECO, 1-2 µg of pEGFP-N1and 2.5 M $CaCl_2$. Infected cells were selected by addition of puromycin (2 µg/ml) to the growth medium for approximately 2 weeks (until all of the untransfected cells had died), with medium being changed every 3 days. Cells were maintained in 1 µg/ml puromycin thereafter.

2.3.5 Transfection of 129Sv cells with plasmid overexpressing CtIP gene

129Sv MEF cells, immortalised with pRS(Puro)-p53shRNA (section 2.2.3), were plated at a concentration of 2 x 10^5 per 10 cm dish (Appleton woods) in 15 ml of culture medium without antibiotics. One dish was seeded to serve as a negative control. Cells were then incubated for 24 h prior to transfection at 37 °C, 5 % CO_2.

Two dishes of cells were transfected and, for each dish, 24 µg of pCMV6-Rbbp8 (OriGene, MC222442) plasmid DNA was diluted in Opti-MEM I Reduced Serum Medium (Invitrogen, Life Technologies) to a total volume of 1.5 ml. 60 µl of Lipofectamine™ 2000 (Invitrogen, Life Technologies) was diluted in Opti-MEM I Reduced Serum Medium to a total volume of 1.5 ml and incubated for 5 min at room temperature. The diluted DNA was combined with the diluted Lipofectamine™ 2000 in a 50 ml falcon tube (Corning), gently mixed by inverting and incubated for 20 min at room temperature. The solution was then added onto the cells and incubated for 6 h at 37 °C, 5 % CO_2. Medium was then removed and 15 ml of full growth culture medium (TABLE 2.2) was added and cells were incubated for a further 24 h at 37 °C, 5 % CO_2. The transfected cells as well as the negative control were split 1:10. Each dish was split into 2, resulting in 4 transfected dishes of cells and 2 non-transfected ones. The selecting agent G-418, an equivalent to neomycin, was added to each dish at a concentration of 1 mg/ml for approximately 1 week (medium was changed every 3 days). Subsequently the concentration of G-418 antibiotic was reduced to 0.5 mg/ml, and cells were incubated for another week (with the medium being changed every 3 days). After approximately 2 weeks, all of the untransfected cells had died and the stably transfected cells were maintained under selection with 0.25 mg/ml of G-418.

2.4 Bioinformatics- algorithms used for CtIP nsSNP prediction

Panther	www.pantherdb.org
PhD-SNP	http://snps.biofold.org/phd-snp/phd-snp.html
Polyphen	http://genetics.bwh.harvard.edu/pph2/
SNAP	https://rostlab.org/services/snap/

SIFT http://sift.jcvi.org/

Meta-SNP http://snps.biofold.org/meta-snp/

2.5 Semi-quantitative PCR

2.5.1 DNA isolation

DNA was isolated from the spleen of CBA/H, C57/BL6 and 129Sv mice using MagNa Pure Compact Nucleic Acid Isolation Kit I (Roche). Tissues were kept in RNAlater® solution (Ambion®, Life Technologies) at -80 ºC. A small piece was cut using a sterile blade and placed into the MagNA Lyser Green Beads (Roche), filled up with 1 ml MagNA Pure DNA Tissue Lysis Buffer (Roche). Samples were then lysed in a MagNa Lyser (Roche) at 6500 rpm for 1 min. The homogenous lysate was transferred into a 1.5 ml microcentrifuge tube. The following steps were carried out according to the MagNa Pure Compact Nucleic Acid Isolation Kit I protocol (Roche). Sample volume: 200 µl; elution volume: 200 µl.

DNA concentration was measured at 260 nm using a Nanodrop ND1000 spectrophotometer (Thermo Scientific).

2.5.2 Semi-quantitative PCR

Polymerase chain reaction (PCR) genotyping was performed with the DNA from the spleen of non-irradiated CBA/H, C57/BL6 and 129Sv mice or the samples from the rAML 129Sv mice. The samples were run on Bio-Rad iCycler using the following cycling conditions: initiation step for 4 min at 95 °C followed by 35 cycles of 30 s each at 95 °C – denaturation step, 60 °C – annealing step, and 72 °C – elongation step, and a final elongation for 10 min at 72 °C. Samples were stored at 4 °C.

TABLE 2.5 The PCR reagents The volume is given per one PCR reaction.

Reagents	Volume (µl)
10x Reaction Buffer (containing 15 mM $MgCl_2$; Qiagen)	1
dNTP mix (10 mM; Invitrogen)	0.2
Q solution (Qiagen)	2
Forward primer (10 µM; Sigma-Aldrich)	0.5
Reverse primer (10 µM; Sigma-Aldrich)	0.5
Taq DNA Polymerase (Qiagen)	0.25
Nuclease-free Water (Ambion)	4.55
Template DNA	1
Total volume	**10**

2.5.3 Agarose gel electrophoresis

The final PCR product was run on a GelRed stained (10 µL/x volume, Biotium) 1 % agarose gel in 1x 2-Amino-2-hydroxymethyl-propane-1,3-diol (tris)/Borate (TBE) buffer (89 mM tris base, 89 mM boric acid and 2 mM EDTA), in order to assess the size and integrity of the nucleic acid. Samples were mixed 1:5 with loading buffer (0.25 % bromophenol blue, 40 % sucrose in H_2O) before loading onto the gel. Electrophoresis was performed in TBE buffer at 5 V/cm at room temperature for approximately 1 h. A 1 kB ladder (Invitrogen, Life Technologies) was used at 0.0625 µg/ml to estimate the size of a product. The gel was visualised using the Gel Doc 2000 system (BioRad).

2.5.4 Sequencing of CtIP and PU.1 gene for the presence of nsSNP

Primers for CtIP nsSNPs were designed and checked by the Oligo Calculator for size, GC content and temperature (Tm) (http://www.basic.northwestern.edu/biotools/OligoCalc-.html), and ordered from Sigma-Aldrich. Primers for PU.1 nsSNP, which can result in a change from arginine to cysteine, serine or histidine (chromosome 2, exon 5) were

designed by Grainne Manning, Public Health England, and ordered from Integrated DNA Technologies (TABLE 2.6)

TABLE 2.6 Primers used for genotyping CBA/H, C57/BL6 and 129Sv mice.

nsSNP **CtIP gene**	**Forward sequence**	**Reverse sequence**	**Product size (bp)**
H388Y **Histidine/Tyrosine**	GGCGTCATCTCCGGTATTT	AAACCGATCTGACAGGTCCA	520
Q418P **Glutamine/Proline**	TGGGTCAGAAGTGAAGGTCA	CTTCCTTTTGGATGCTTTGC	177
A498T **Alanine/Threonine**	CCTTTCCCAATGGAGAATCA	AGGAGGAGCCCTTTGGAAT	187
A882V **Alanine/Valine**	AGTCCTCGTCCCAAAAGACG	CTTGCATGTCAAAAGCTGGT	507
PU.1 gene **R235C** **Arginine/Cysteine** **R235S** **Arginine/Serine** **R235H** **Arginine/Histidine**	CGACATGAAGGACAGCATCT	TTTCTTCACCTCGCCTGTCT	181

2.5.4.1 Sequencing

The PCR products were gel purified according to the MinElute® PCR Purification Kit protocol using a microcentrifuge (Eppendorf) or left unpurified, if only one product was visible on the gel. Samples were then sent for sequencing at the DNA Sequencing Lab, Source BioScience Life Sciences, Department of Biochemistry, South Parks Road, Oxford. The Sanger sequencing method was used with the following sample requirements: PCR product 1 ng/µl per 100 bp, primer 3.2 pmol/µl.

2.6 Multiplex Quantitative Real-Time-PCR (MQ-RT-PCR)

2.6.1 RNA isolation

RNA was isolated from blood, bone marrow, brain, spleen and thymus of CBA/H, C57/BL6 and 129Sv mice using miRNeasy Mini Kit (Qiagen).

2.6.1.1 RNA isolation from solid tissues

Tissues were stored in RNAlater® solution at -80 ºC. A piece of tissue was cut using sterile blade and placed into the MagNA Lyser Green Beads (Roche) and filled up with 700 µl QIAzol Lysis Reagent (Qiagen). Tissue was then homogenised in MagNa Lyser at 6500 rpm for 1 min and incubated at room temperature for 5 min. The following steps were carried out according to the manufacturer's protocol. 140 µl of chloroform was added to each sample and the tube was shaken vigorously for 15 seconds to separate the phases of the homogenate. Sample was then centrifuged for 15 min at 8000 x g at 4 ºC (Eppendorf), supernatant was carefully removed and placed into a new collection tube. 100 % ethanol (x 1.5 volume) was added into the tube and mixed thoroughly by pipetting up and down several times. Up to 700 µl of the sample was pipetted into an RNeasy Mini spin column and placed in a 2 ml collection tube. Sample was centrifuged at 8000 x g for 15 seconds at room temperature and the flow-through was discarded. This step was repeated with the remainder of the sample.

In order to perform DNase digestion step, 350 µl washing buffer- Buffer RWT was added onto the RNeasy Mini spin column and centrifuged at 8000 x g for 15 seconds at room temperature; the flow-through was discarded. Subsequently, DNase I incubation mix, consisting of 10 µl DNase I stock solution and 70 µl Buffer RDD, was added directly onto the RNeasy Mini spin column and incubated for 15 min at room temperature. Buffer RWT (350 µl) was then added onto the RNeasy Mini spin column and centrifuged at 8000 x g

for 15 seconds at room temperature. The flow-through was discarded 500 µl Buffer RPE (second washing buffer) was added onto the RNeasy Mini spin column, centrifuged at 8000 x g for 15 seconds at room temperature and the flow-though was discarded. 500 µl Buffer RPE was added onto the column again and centrifuged at 8000 x g for 2 min at room temperature, in order to dry the RNeasy Mini spin column membrane. The flow-through was discarded together with the collection tube. The RNeasy Mini spin column was placed into the fresh collection tube and centrifuged at 14,000 x g at room temperature. The RNeasy Mini spin column was then transferred into a new collection tube and 30 µl of RNase-free water was added directly onto the RNeasy Mini spin column membrane and centrifuged at 8000 x g for 1 min to elute RNA.

RNA quantity was measured at 260 nm using a Nanodrop ND1000 spectrophotometer, and RNA quality was assessed on 1 % agarose gel, as described in section 2.5.3.

2.6.1.2 RNA isolation from bone marrow

Bone marrow cells were stored in RNAlater® solution at -80 ºC. Around 500 µl to 1 ml of the cells was placed into the MagNA Lyser Green Beads and centrifuged at 12,000 x g for 10 min at room temperature. The RNAlater® solution (supernatant) was removed and discarded. 700 µl of QIAzol Lysis Reagent was then added and the RNA isolation was carried out as described in section 2.6.1.1.

2.6.2 Reverse Transcription (RT)

Reverse transcription reactions were performed using a High Capacity cDNA Reverse Transcription Kit (Applied Biosystems). A master mix containing listed reagents was prepared (TABLE 2.7) with 35 µl of diluted RNA added per reaction (700 ng of RNA in a 50 µl reaction volume). The reaction was performed using the iQ5 Real-Time PCR detection system (Bio-Rad), using the following cycling conditions: 10 min at 25 °C - to

allow primers to anneal, 2 h at 37 °C - reverse transcription and 5 min at 85 °C – reverse transcriptase inactivation. Samples were stored at 4 °C.

TABLE 2.7 Reagents used for preparation of RT master mix; the volumes are given per one reaction.

Reagent for master mix solution	Volume (µl)
RT Buffer	5
dNTP mix	2
Random primer	5
Multi scribe RT	2.5
H_2O	0.5
RNA+ H_2O	35
Total volume	**50**

2.6.3 Multiplex Quantitative Real-Time-PCR

Real-time PCR was performed using Rotor-Gene (Qiagen). All reactions were run in triplicate using PerfeCTa® MultiPlex qPCR SuperMix (Quanta Biosciences), primer and probe sets for target genes at 300 nM concentration each and 2.5 µl of cDNA in 30 µl reaction volume. 3'-6-Carboxyfluorescein (FAM), 6-Hexachlorofluorescein (HEX), Texas Red (TEX), ATTO680 and Cy5 (Eurogentec ltd.) were used as fluorochrome reporters for the hydrolysis of the probes analysed in multiplexed reactions. The Black Hole Quencher® dye (BHQ) was used as a quencher of fluorescence at one end of the probe (**FIGURE 2.3** and **TABLE 2.8**). Cycling parameters were 2 min at 95 °C- initiation step, then 45 cycles of 10 sec at 95 °C- denaturation, 60 sec at 60 °C- annealing and elongation. Samples were stored at 4 °C. Data was collected and analysed by Rotor-Gene Q associated software. Gene target cycle threshold (Ct) values were normalised to a Hypoxanthine–Guanine phosphoribosyltransferase 1 (HPRT1) internal control. Ct values were converted to transcript/sample quantity (SQ) using standard curves obtained by serial dilution of PCR-amplified DNA fragments of each gene and run in each MQ-RT-PCR reaction. The linear

dynamic range of the standard curves covering six orders of magnitude (serial dilution from 3.2 x 10^{-4} to 8.2 x 10^{-10}) gave PCR efficiencies between 93% and 105% for each gene with R^2>0.998. Relative gene expression levels after irradiation were similarly obtained for comparison with sham irradiated controls.

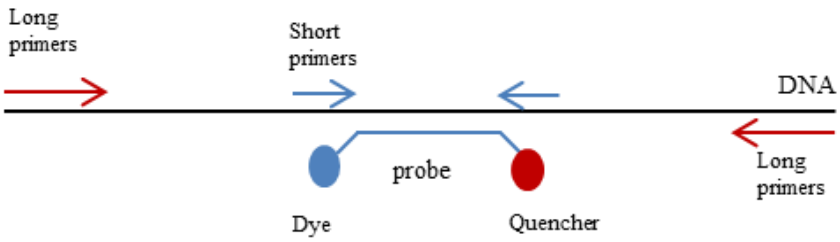


FIGURE 2.3 The illustration of a probe specific to the amplified sequence. The probe has a fluorescent reporter at one end and a quencher of fluorescence at the opposite end. The long primers were designed to flank the assay primers (short primers) to prepare the PCR product used for construction of the standard curve.

The primers and probes were designed by Grainne Manning and Sylwia Kabacik, Public Health England.

TABLE 2.8 Primers and probes used for MQ-RT-PCR.

Gene	Forward / Reverse sequence	Probe sequence	Dye	Quencher
Hprt1	GGACAGGACTGAAAGACTTG/ TAATCCAGCAGGTCAGCAAA	CCCTTGAGCACACAGAGGGCCACA	FAM	BHQ1
CtIP	TGCCAGCAGAAGAAAGAGAA / GTCTTTTGGGACGAGGACTA	AGTTGGCTTCCTGCTCAAGACACCG	Cy5	BHQ3
Cables	GGAAGCTGAACAAGCAGAAC/ CAGTCGGAACTTCTCTTCCA	CTTGGCCGCTAGCAGCACACAGGC	TEX	BHQ2
Ccng1	TGAAAGCGACTGAAGAGGAA/ GGTCTGAAACCGTGAACCTA	CCCACTGGCGACTGATTTGATCCGA	ATTO680	BHQ3
PU.1	AGAAGCTGATGGCTTGGAGC/ GCGAATCTTTTTCTTGCTGCC	TGGGCCAGGTCTTCTGCACGG	HEX	BHQ1

2.7 Induction and detection of DNA double strand breaks

2.7.1 Ionising radiation

2.7.1.1 γ-radiation

Exponentially growing cell lines (section 2.2) were plated at 1 x 10^5 in 2 ml of growth medium (TABLE 2.2) into 3 cm glass walled, number 1 glass cover-slip based dishes, 24 h prior to irradiation. Cells were cooled on ice for 10 min prior to irradiation to slow cellular processes including DNA repair. Cells were irradiated at room temperature in the culture medium with 0.662 MeV (LET=0.3 keV/µm) ^{137}Caesium γ-rays (GSR D1 irradiator, Gamma-Service Medical GmbH) at a dose rate of 1.7 Gy/min. Dosimetry was performed by James Thompson (Gray Institute) using gafchromic film.

2.7.1.2 α-particle irradiation

Exponentially growing cell lines (section 2.2) were plated at 1 x 10^5 in 2 ml of growth medium (TABLE 2.2) into 3 cm glass walled, 2.5 µm mylar based dishes, 48 h prior to irradiation. Cells were irradiated at room temperature directly through the mylar base with ^{238}Plutonium α-particles at a dose rate of 0.5 Gy/s and an incident energy of 3.26 MeV (LET=120 keV/µm). The range of the α-particles in water is 20 µm. Irradiations were carried out by James Thompson (Gray Institute) who also performed the dosimetry.

2.7.2 Immunofluorescent staining for γH2AX, 53BP1, Rad51 and RPA32

TABLE 2.9 Antibodies used for immunofluorescent staining.

Primary antibody	Dilution	Company & Catalogue Number	Secondary antibody	Dilution	Company
rabbit anti-53BP1	1:500	Abcam ab36823	Goat anti-rabbit, Alexa Fluor®633	1:1000	Invitrogen, Life Technologies
mouse anti-γH2AX (phospho-S139, JBW301)	1:1000	Millipore 05636	Goat anti-mouse, Alexa Fluor®488	1:1000	Invitrogen, Life Technologies
mouse anti-Rad51 (14B4)	1:500	GeneTex GTX70230	Goat anti-mouse, Alexa Fluor®488	1:1000	Invitrogen, Life Technologies
Rat anti-RPA32 (4E4)	1:200	Cell Signalling Technology 2208,	Goat anti-rat, Alexa Fluor®555	1:1000	Invitrogen, Life Technologies

Following irradiation, exponentially growing cell lines (section 2.2) were resuspended in 2 ml of culture medium (**TABLE 2.2**) warmed to 37 °C and incubated at 37 °C for the stated repair times. Cells were then washed with PBS for 5 min and fixed in 500 µl of 3 % paraformaldehyde (Sigma-Aldrich) in PBS at room temperature for 15 min. The paraformaldehyde was removed and cells washed with PBS for 5 min at room temperature and then permeabilised with ice-cold 500 µl of 1 % Triton X-100 (Sigma-Aldrich) in PBS for 10 min at room temperature. Cells were blocked with 500 µl of 2 % bovine serum albumin (BSA, Sigma-Aldrich) in 0.1 % Triton X-100 in PBS for a minimum of 1 h at room temperature. Cells were washed with ice-cold 0.25 % Triton X-100 in PBS for 5 min and then incubated with primary antibodies (**TABLE 2.9**) diluted in 2 % BSA in 0.1 % Triton X-100 in PBS, for at least 4 h at room temperature, or overnight at 4 °C. Cells were washed a further 3 times with ice-cold 0.25 % Triton X-100 in PBS for 5 min and then incubated with corresponding secondary antibodies (**TABLE 2.9**) diluted in 2 % BSA in

0.1 % Triton X-100 in PBS, for 1 h at room temperature. After two washes with ice-cold 0.25 % Triton X-100 in PBS for 5 min, a drop of Vectashield® mounting medium containing 2-(4-amidinophenyl)-1H -indole-6-carboxamidine (DAPI) (Vector Laboratories) was added to each dish and the cells were covered with a 25 mm diameter number 1 glass cover-slip. Cells were viewed using confocal microscope Zeiss LSM T-PMT with a x40 oil objective.

2.8 Sister chromatid exchange

2.8.1 Mitomycin C (MMC) treatment

Exponentially growing immortal MEFs were cultured in growth medium (**TABLE 2.2**) and split into two T_{75} flasks. The next day one flask from each cell line was treated with MMC (Sigma-Aldrich), a well-known inducer of SCE [187], at a final concentration of 0.5 µg/ml and incubated at 37 ºC, 21 % O_2, 5 % CO_2 for 2 h. An equivalent volume of vehicle control (PBS) was added to the second flask. The cells were then washed three times with growth medium and subsequently incubated in growth medium containing 15 µM bromodeoxyuridine (BrdU, Invitrogen, Life Technologies) for 48 h. After 48 h, 10 µl of colcemid (100 µg/µl, Fluka) was added per 10 ml to each culture, in order to arrest cells in metaphase, and incubated at 37 ºC for 3 h. Using the mitotic shake-off technique, only cells in mitosis, therefore not strongly attached to the flask, were collected. After a few minutes of extensive 'shake-off', medium was removed from the flasks into 15 ml Falcon tubes (Corning). Cells were centrifuged at 1200 rpm for 5 min (Sorvall Heraeus 75006445). The pellets were then resuspended in 2 ml of pre-warmed 0.075M KCl and incubated for 6 min at 37 ºC. Cells were fixed in methanol:acetic acid (3:1) which was added to the cells drop wise (approximately 10 drops per tube) without mixing. Cells were centrifuged at 1200 rpm for 5 min, supernatant was removed and the pellet resuspended in

5 ml fixative solution by vortexing. This procedure was repeated twice and cells left in fixative solution at 4 ºC overnight. The next day, cells were centrifuged and the supernatant was resuspended in several drops of fixative solution. Around 500 µl of this solution was then splashed on a glass microscope slide ('chromosome drop'). In order to obtain optimal temperature and humidity, this was carried out in a fume hood under a heat lamp. The slides were left to dry in the fume hood for 24 h before being stained by the fluorescence plus Giemsa technique.

2.8.1.1 Fluorescence plus Giemsa (FPG) staining

Slides were stained with 0.5 µg/ml Hoechst 33258 solution (Sigma-Aldrich) for 20 min, rinsed in dH_2O and mounted in 2-3 drops of Hoechst 33258 solution underneath a coverslip. Slides were then placed on a sheet of aluminium foil beneath an ultraviolet lamp for 20 min. Coverslips were removed and slides rinsed in dH_2O. Slides were placed in 5 % Giemsa solution (Giemsa stain [VWR International] diluted in pH 6.8 buffer [Gibco]) for 2.5-3 min, rinsed in dH_2O and left to dry for several hours. A drop of xylene was placed on the dried slides and then covered with a coverslip.

Lastly, the frequency of SCEs was evaluated in second-division metaphases, under a light microscope (Olympus BX60, 100 x objective).

2.8.2 α-particle irradiation

Cells were plated and irradiated as described in section 2.7.1.2. Immediately following irradiation cells were trypsinised and two dishes (2×10^5 cells) per treatment placed into a T_{75} flask. BrdU was subsequently added to the growth medium to give a final concentration of 15 µM and cells were incubated at 37 ºC for 48 h. The subsequent steps were performed as described in section 2.8.1.

2.9 Western blotting

2.9.1 Preparation of whole cell lysates

Exponentially growing cells were washed with cold PBS and 500 µl of lysis buffer (Cell Signalling Technologies: 20 mM Tris-HCl (pH 7.5), 150 mM NaCl, 1 mM Na_2EDTA, 1 mM ethylene glycol tetraacetic acid (EGTA), 1% Triton X-100, 2.5 mM sodium pyrophosphate, 1 mM β-glycerophosphate, 1 mM Na_3VO_4 and 1 µg/ml leupeptin), supplemented with 1 mM of the serine protease inhibitor phenylmethanesulfonyl fluoride (Sigma-Aldrich), was added to a T_{75} flask and incubated on ice for 15 min. Lysed cells were then scraped, transferred into chilled 2 ml microcentrifuge tubes and kept on ice. Lysates were sonicated (BioLogics, Inc.) twice for approximately 10 seconds and centrifuged at 14,000 x g in a microcentrifuge (Eppendorf) at 4 °C for 10 min. The supernatants were transferred into fresh tubes and stored at -80 °C.

2.9.2 Preparation of nuclear and cytoplasmic cell lysates

Nuclear and cytoplasmic extracts were prepared according to Thermo Scientific NE-PER® Nuclear and Cytoplasmic extraction protocol. Exponentially growing cells were harvested as described in section 2.2.4. Following the centrifugation, supernatant was removed and the pellet, representing the content of a 70-80 % confluent T_{175} flask, was resuspended in 100 µl ice-cold cytoplasmic extraction reagent I (CER I) by vigorous vortexing at the highest setting for 15 sec to fully resuspend the cell pellet. Samples were incubated on ice for 10 min, subsequently 11 µl of ice-cold cytoplasmic extraction reagent II (CER II) was added to each sample, vortexed for 5 sec at the highest setting and incubated on ice for 1 min. The samples were further vortexed for 5 sec at the highest setting and centrifuged in the microcentrifuge at 16,000 x g (Eppendorf). The supernatant (cytoplasmic extract) was immediately transferred into to a fresh pre-chilled tube and stored on ice until use or

storage. The pellet, containing nuclei, was resuspended in 50 µl ice-cold nuclear extraction reagent (NER) by vortexing at the highest setting for 15 sec and placed on ice. The sample was vortexed every 10 min for a total of 40 min. The tube was then centrifuged at 16,000 x g for 10 min. The supernatant (nuclear extract) was immediately transferred into to a fresh tube and placed on ice. Cytoplasmic and nuclear extracts were stored at -80 °C.

The lowest volume of CER I (100 µl) and II (5.5 µl) as well as NER (50 µl) solution were used in order to obtain higher protein concentrations.

2.9.3 Determination of a protein concentration

Protein concentration was measured by performing a Bradford assay, a colorimetric protein assay based on an absorbance shift of the dye Coomassie Brilliant Blue G-250 from its red form into a blue form on binding of protein. The binding of protein stabilises the blue form of the Coomassie dye, therefore the amount of the complex present in solution is a measure of the protein concentration, and can be estimated by use of an absorbance reading.

2 µl of each protein lysate was diluted in dH_2O to 40 µl and placed in a cuvette (Fisher Scientific). 40 µl of dH_2O was used as a negative control and 40 µl of 8 µg/µl BSA as a positive control. 960 µl of diluted 1:5 in dH_2O Bradford Protein Assay Reagent (BioRad) was added to each cuvette (final volume of 1 ml) and incubated for 5 min at room temperature.

The absorbance was read at OD_{595nm} using a UV spectrophotometer (Ultraspec 2000, Pharmacia Biotech). The standard curve was performed using a dilution series of BSA protein (**FIGURE 2.4**). The concentration of the lysates was determined according to the equation obtained from the standard curve, where ‘y’ is the absorbance measured and ‘x’ is the protein concentration: $y = 0.042x + 0.0245$.

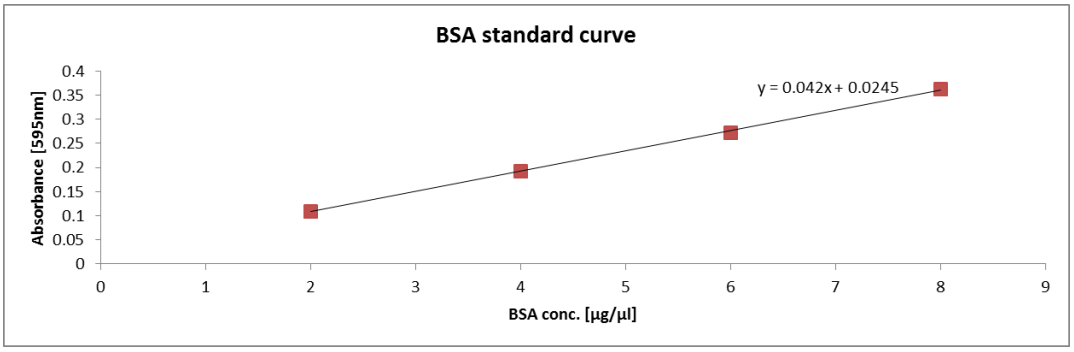


FIGURE 2.4 The standard curve prepared using: 2, 4, 6 and 8 µg/µl of BSA protein, used to determine concentration of the protein lysates.

2.9.4 Western blotting

2.9.4.1 Reagents

TABLE 2.10 Reagents used for western blot technique.

Laemmli buffer	50 mM Tris-HCl (pH 6.8), 2% SDS, 0.1% bromophenol blue, 10% glycerol, 10% β-mercaptoethanol	Sigma-Aldrich
PBS-T	PBS + 0.1% Tween 20	Sigma-Aldrich
TBS	137 mM NaCl, 2.68 mM KCl, 3.71 mM Triza Base	Sigma-Aldrich
TBS-T	TBS + 0.1% Tween 20	Sigma-Aldrich
Running buffer	2 mM Trizma-Base, 0.25 M glycine, 0.1% SDS	Sigma-Aldrich
Transfer buffer	3.9mM glycine, 4.8mM Trizma-Base, 0.0037 % SDS, 20% methanol	Sigma-Aldrich

2.9.4.2 Western blotting

Cell lysates were mixed with Laemmli buffer and heated at 100 °C for 5 min. This denatures or unfolds the protein enabling antibody access. The β-mercaptoethanol in the Laemeli buffer reduces protein disulphide bridges allowing proteins to be separated by size

when electrophoresed in running buffer containing sodium dodecyl sulphate (SDS). Reduced and denatured samples were loaded onto a pre-cast Novex® Tris-Glycine gels 4-20 % (1.5 mm, 15 wells, Novex, Life Technologies), placed in an XCell SureLock™ Mini-Cell Electrophoresis System (Invitrogen, Life Technologies). The inner chamber was filled with running buffer (**TABLE 2.10**) and approximately 200 ml running buffer added to the outer chamber. The samples ran alongside a 10-250 kDa molecular weight marker (Precision Plus Protein All Blue Standards, BioRad) at 125 V for 2.5 h at room temperature.

The Tris-Glycine gel was placed next to a nitrocellulose membrane, which had been soaked in transfer buffer, and sandwiched between a sponge and filter paper (also soaked in transfer buffer), ensuring no air bubbles were present between the gel and membrane. This sandwich was clamped in a XCell SureLock Min-Cell Blot Module (Invitrogen, Life Technologies) and placed in a XCell II™ Blot Module (Invitrogen, Life Technologies). The inner chamber was filled with transfer buffer (**TABLE 2.10**) and the outer chamber filled with cold water. The SDS used in the Laemmli buffer results in the proteins becoming negatively charged. The sandwich is positioned so that as the proteins travel towards the positively-charged electrode they become bound to the membrane. The gel was transferred at 25 V for 2 h at 4 °C.

Using the molecular weight marker as a guide, the membrane was cut at approximately 75 kilodaltons (kDa), the top part was used to detect higher molecular weight proteins (CtIP and ATR proteins, approximately 130 and 300 kDa, respectively) and the bottom part was used to detect lower molecular weight proteins (RPA32 (approximately 32 kDa), pRPA S4/S8 (approximately 32 kDa), or β-actin (approximately 42 kDa). The membranes were blocked in the relevant blocking buffer (**TABLE 2.11**) for a minimum of 1 h at room temperature and incubated with the primary antibodies overnight at 4 °C. The membranes

were washed 3 times for 5 min in the solution corresponding to the antibody used (**TABLE 2.11**). The membranes were then incubated with the secondary antibodies (**TABLE 2.11**) for 1 h at room temperature. The membranes were further washed 3 times for 5 min and either scanned by the Odyssey®Sa Infrared Imaging System (LI-COR) or developed using Bio-Rad developing solution in conjunction with X-ray film. The developing solution was diluted 1:1 with PBS or TBS, and incubated with the membrane for 5 min at room temperature under safe light conditions. The excess solution was removed and the membrane was placed into an X-ray cassette (Hypercassette, Amersham Biosciences) together with the developing film (GE Heathcare) for a set amount of time (10 seconds for β-actin, 3-5 min for the remaining proteins). The films were developed using an X-ray developer (SRX-101A, Konica Minolta).

TABLE 2.11 Antibodies and conditions used during western blot technique.

Primary antibody	Company	Blocking buffer used	Dilution	Diluted in	Secondary antibody	Dilution	Company	Diluted in	Washes performed in	Development system
Mouse anti-CtIP(14-1)	A gift from Richard Baer, Columbia University, New York	5 % powder milk in PBS	1:50	5 % powder milk in PBS-T	Goat anti-mouse / HRP	1:5000	DAKO	5 % powder milk in PBS-T	PBS-T	X-ray developer SRX-101A, Konica Minolta
Rat anti-RPA32 (4E4)	2208, Cell Signalling Technology	1:1 Odyssey® Blocking Buffer (LI-COR): PBS	1:1000	1:1 Odyssey® Blocking Buffer: PBS-T	Goat anti-rat Alexa Fluor®680	1:10,000	LI-COR	1:1 Odyssey® Blocking Buffer: PBS-T	PBS-T	Odyssey® Sa Infrared Imaging System (LI-COR).
Rabbit anti-pRPA32 (S4/S8)	A300-245A, Bethyl	5 % powder milk in TBS	1:1000	5 % powder milk in TBS-T	Goat anti-rabbit IRDye®800	1:5000	DAKO	5 % r milk in PBS-T	TBS-T	Odyssey System
Mouse anti-β-actin	ab8226, Abcam	1:1 Odyssey® Blocking Buffer: PBS-T	1:2000	1:1 Odyssey® Blocking Buffer: PBS-T	Goat anti-mouse IRDye® 680	1:10,000	LI-COR	1:1 Odyssey® Blocking Buffer: PBS-T	PBS-T	Odyssey System
Goat anti-ATR (N-19)	sc-1887, Santa Cruz	5 % powder milk in TBS	1:500	5 % powder milk in TBS-T	Donkey anti-goat / HRP	1:5000	Jackson ImmunoResearch	5 % milk in TBS-T	TBS-T	X-ray developer

2.9.5 Survival assay

2.9.5.1 Clonogenic assay- dilution assay

The dilution assay [188], a well-established variation of the clonogenic assay, can be used to measure the survival of the cells which do not readily form colonies [189], and was therefore used to examine the radiosensitivity of the MEF cell lines.

Exponentially growing MEFs in culture medium (**TABLE 2.2**) were irradiated with 0, 1, 5 and 10 Gy γ-rays (section 2.7.1.1). 200 µl of the 6.25 x 10^5 / ml concentration of irradiated or untreated cells was seeded into 2 rows (1 and 7; making it two repeats) of a 96 well plate (Appleton Woods) and diluted 1:10 in 6 series of dilutions. Cells were then incubated at 37 °C and in 5 % CO_2 for 7 days. Subsequently medium was removed and cells were stained with approximately 100 µl of crystal violet (0.5 % in ethanol) per well. The stain was removed and the plates were rinsed with tap water and left to dry.

The wells with no visible cell growth were counted and the survival fraction was determined according to the following equation, where 'c' is the number of cells plated per well, 'n' is the total number of wells and 'x' is the number of wells with no growth [190].

$$S= (-1/c)\ln(x/n)$$

The cell survival data was plotted as the logarithm of the surviving fraction versus dose.

2.9.5.2 Proliferation assay

Resazurin is a blue dye, which is reduced to the pink coloured fluorescent resorufin in cell mitochondria indicating cell proliferation. The use of resazurin has been shown to correlate well with colony formation assays in radiation studies [191]. It was used to measure cell response to ionising radiation and HU in primary and immortal CBA/H, C57BL/6 and 129Sv MEF cell lines.

Exponentially growing MEFs in culture medium (TABLE 2.2) were plated into 96 well plates (Appleton Woods), 1500 cells per well, 12 wells per cell line, per dose and either irradiated with 0, 1, 3, 5, 10 Gy γ-rays (section 2.7.1.1) and incubated at 37 °C and in 5 % CO_2 for 6 days without changing the medium or treated with 0, 0.5, 1, 1.5, 2 mM HU for 6 h and incubated at 37 °C and in 5 % CO_2 for 6 days after the exchange of the medium.

The medium was removed and resazurin (1 mg/ml, Santa Cruz) was diluted 1:100 in the culture medium. 100 µl of diluted resazurin was then added per well and incubated at 37 °C and in 5 % CO_2 for 2 h. The absorbance was measured using POLARstar Omega spectrophotometer, excitation 544 nm, emission 590 nm.

2.9.5.3 Clonogenic assay – colony formation

2.9.5.3.1 X-ray radiation

Cells were plated into T_{75} flasks at a concentration allowing exponential growth before the irradiation. Cells were irradiated in T_{75} flasks at room temperature in the culture medium with X-rays (AGO HS X-ray system; Xray tube- NDI-321 with 2 filters: copper and aluminium, thickness of each filter-1 mm) at a dose rate of 1.7 Gy per min (LET=2 keV/µm).

Clonogenic survival assays were performed to determine survival of immortal MEF cell lines following X-ray and γ-ray irradiation. Exponentially growing cells in culture medium (**TABLE 2.2**) were split into T_{75} flasks and irradiated with 30 Gy X-rays or γ-rays (section 2.7.1.1 and 2.9.5.3.1) to create a population of feeder cells, which created a suitable environment for MEFs to form colonies. Feeder cells were then seeded in triplicates for each dose, into 6 well plates (Appleton Woods), 10,000 cells per well in 2 ml of culture medium. The next day exponentially growing cells from the 3 MEF cell lines were irradiated with stated doses of X-rays, γ-rays or HU and the pre-optimised cell numbers presented in **TABLE 2.12**, **TABLE 2.13** and **TABLE 2.14** were seeded in triplicate for each dose in 2 ml of medium, into 6 well plates containing feeder cells. After irradiation, cells were incubated at 37 °C and in 5 % CO_2 for 7-8 days, until countable colonies were formed (defined as a group of 50 or more cells originating from a single cell). The medium was removed from the 6 well plates and approximately 1 ml of crystal violet stain (0.5 % in ethanol) was added to each well and incubated for 5-10 min. The stain was removed and the plates were rinsed with tap water and left to dry. The feeder cells alone were also seeded in 6 well plates (10,000 cells / well) to make sure no colonies were formed.

The plating efficiency (PE) for each cell line was calculated using the following equation.

$$PE = \frac{\text{number of colonies counted}}{\text{number of cells seeded}} \times 100$$

The PE was used to calculate a surviving fraction (SF) for each irradiated population normalised to the control

$$SF = \frac{\text{number of colonies counted after IR}}{\text{number of a cells seeded x PE}} \times 100$$

The cell survival data was plotted as the logarithm of the surviving fraction versus dose.

TABLE 2.12 Seeding densities for each dose of X-ray radiation and cell line used in the clonogenic survival assay.

Dose (Gy)	Number of cells plated		
	CBA/H	**C57BL/6**	**129Sv**
0	250	250	250
1	250	250	250
2	250	250	250
3	500	500	500
4	500	500	500

TABLE 2.13 Seeding densities for each dose of γ-ray radiation and cell line used in the clonogenic survival assay.

Dose (Gy)	Number of cells plated		
	CBA/H	**C57BL/6**	**129Sv**
0	250	250	250
1	250	250	250
5	500	500	500
10	1000	1000	1000

TABLE 2.14 Seeding densities for each dose of HU treatment and cell line used in the clonogenic survival assay.

Dose (mM)	Number of cells plated		
	CBA/H	C57BL/6	129Sv
0	250	250	250
0.5	250	250	250
2	250	250	250
5	250	250	250

2.9.6 Detection of S-phase cells using EdU

Detection of the S-phase population in exponentially growing immortal MEFs following exposure to γ-radiation was performed using the Click-iT® EdU Imaging Kit (Invitrogen). 5-ethynyl-2´-deoxyuridine (EdU) is a nucleoside analog of thymidine and is incorporated into DNA during active DNA synthesis. The detection is based on a click reaction, a copper-catalysed covalent reaction between an azide and an alkyne. The EdU contains the alkyne and the Alexa Fluor® dye contains the azide.

MEFs were plated in 2 ml of growth medium (TABLE 2.2) onto the 3 cm glass dishes, 1 x 10^5 per dish, 24 h prior to irradiation with 1 Gy γ-rays. The procedure was performed according to manufacturer's protocol. Cells were pulse labeled with EdU prior to fixation. 2 ml of pre-warmed 2x EdU solution was added to 2 ml of medium containing cells, to obtain 1x EdU solution (10 μM) and incubated at 37 °C for 20 min. This allows direct measurement of cells synthesizing DNA. Medium was subsequently removed and 1 ml of 3 % paraformaldehyde in PBS was added into each dish and incubated for 15 min at room temperature. Cells were then washed twice with 1 ml 3 % BSA in PBS. In order to permeabilise the cell membrane 500 μl 0.5% Triton® X-100 in PBS was added and incubated at room temperature for 20 min. During incubation, the Click-iT® reaction cocktail was prepared. The ingredients were added in order recommended in the manufacturer's protocol: 1x Click-iT® reaction buffer, $CuSO_4$, Alexa Fluor®647 azide, reaction buffer additive. The total volume of all the components per dish was 500 μl. Following two washes with 1 ml 3 % BSA in PBS, the reaction cocktail was added onto the cells within 15 min of preparation and incubated for 30 min at room temperature, protected from the light. After the incubation cells were washed with 1 ml 3 % BSA in PBS and co-stained with rabbit anti-53BP1 antibody (TABLE 2.9). Cells were incubated overnight at 4 °C and then washed 3 times with PBS, incubated with secondary antibody,

goat anti-rabbit, Alexa Fluor®488 for 1 h and washed a further 3 times with PBS. A drop of Vectashield® mounting medium containing DAPI was added to each dish and the cells were covered with a 25 mm diameter number 1 glass cover-slip. Cells were viewed using a confocal microscope Zeiss LSM T-PMT and a x 40 oil objective.

2.9.7 Determination of the cell cycle distribution using flow cytometry

The CBA/H, C57BL/6 and 129Sv primary and immortal MEFs were plated in growth medium (TABLE 2.2) at the concentration of 1 x 10^5 cells per T_{25} flask 48 and 24 h prior to irradiation, respectively. Cells were irradiated with 0, 1, 5 and 10 Gy γ-rays and fixed at the stated times. Cells were pulse labelled with 10 µM BrdU for 30 min prior to fixation. BrdU is incorporated into a newly synthesized DNA, as a substitution for thymidine, during the S-phase of the cell cycle.

Cells were harvested as described in section 2.2.4 and placed into 15 ml centrifuge tubes (Corning), followed by centrifugation at 250 x g for 5 min at room temperature. The medium was removed and the cell pellet (residue left in tube after discarding the supernatant) was resuspended in 100 µl PBS. The cells were fixed in 100 µl of ice cold 70 % ethanol, added drop wise while vortexing. Cells were then incubated at 4 °C for a minimum of 30 min (usually overnight). The fixative was removed by centrifugation at 250 x g for 5 min at room temperature, followed by addition of HCl (1 ml, 2 M) containing 0.1 mg/ml pepsin, and incubation for 20 min at room temperature. Samples were centrifuged at 250 x g for 5 min at room temperature, the tubes inverted in order to remove the liquid, and the pellets were resuspended in the remaining solution by vortexing. Cells were washed with 2 ml PBS and centrifuged at 350 x g for 5 min at room temperature, supernatant was removed by inverting the tubes and the pellets were resuspended in 1 ml

2% FBS in PBS, used as a blocking buffer, and spun at 350 x g for 5 min at room temperature. Supernatants were removed by inverting the tubes and the pellets were resuspended in the remaining solution by vortexing. The pellets were resuspended in 100 µl mouse anti-BrdU antibody (BD Biosciences) diluted in 2 % FBS (1:100) in PBS and incubated for 90 min at room temperature, mixing every 30 min. 1 ml 2 % FBS in PBS was added followed by centrifugation at 350 x g for 5 min at room temperature. The pellets were resuspended in 100 µl of goat anti-mouse Alexa488 secondary antibody, diluted 1:200 in 2 % FBS in PBS and incubated for 60 min at room temperature, protected from the light. Cells were washed in 1 ml PBS followed by centrifugation at 350 x g for 5 min at room temperature. Pellets were then resuspended in 500 µl PBS containing 5 µl of a propidium iodide (1 mg/ml stock) at room temperature and analysed using a Becton Dickinson FACS Sort. The percentage of cells in each cell cycle phase was calculated using Cell Quest^{TM} software (Becton Dickinson).

2.10 Statistics

All statistical analyses were performed using Prism version 5.04 (GraphPad Software). Data points are expressed as means and bars are standard errors of the mean (SEM). The survival data was analysed using Kaplan Meier analysis with a Mantel-Cox test. Analyses performed on comparing mean values of groups (Chapter 3) were either two-tailed t-tests or one-way analysis of variances (ANOVAs). *P*-values of <0.05 are considered statistically significant and denoted with a * on graphs. (*P*<0.01=**; *P*<0.001 =***; *P*<0.0001=****).

3 Association between CtIP nsSNP and the onset of radiation-induced AML

3.1 Introduction

Exposure to ionising radiation increases the risk of cancer, including acute myeloid leukemia (AML), the most common form of myeloid leukaemia [154]. Using a surrogate assay of susceptibility to radiation-induced AML (rAML), based on chromosomal radiosensitivity, a group at Public Heath England led by Dr Christophe Badie, identified the CtIP gene as a strong candidate for susceptibility to rAML [2]. CtIP is essential for embryonic development and its heterozygous inactivation leads to early development of tumours [22, 23].

3.1.1 Mouse models

Three mouse models were studied in this project: CBA/H, C57BL/6 and 129Sv. The CBA/H mouse model of rAML has been extensively used for decades [175]. It serves as a good model for human rAML as the incidence of *de novo* AML in control CBA/H is very low (0.1 %) [176]. The key feature of the CBA/H mouse strain is the deletion of one copy of chromosome 2 following exposure to X-ray radiation [175]. The deleted region includes the transcription factor gene PU.1/Sfpil [179], which is essential for the development of myeloid and lymphoid cell types. A high proportion of AML mice with a chromosome 2 deletion carry highly specific point mutations in the DNA-binding domain of the

remaining PU.1 allele [192]. Mutations in PU.1 gene, lead to disruption of its function and this has been described in some cases of human AML [193].

The C57BL/6 mouse strain is described as being resistant to rAML [176]. It is, however, susceptible to radiation-induced thymic lymphoma [176].

The sensitivity of the 129Sv strain to rAML, as well as the presence of chromosome 2 aberrations is as yet unknown. There is low overall tumour incidence in the 129Sv strain [180, 181], apart from the 129Sv teratoma sub-strain, which has high incidence of spontaneous testicular teratomas (1-3 % in 129Sv parental substrains; 30 % in teratoma substrains) [194]. The 129Sv sub-strain used in this project is 129S2/SvHsd from Harlan Laboratories (UK) and is genetically different to 129Sv substrain bred in The Jackson Laboratory (USA). 129S2/SvHsd is referred to as 129Sv in the text.

The historical median lethal dose (LD_{50}) data, where 129S/J mice (129Sv strain bred in The Jackson Laboratory) were exposed daily to 1 Gy X-rays until death, showed that 129S/J strain is the most radio-resistant. CBA/J mice (CBA strain bred in the Jackson Laboratory, genetically identical to CBA/H bred in Harwell, UK) were shown to be the most radio-sensitive with C57BL/6 falling in the middle of this radio-resistance range, post 1 Gy X-rays daily exposure [195, 196]. Apart from this historical data referring to 129S/J as radio-resistant, no other information is available in the literature on 129Sv mice exposed to radiation.

3.1.2 Single nucleotide polymorphism in CtIP gene of 129Sv strain

Single nucleotide polymorphism (SNP) is a substitution of one nucleotide (adenine [A], thymine [T], cytosine [C] or guanine [G]) for another in the gene sequence [197]. SNPs may be present within coding and non-coding regions of the genes. SNPs in the coding region are divided into two types, synonymous, where the amino acid sequence does not change and non-synonymous SNPs (nsSNPs) [198], which are further divided into missense and nonsense mutations. The missense mutation is a sequence variant that changes one base, resulting in a different amino acid and possibly protein malfunction [199]. The substitution of one amino acid for another generally results in conformational changes which lead to a significant alteration in thermodynamic stability of the resulting protein [200]. Nonsense mutations occur when the new sequence results in a premature stop codon and therefore a truncated, often non-functional, protein (definition from the Ensembl genome browser). nsSNPs within a particular gene can lead to early development of cancer [201-203] or neurodegenerative disorders, like Alzheimer's or Parkinson's disease [204, 205].

According to the Ensembl genome browser, at the time of initial investigation there were seven nsSNPs present within the mouse CtIP gene: G7S, A16V, H338Y, Q418P, A498T and A882V (**TABLE 3.2** provides detailed description). The Mouse Genome Informatics (MGI) website provides information about polymorphisms in various strains of mice (MGI website details can be found in section 2.1.1). Five out of the seven nsSNPs, were found within the CtIP gene of 129S1/SvImJ, one of the 129Sv sub-strains bred in The Jackson Laboratory. The presence of CtIP nsSNPs in 129S2/SvHsd (the strain from Harlan Laboratories used in this project) was, however, unknown.

3.1.3 Prediction of an effect on a protein caused by an amino acid substitution

Various algorithms for the automatic prediction of the effects of amino acid substitutions on protein function have been developed in recent years and have improved identification of different mutations, including those in cancer genomes [199, 206].

The Sorting Intolerant from Tolerant (SIFT) algorithm [207] is a well-recognised tool for prediction of disease-causing nsSNPs by analysing disruption of conserved sequences [198, 199]. The SIFT score ranges from 0 to 1. If the score is between 0 and 0.05 the amino acid substitution is predicted to be damaging [207]. Protein ANalysis THrough Evolutionary Relationships (PANTHER) is another algorithm which is based on an alignment of evolutionarily related proteins [208]. Single Nucleotide Polymorphism Annotation Platform (SNAP) is a server designed to analyse single genes and relationships between genes based on SNPs in the genome [209]. Predictor of human Deleterious Single Nucleotide Polymorphism (PhD-SNP) is a Support Vector Machines (SVMs) based method trained to predict disease-associated nsSNPs using sequence information [205]. A score above 0.5 by Panther, PhD-SNP and SNAP predicts a mutation to be disease-causing.

Recently a meta-predictor of SNPs (Meta-SNP) has been developed, which identifies disease-causing nsSNPs by coupling predictions from Panther, PhD-SNP, SIFT and SNAP [210]. Meta-SNP takes the output of the four predictors and gives the probability that a given nsSNP is disease-related where the score is higher than 0.5.

3.2 Aim

The aim of this chapter is to evaluate the disease-causing potential of nsSNPs present in the CtIP mouse gene using the various algorithms described, to characterise a mouse strain carrying a missense variant within this gene and examine the effect of this variant on rAML development and survival, following exposure to an acute dose of 3 Gy of X-rays.

3.3 Results

3.3.1 Evaluation of disease-causing potential of nsSNP within CtIP gene.

The nsSNPs present within the mouse CtIP gene (G7S, A16V, H338Y, 1366T, Q418P, A498T, A882V) were initially checked by five algorithms (Panther, PhD-SNP, SIFT, SNAP) for disease prediction, and four (H338Y, Q418P, A498T, A882V) were predicted as disease-causing. This result was subsequently reinforced by the meta-prediction algorithm, Meta-SNP (TABLE 3.1). Of these nsSNPs, the Q418P nsSNP was predicted by two out of the five algorithms as disease-causing. In addition, it had a score very close to 0.5, the lower limit for prediction of disease-causing, obtained with the PhD-SNP and Meta-SNP algorithms. Overall, these predictions indicate that Q418P is the most likely disease-causing missense variant of the seven CtIP nsSNPs assessed.

TABLE 3.1 The predictions of disease-causing status of nsSNPs by five algorithms: Panther, PhD-SNP, SIFT, SNAP and Meta-SNP using Meta-predictor website. Dis- disease-causing; N/A- not available; Panther, PhD-SNP, SNAP, Meta-SNP: a score >0.5 predicts a mutation to be disease-causing; SIFT: score < 0.05 predicts a mutation to be disease-causing; orange colour- almost disease-causing.

	ALGORITHMS				
nsSNP	PANTHER	PhD-SNP	SIFT	SNAP	Meta-SNP
G7S	0.094	0.012	1.000	0.115	0.091
A16V	0.212	0.052	0.080	0.310	0.043
H388Y	0.339	0.238	0.100	*Dis* 0.530	0.126
I366T	0.102	0.091	1.000	0.215	0.045
Q418P	0.363	0.490	*Dis* 0.000	*Dis* 0.730	0.496
A498T	N/A	0.258	*Dis* 0.000	*Dis* 0.570	0.129
A882V	0.169	0.092	*Dis* 0.000	*Dis* 0.665	0.122

3.3.2 Identification of the presence of nsSNP in CtIP gene in the mouse strains CBA/H, C57BL/6 and 129Sv

The CBA/H, C57BL/6, and 129Sv strains of mice were tested for the presence of H338Y, Q418P, A498T, A882, potentially disease-causing CtIP nsSNPs. DNA from the spleen of the CBA/H, C57BL/6 and 129Sv mouse strains was sequenced (Appendix B) and only the Q418P nsSNP was found in the 129Sv mouse strain (**TABLE 3.2**). It was therefore decided to study the potential impact of Q418P on cancer induction in vivo, focusing on rAML (section 3.3.3). The Q418P nsSNP results in a change from glutamine (CAG) to proline (CCG) (**FIGURE 3.1**). This amino-acid change results in an acyclic amino acid being transformed into a cyclic one and this has been shown to lead to conformational changes in proteins, which can result in a disease [200, 211].

TABLE 3.2 The presence of: H338Y, Q418P, A498T and A882V CtIP nsSNPs in spleen DNA of mouse strains CBA/H, C57BL/6, and 129Sv. '-'sequencing not successful; 'x' SNP not present; '✓' SNP present.

nsSNP	Amino acids	Allele	Exon	Mouse strains		
				CBA/H	C57BL/6	129Sv
H388Y	Histidine/Tyrosine	C/T	11	x	x	x
Q418P	Glutamine/Proline	A/C	11	x	x	✓ **SNP**
A498T	Alanine/Threonine	G/A	11	x	x	x
A882V	Alanine/Valine	C/T	19	x	x	-

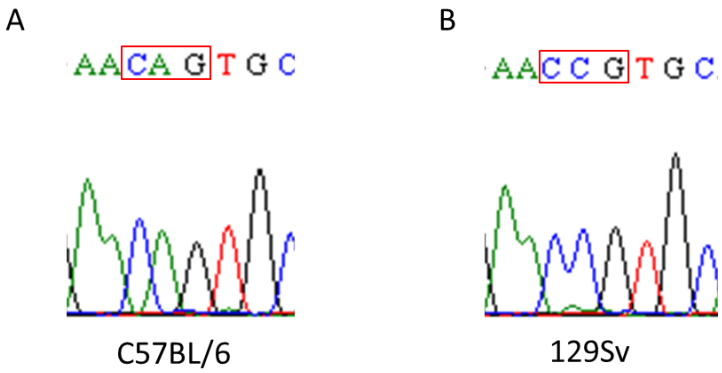


FIGURE 3.1 The sequence of DNA from C57BL/6 (A) and 129Sv (B) mice without (A) or with (B) a Q418P nsSNP, respectively. Substitution of alanine (A) by cytosine (C) results in amino acid change from glutamine (C**A**G) to proline (C**C**G).

3.3.3 The survival rate of CBA/H, C57/BL6 and 129Sv mice post-irradiation with 3Gy X-rays

Differences in the survival rates of CBA/H, C57BL/6 and 129Sv mouse strains (**TABLE 3.3**) were investigated after exposure to whole body, single acute doses of 3 Gy X-rays at the age of 12-15 weeks. The irradiation and maintenance of the 129Sv mouse strain was undertaken during the time frame of this project. The survival data for CBA/H and C57BL/6 mice, as well as CBA/H AML data, were produced by Carl Olme during his doctoral project (Dr Carl Olme '*Role and functional consequences of PU.1 transcriptional factor loss and mutations in a mouse model of radiation-induced acute myeloid leukaemia'* doctoral thesis, Imperial College London, 2011). The mean life span of non-irradiated C57BL/6 was obtained from the study performed by The Jackson Laboratory.

According to institutional regulations, animals were euthanised for humane reasons as soon as they developed an untreatable disease (section 2.1.3). The survival of irradiated CBA/H and 129Sv mice is compared with non-irradiated controls in **FIGURE 3.2**. This shows that irradiated CBA/H and 129Sv mice had to be euthanised sooner in comparison to their non-irradiated controls, indicating that radiation shortens their life span. In contrast, irradiated C57BL/6 mice showed only slightly shorter mean life span when compared to control mice (**TABLE 3.3**). **FIGURE 3.3** compares the survival of CBA/H, C57BL/6 and 129Sv mouse strains exposed to radiation. CBA/H mice needed to be sacrificed at earlier times post-irradiation when compared to C57BL/6, consistent with published reports showing that the CBA strain is radio-sensitive and the C57BL/6 radio-resistant [196]. 129Sv mice however are significantly more sensitive to radiation than CBA/H mice, what is in contrast to results from 50 years ago showing that 129S/J mice are radio-resistant [196]. As previously described, the 129S/J strain is genetically different to the 129Sv strain used in this study. Additionally, 129Sv mice were exposed to a single

dose of 3 Gy X-rays whereas in the previous study 129S/J mice were irradiated daily with 1 Gy X-rays until death [196].

When the mean life span of the three mouse stains exposed to radiation was normalised to the mean life span of corresponding controls, CBA/H and 129Sv showed similar decrease in survival post-radiation (25 and 30 %, respectively) (TABLE 3.3). The radiosensitivity of these strains to X-rays is similar, whereas the mean life span of C57BL/6, the radio-resistant strain, decreases only by 1 % when irradiated. However, the number of irradiated C57BL/6 mice was very low (10), therefore no definite conclusion can be made.

TABLE 3.3 The number of CBA/H, C57BL/6 and 129Sv control mice and 3 Gy X-ray irradiated used in this study and their mean life span; * data taken from The Jackson Laboratory (the mean of study 1 and 2 for male C57BL/6)

Strain	Controls (No. of mice)	Mean life span controls (days)	3 Gy X-rays (No of mice)	Mean life span 3 Gy X-rays (days)	Mean life span 3 Gy X-rays normalised to controls (%)
CBA/H	12	778.5	94	582.5	75
C57BL/6	226*	789*	10	778.5	99
129Sv	20	635	78	447	70

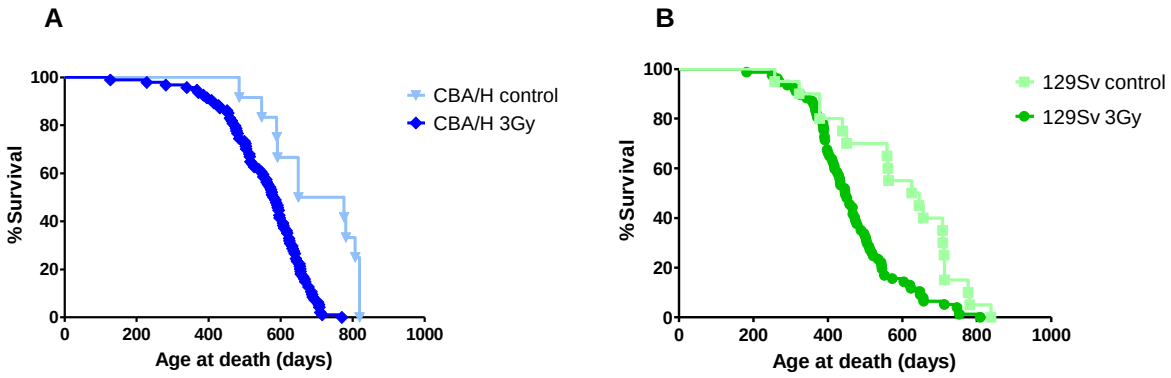


FIGURE 3.2 The survival percentage of controls versus 3 Gy X-ray irradiated mouse strains: CBA/H (A), and 129Sv (B). The differences between irradiated mice and controls are statistically significant, A: p value < 0.0001, B: p value < 0.01.

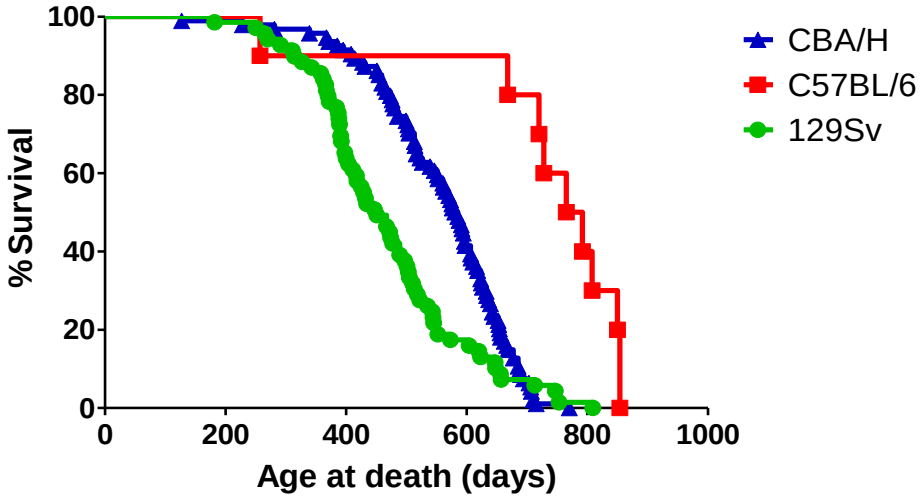


FIGURE 3.3 The comparison of CBA/H, C57BL/6* and 129Sv mouse strains survival post 3 Gy X-ray radiation. The difference between the strains is statistically significant: p value < 0.0001. * data taken from The Jackson Laboratory

3.3.4 Post-radiation development of AML

3.3.4.1 The diagnosis of rAML in 129Sv stain

As previously described in the introduction of this chapter, CBA/H mice are known to be sensitive to rAML in contrast to C57BL/6 mice, which have been shown to be resistant. Identification of a possible link between CtIP and rAML directed the investigation of rAML in the 129Sv mouse strain, carrying the Q418P nsSNP within the CtIP gene.

129Sv mice irradiated with 3 Gy X-rays, as an optimal dose for leukaemia incidence [212], were observed daily for signs of AML (section 2.1.3). Animals were sacrificed following identification of outward physical signs of haematological malignancy and a post mortem was carried out. This included taking a sample of blood to generate a blood smear to check for the presence of immature forms of leukocytes as well as performing a white blood cell count and neutrophil count (section 2.1.3; work done by Dr Rosemary Finnon (PHE)). **TABLE 3.4** shows the number of neutrophils and total white blood cells as well as weight of the spleen in 129Sv potential rAML mice. The total white blood cell count was elevated in each of the nine rAML mice in comparison to the mean white blood cell count of 129Sv controls. An enlarged spleen and lower level of neutrophils (apart from AN 39) was also observed in 129Sv rAML mice when compared with the mean size of the spleen and the percentage of neutrophils present in the controls.

TABLE 3.4 A sample of blood was taken from each animal (3 Gy X-rays irradiated as well as controls) shortly after they were sacrificed. Total white blood cell count as well as count of neutrophils was performed; the weight of spleen was also assessed. Described are 9 potential rAML cases: AN 9, AN 13, AN 14, AN 29, AN 32, AN 36, AN 39, AN 43, AN 59, and controls (the mean was taken from 20 control mice).

Characteristics	129Sv mice									
	AN 9	AN 13	AN 14	AN 29	AN 32	AN 36	AN 39	AN 43	AN 59	Controls (mean)
Total white blood cell count (x 10^6/ml)	19.4	5.6	13.8	8.8	4.8	6.2	7.6	13.2	35	4.7 ± 2.2
Spleen weight (g)	0.415	0.34	1.067	0.649	0.423	0.617	0.685	0.129	1.25	0.18±0.16
Neutrophils count (%)	8.2	0	21.5	0	2.5	0	30	5.7	0	30± 1.8

The presence of immature and functionally abnormal hematopoietic cells/blasts was also examined by staining spleen cells with antibodies recommended by the hematopathology subcommittee of the Mouse Models of Human Cancers Consortium [152]. Seven out of nine 129Sv mice with potential rAML were analysed for the presence of blasts, as the cells from AN 29 and AN 36 were not available. Data obtained by flow cytometry showed a notable difference between normal and leukaemic samples. The region with high side scatter (region 3 [R3], pink) representing immature forms/blast cells was present in leukaemic samples from 129Sv irradiated mice but not in the controls (**FIGURE 3.4**). It has been reported that 20 % or more of immature forms/blasts present in a sample is one defining feature of leukaemia [152]. This criterion was met in all cases apart from one (AN 14) (**TABLE 3.5**). The analysis of surface markers was performed on the gated region with immature forms/blasts from spleen cells of 129Sv potential rAML samples (**TABLE 3.5**), but not the control samples as there were hardly any blasts present in the R3 region.

All the tested surface markers for immature myeloid or lymphoid cells were detected in all of the potential rAML cases. A high level of Gr-1 is characteristic for cells with a

granulocytic phenotype [213] and high Mac-1 expression levels indicates a more monocytic cell component [214]. Together, high levels of Gr-1 and Mac-1 indicate granulocytic leukaemia, whereas low or negative Gr-1 and positive Mac-1 are classified as monocytic leukaemia [152]. All 129Sv rAML mice showed positivity for both markers. However, AN 59 exhibited a very low percentage of Gr-1 and Mac-1 markers. The low expression may indicate that immature forms/blasts were less differentiated in this particular case, compared to other samples. CD31 and Ly6C, markers for myeloid progenitors [157], were also expressed in all cases with Ly6C showing very highly expression levels (apart from AN 14). When expressed together, Sca-1 and c-Kit are markers for haematopoietic stem cells [158] whereas a high level of c-Kit alone usually indicates the presence of myeloid progenitors [159]. The expression of Sca-1 and c-Kit did not differ greatly within each sample, with the exception to AN 59 which showed very high expression of c-Kit and very low expression of Sca-1. These expression levels indicate the presence of haematopoietic stem cells in the spleens of all the potential rAML cases. T- and B-cells markers such as CD3 [160] and B220 [161], respectively are very low or not expressed in non-lymphoid leukaemias [152]. All of the cases examined showed low expression of T- and B-cell markers apart from AN 14, which exhibited co-expression of B220 along with both Gr-1 and Mac-1, possibly indicating the presence of biphenotypic leukaemia, also known as a non-lymphoid leukaemia [152].

Taken together, the causes of death for the 129Sv stain varied (Appendix B); however there were indications of increased incidence of rAML, and these cases were examined in greater detail. Nine 129Sv irradiated mice showed signs of rAML based on elevated white blood cell counts, increased spleen weight and neutropenia, when compared to non-irradiated 129Sv control mice. Six out of the nine cases analysed by flow cytometry exhibited a high percentage of immature forms/blasts compared to control samples. Within

this population, markers for myeloid progenitors and haematopoietic stem cells were also strongly expressed. Three out of the nine potential rAML cases were confirmed by a mouse pathologist (Professor Cheryl Scudamore, MRC, Harwell). The spleens from the six rAML mice were not available to the pathologist as they were frozen in RNA later solution for future DNA/RNA extraction.

Based on the criteria described above, these findings quite clearly indicate presence of rAML in three out of nine 129Sv presented cases, leaving six as probable rAMLs.

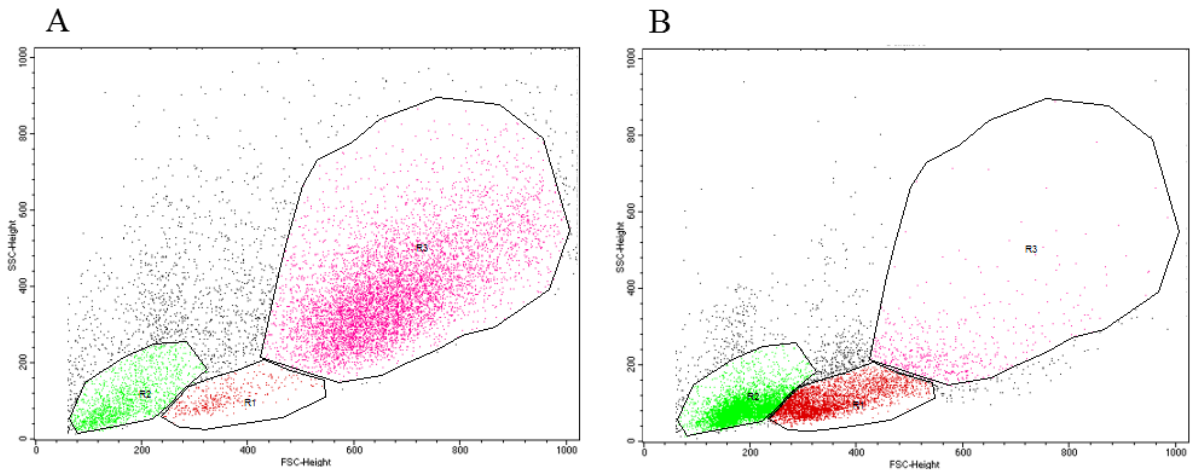


FIGURE 3.4 Representative FACS images of the spleen cells from 129Sv 3 Gy X-ray irradiated mouse diagnosed with rAML (AN 59) (A), and cells from 129Sv non-irradiated control (B); R3: immature forms/blast cell population equals 68.6 % in rAML sample (A) and 5 % in the control (B); R1 and R2 are splenocyte and lymphocyte cells.

TABLE 3.5 Spleen cells from seven 129Sv potential AML mice stained with antibodies for immature forms/blasts as well as with isotope control to eliminate non-specific binding; ND: not done.

Immature forms/blasts (%)	**129Sv mice**						
	AN 9	AN 13	AN 14	AN 32	AN 39	AN 43	AN 59
Gr-1	62.6	66.6	23.02	54.7	62.7	59.22	0.41
Mac-1	85.2	82.6	20.62	64.6	85.2	77.37	1.83
Ly6c	91.6	87.3	30.84	80.52	96.7	88.77	99.7
c-Kit	12.2	18.8	44.65	11.2	16.02	27.9	99.8
Sca-1	17.6	30.7	24.92	28.4	23.14	24.35	2.20
CD31	33.7	51.6	19.86	27.6	33.44	ND	98.6
B220	17.4	21.4	64.02	29.3	10.9	17.3	0.39
CD3	1.14	2.34	10.61	3.05	1.35	2.17	0.22
Isotope control (%)	**1.84**	**1.76**	**6.37**	**2.38**	**1.26**	**2.35**	**0.15**
Total population of blasts (%)	35	27.8	15	21	33.4	23	68.6

3.3.4.2 The rate of AML in CBA/H, C57/BL6 and 129Sv mice post 3 Gy X-rays radiation

Based on the diagnosis described in section 2.1.3, after exposure to 3 Gy X-rays, 28, 11 and 0 percent of CBA/H, 129Sv and C57/BL6 mice respectively, were diagnosed with rAML (**FIGURE 3.5**). Nine out of 78 (11 %) irradiated 129Sv mice were diagnosed with rAML based on observation, FACS data, white blood cell and neutrophil count and blood smear data. Three out of the nine cases were confirmed by a mouse pathologist. AML was not observed in any of the control mice from the three different strains. Comparison of rAML incidence between irradiated strains shows that 129Sv mice exhibit higher incidence of rAML than C57BL/6 (rAML resistant strain) and lower than CBA/H (rAML sensitive strain). **FIGURE 3.6** shows the development of rAML in 129Sv and CBA/H mice. The 129Sv strain started to develop rAML earlier than the CBA/H strain, around 370 and 450 days post-irradiation, respectively. 129Sv mice diagnosed with rAML post 3 Gy X-ray radiation needed to be sacrificed earlier than the rest of 129Sv irradiated non-rAML mice but only at a later stage (>450 days). The life span of CBA/H mice with rAML was significantly shorter when compared to irradiated mice without rAML.

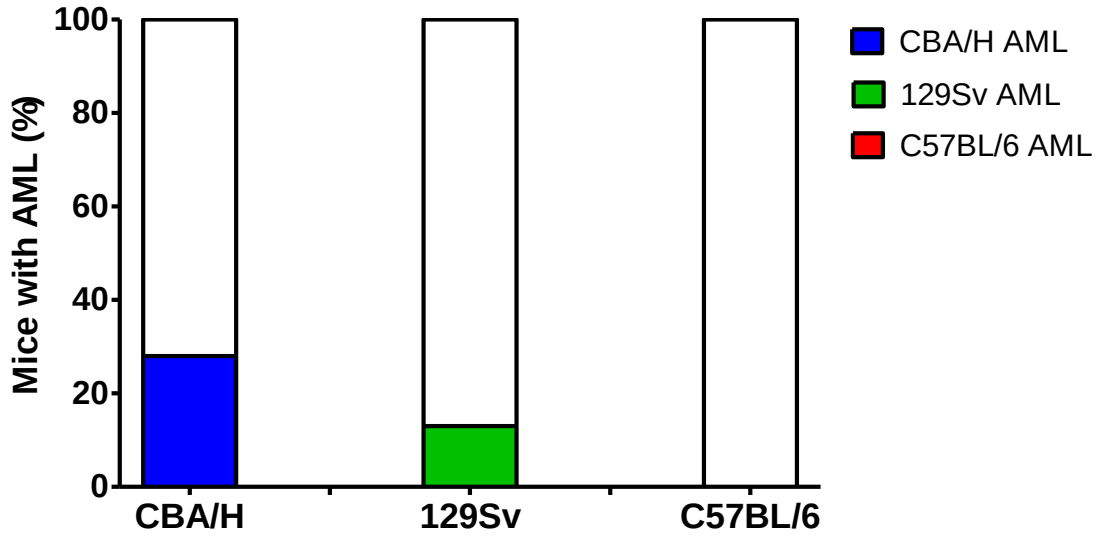


FIGURE 3.5 The percentage of rAML cases in CBA/H (28 %), 129Sv (11 %) and C57BL/6 (0 %) mouse strains post 3 Gy X-rays; AML was not observed in any of the control mice.

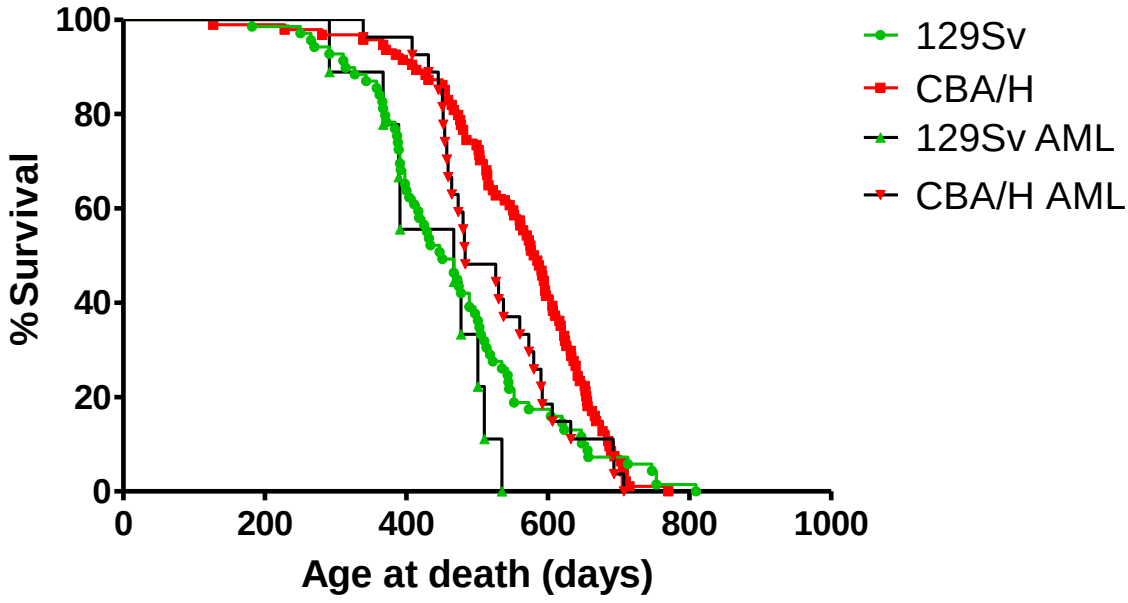


FIGURE 3.6 Comparison of survival rate in the whole population after acute 3 Gy X-ray irradiation of CBA/H and 129Sv mice and those irradiated mice diagnosed with rAML. CBA/H data has been taken from Carl Olme's doctoral thesis.

3.3.5 Confirmation of the Q418P nsSNP in CtIP gene and evaluation of a potential nsSNP in the PU.1 gene of 129Sv rAMLs

A mutation in the PU.1 gene reported in rAML mice (including the CBA/H mouse strain) affects amino acid arginine in position 235 of the protein, resulting in cysteine (R235C), serine (R235S) or histidine (R235H) [179, 192]. The DNA from 129Sv mice diagnosed with rAML was sequenced to check for a potential nsSNP present in position 235 of the PU.1 gene, as well as to confirm the presence of Q418P nsSNP within the CtIP gene (section 3.3.2). The presence of the Q418P nsSNP was confirmed in the CtIP gene, however, no mutations were found within the PU.1 gene.

3.3.6 Post-irradiation expression of the CtIP gene in the different CBA/H, C57BL/6 and 129Sv mouse strain tissues

In order to check whether low LET radiation changes the expression level of CtIP, rAML sensitive and resistant mouse strains (CBA/H and C57BL/6, respectively) were exposed to 3 Gy X-ray radiation. CtIP transcript levels were measured 2 h, 24 h and 1 month post-irradiation in blood, brain, bone marrow, spleen and thymus. CtIP was expressed in all non-irradiated tissues tested. The results were normalised to the housekeeping gene Hprt1 and to non-irradiated controls (the mean of three control mice). A small upregulation of CtIP expression was visible, mainly 2 h post-irradiation, in all tested tissues from both mouse strains (**FIGURE 3.7**). Bone marrow and spleen are the main tissues for haematopoietic stem cell development and maturation, and therefore are the most relevant for the development of AML [152]. 129Sv mice were also exposed to 3 Gy X-rays and CtIP transcript levels were measured 2 h, 24 h and 1 month post treatment in spleen and bone marrow tissues. Upregulation of CtIP was observed 2 h post-irradiation (**FIGURE 3.8**), which was consistent with the results obtained from the spleen and bone marrow of the CBA/H and C57BL/6 mouse strains (**FIGURE 3.7**).

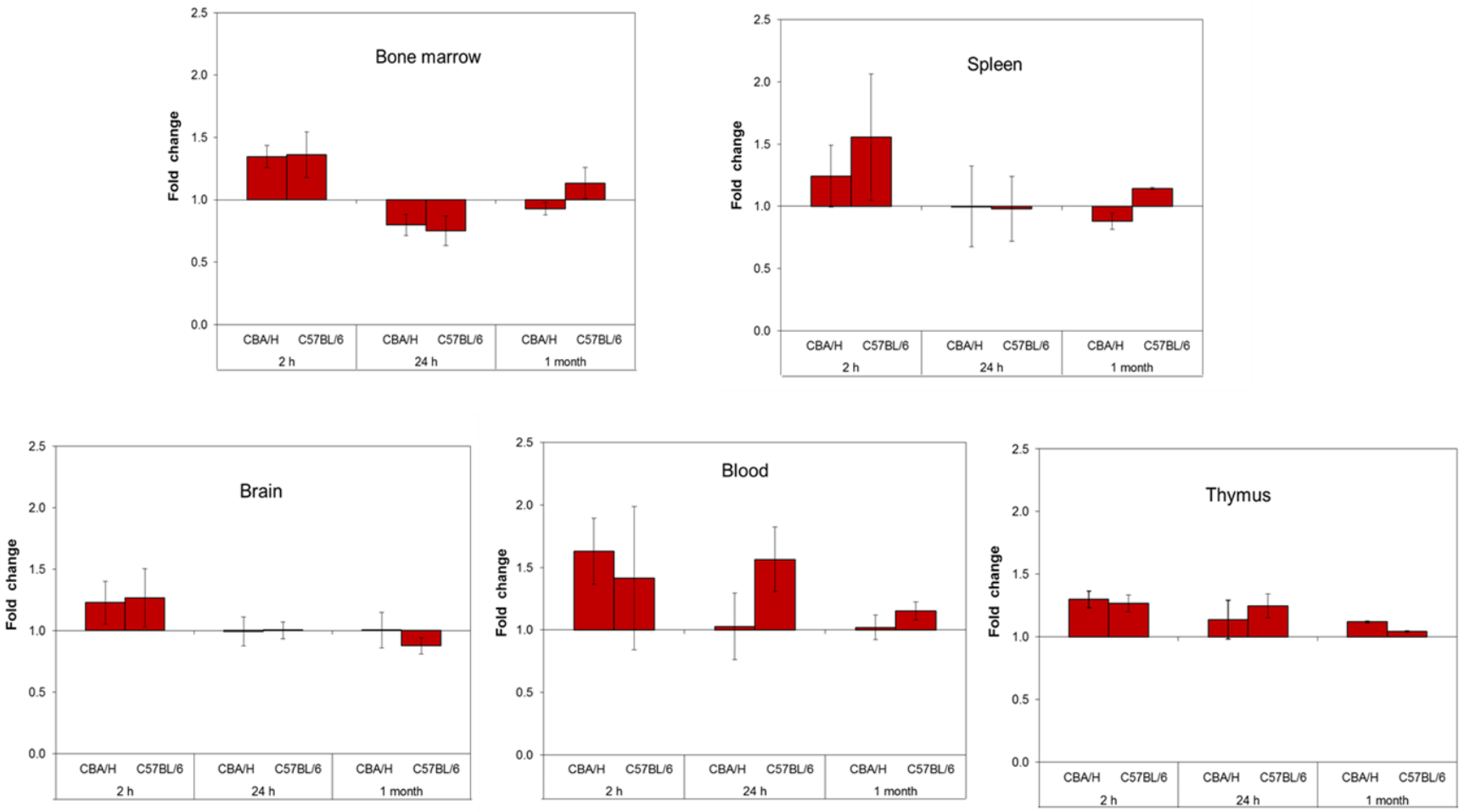


FIGURE 3.7 The expression of CtIP gene in CBA/H and C57BL/6 mouse tissues irradiated with 3 Gy X-rays. CtIP transcriptional levels were measured 2 h, 24 h and 1 month post-irradiation in mouse tissues. The gene of interest copy numbers were divided by Hprt1 copy numbers in irradiated as well as non- irradiated control mice. The results from irradiated mice were then divided by the results from control mice; number of mice per time point= 3; Error bars are SEM.

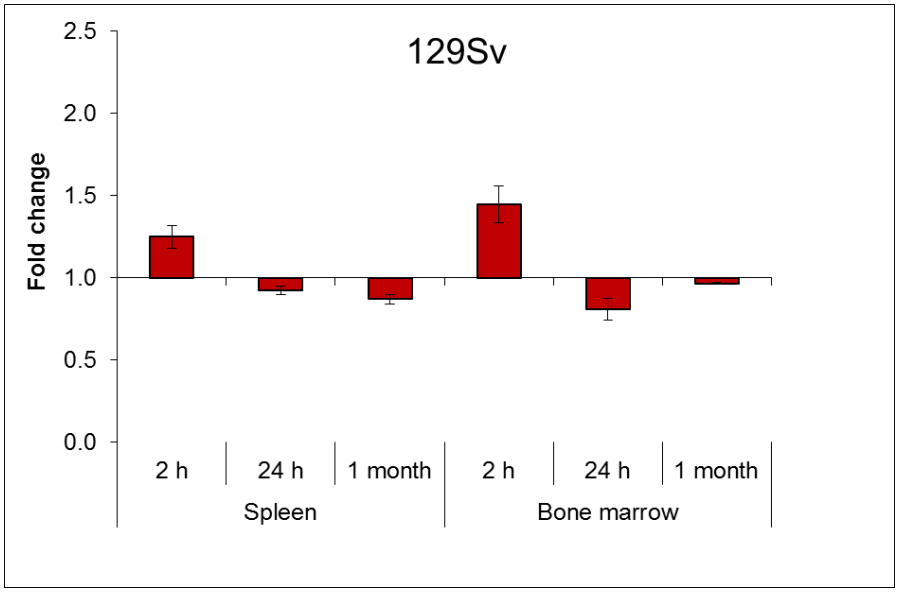


FIGURE 3.8 The expression of CtIP gene in bone marrow and spleen of 129Sv mouse strain irradiated with 3 Gy X-rays. CtIP transcriptional levels were measured 2 h, 24 h and 1 month post-irradiation in mouse tissues. The gene of interest copy numbers were divided by Hprt1 copy numbers in irradiated as well as non- irradiated control mice. The results from irradiated mice were then divided by the results from control mice; number of mice per time point= 3; Error bars are SEM.

3.3.7 Expression of CtIP and PU.1 gene in 129Sv mice diagnosed with rAML

In order to examine the differences between 129Sv mice which were diagnosed with AML post-irradiation and their controls, the CtIP and PU.1 transcript levels were measured in splenic tissue of six 129Sv rAML mice. The results were normalised to the housekeeping gene Hprt1 and to the non-irradiated control. Upregulation of CtIP gene expression was not found in any of the cases (**FIGURE 3.9A**). In contrast, upregulation of PU.1 was visible in all six rAML samples compared to non-irradiated controls (**FIGURE 3.9B**). It has been shown that rAMLs without a PU.1 point mutation exhibit downregulation of PU.1 in splenic tissue [215].The R235C, R235S or R235H nsSNPs were not found in the PU.1 gene of 129Sv rAML mice, as described in section 3.3.5. However, upregulation was detected which may indicate that gene expression levels of PU.1 in the spleen of rAML mice do not correlate with the presence/absence of the nsSNPs.

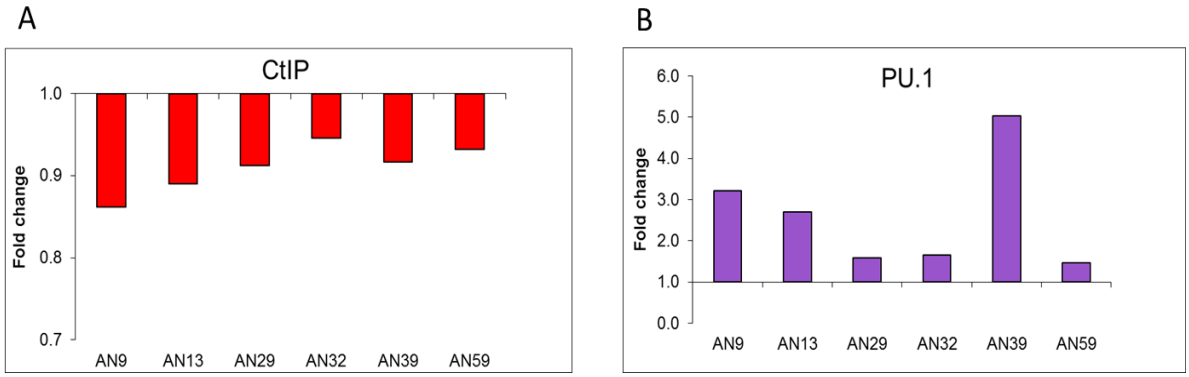


FIGURE 3.9 The expression of CtIP (A) and PU.1 (B) gene in the spleen of 129Sv rAML mice. The gene of interest copy numbers were divided by Hprt1 copy numbers in irradiated as well as non- irradiated control mice. The results from irradiated mice were then divided by the results from control mice; n=1.

3.4 Discussion

The Q418P nsSNP, identified by several algorithms as disease-causing, was detected in the CtIP gene of 129Sv mouse. As CtIP is a crucial gene in embryonic development and has been identified as a strong candidate for rAML susceptibility, a nsSNP which affects its protein function could possibly lead to tumour development. After a single 3 Gy X-ray exposure, the mean life span of 129Sv mice decreased by 30 % in comparison to the life span of non-irradiated mice. This decrease is slightly more than the decrease in life span of CBA/H (25 %), the mouse strain sensitive to rAML. The C57BL/6 mice, which are rAML resistant, did not show any decrease in viability post-irradiation. Nine out of 78 (11%) irradiated 129Sv mice were diagnosed with possible rAML. This level is lower than that for irradiated CBA/H (28 %) but greater than seen with C57BL/6 (0%). A small upregulation of CtIP gene expression levels was observed in CBA/H and C57BL/6 mice mainly 2 h post-irradiation in bone marrow, spleen, brain, blood, thymus. This upregulation was also seen in the bone marrow and spleen of 129Sv mice. However, upregulation of CtIP was not seen in the spleen of mice diagnosed with rAML. This could be due to the fact that the CtIP expression was checked several months after exposure of mice to X-ray radiation (depending on the time of death). In contrast, CtIP expression was measured 2 h post-irradiation in the spleen of irradiated non-AML 129Sv mice (**FIGURE 3.8**)

The results suggest that the Q418P nsSNP of CtIP, found only in the 129Sv mouse strain, may influence early onset of radiation-induced carcinogenesis, including rAML, upon exposure to X-ray radiation. This could be due to an impairment of the role of CtIP in DNA double stand break repair, particularly by HR post-irradiation. Unrepaired or misrepaired double stand breaks can lead to chromosomal aberrations and possibly genomic instability, which as a consequence could increase cancer risk [50].

4 The influence of the Q418P nsSNP on the role of CtIP in the repair of radiation-induced DSBs

4.1 Introduction

The results presented in Chapter 3 showed that the mouse strain 129Sv containing a nsSNP within the CtIP gene is radiosensitive and develops early onset of cancer, including rAML, in contrast to the radioresistant C57BL/6 strain. This Chapter investigates the potential role of CtIP, carrying the Q418P nsSNP, in the repair of radiation-induced DSBs. CtIP is known to be involved in short range resection of DSB ends resulting in ssDNA, and in part controlling DNA repair pathway choice [51, 216]. Such DSB resection is required in HR in order to generate ssDNA which is necessary for homology searching and strand invasion [63]. It has been shown that CtIP is required for DSB resection, and therefore for HR [22, 61]. However it has also been reported that CtIP is involved in DSB repair in G1 phase to resect just a few nucleotides at DSB ends required for MMEJ [8, 62]. RPA is a key protein involved in HR of DSBs. RPA binds ssDNA following CtIP mediated resection [61]. RPA32, one of three RPA subunits, is differentially phosphorylated during the cell cycle and in response to DNA damage [217]. Hyperphosphorylation of RPA32 at serine 4 and serine 8 (S4, S8) has been used as a marker for activation of the DNA damage response [71]. The S4 and S8 sites have been reported to be mainly phosphorylated by DNA-PK *in vitro* and *in vivo* [71, 72]. Active RPA recruits ATR checkpoint protein which in response phosphorylates Chk1 to promote checkpoint activation [10]. Inactivation of

ATR or Chk1 leads to fork collapse and high levels of DSBs [218, 219], which can cause genomic aberrations [220].

It has been reported that CtIP depletion impairs RPA hyperphosphorylation and ATR activation [61, 221]. Rad51 mediated DNA strand invasion occurs post DSB resection and is therefore CtIP dependent and required to initiate HR [70]. CtIP also plays a role in DNA-damage induced cell cycle checkpoint control. The interaction of CtIP with RB is essential for G1 to S phase progression [22] and its interaction with the tumour suppressor BRCA1 is required for the G2/M transition [68].

4.2 Aim

The aim of this chapter is to investigate whether the Q418P nsSNP identified within the CtIP gene may impair repair of radiation-induced DSBs, and more specifically whether it impairs Rad51 and RPA binding to the damage sites and therefore their activation, which is crucial for HR progression.

4.3 Results

4.3.1 The influence of oxidative stress on the growth of CBA/H, C57BL/6 and 129Sv primary and immortal MEFs

It has been previously demonstrated that primary MEFs grow better in low oxygen to minimise the harmful effects of oxidative stress, such as chromosomal breaks [222]. Therefore the experiments were initially conducted to compare cell growth under low (3 %) and normal (21 %) oxygen tensions. Primary MEF cell-lines, established from the mouse strains CBA/H, C57BL/6 and 129Sv (section 2.2.2) were grown for up to 12 days under different oxygen conditions and cell numbers were counted at stated time points. No major differences in growth rate between the cell lines were observed, although proliferation rates of the three cells lines were strongly influenced by the oxygen tension (FIGURE 4.1). Primary MEFs were unable to grow under high oxidative stress conditions, which is consistent with previous reports [222]. As a consequence primary MEFs were maintained in low (3 %) oxygen incubator throughout the project.

Following immortalisation of the three MEF cell lines, their growth rates were re-examined under the different oxygen conditions. Again, no major differences in growth rate were observed between the three cell lines. In contrast to primary MEFs, the growth of immortal MEFs was not significantly influenced by the oxygen concentration (FIGURE 4.2). It was therefore decided to maintain immortal MEFs under normal (21 %) oxygen tension.

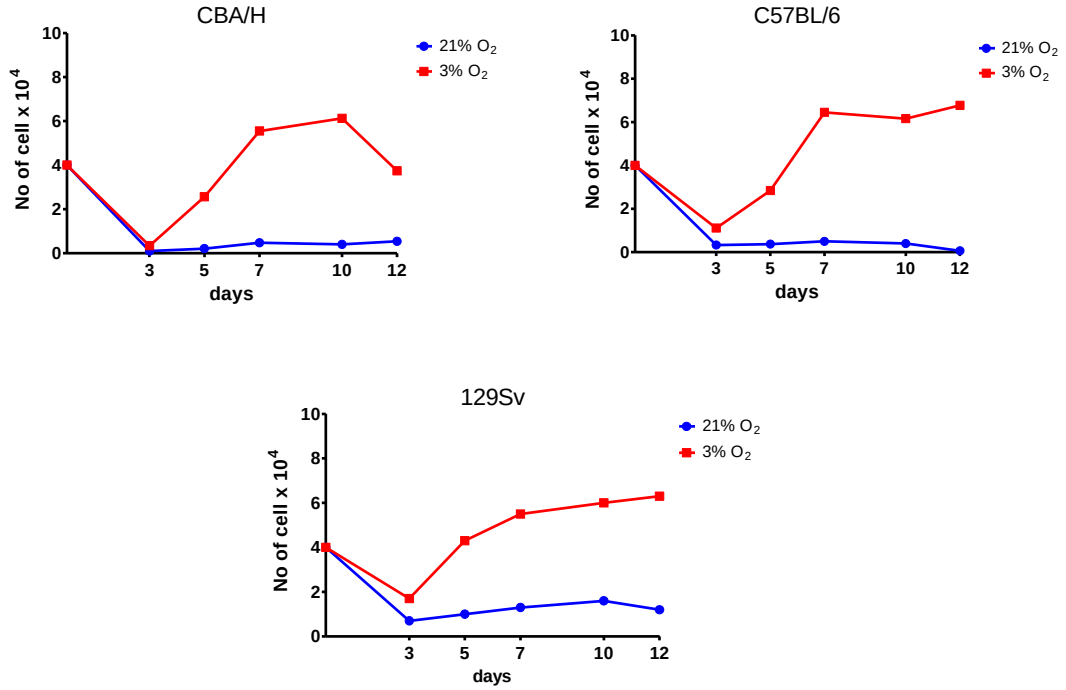


FIGURE 4.1 Comparison of cell growth of CBA/H, C57BL/6 and 129Sv primary MEFs under low (3 %) and normal (21 %) oxygen tensions. Cells were counted after 3 days (1st time point) and every 2 days thereafter for 12 days. n=1.

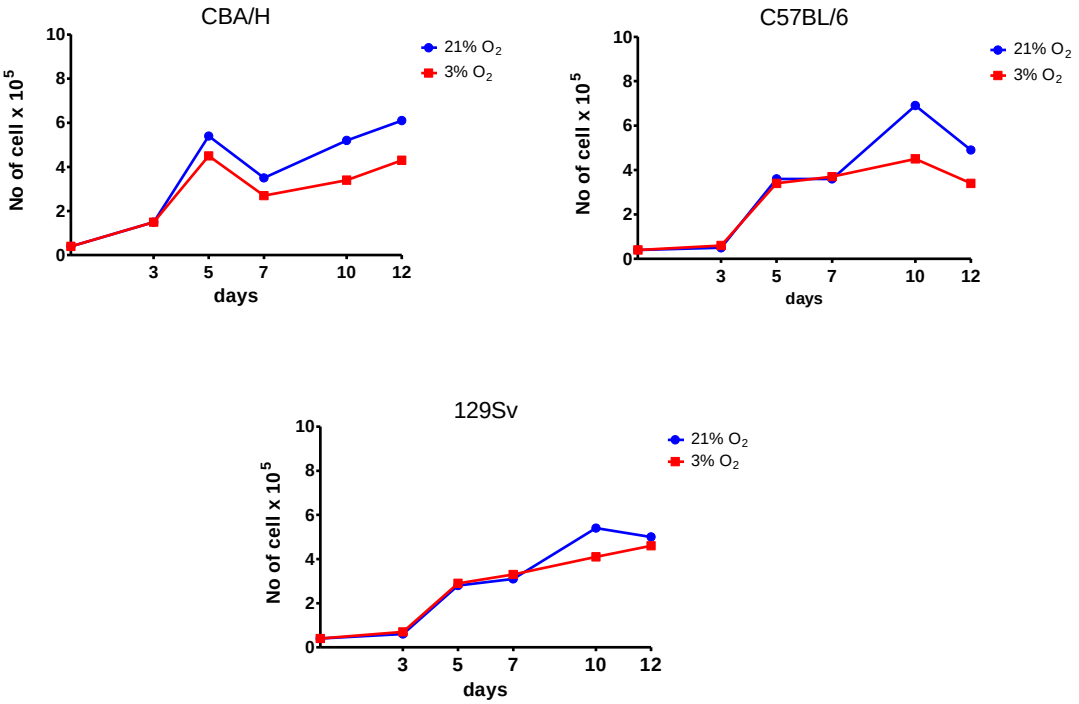


FIGURE 4.2 Comparison of cell growth of CBA/H, C57BL/6 and 129Sv immortal MEFs under low (3 %) and normal (21 %) oxygen tensions. Cells were counted after 3 days (1st time point) and every 2 days thereafter for 12 days. n=1.

4.3.2 Efficiency of DSB repair assessed from the dynamics of formation and loss of γH2AX and 53BP1 foci induced in primary MEFs by γ-radiation and α-particles

Having identified the Q418P nsSNP in CtIP of the 129Sv mouse strain (section 3.3.2), CBA/H, C57BL/6 and 129Sv MEF cell lines were exposed to either 1 Gy of low-LET γ-radiation or high-LET α-particles to assess whether the presence of the nsSNP would affect the reparability of radiation-induced DSBs and show an effect of radiation quality. Changing radiation quality from low to high LET results in decreasing the contribution of simple DSBs in favour of more complex DSBs. This is seen as decreased reparability as the radiation quality increases [37,62,92].

At stated time points post-irradiation, DNA DSB repair was assessed using either γH2AX or 53BP1, which are known markers of DSBs [100]. Representative images are shown in **FIGURE 4.3** and **FIGURE 4.4** for γ- and α- irradiation of C57BL/6 MEFs respectively with a dose of 1 Gy. All three MEF cell lines, CBA/H, C57BL/6 and 129Sv, showed similar rates of DSB repair after irradiation with 1 Gy γ-rays, with the number of γH2AX and 53BP1 foci approaching background levels at 24 h (**FIGURE 4.5 A,B**). Up to 6 h post α-particle irradiation (**FIGURE 4.5 C,D**), the rate of DSB repair in CBA/H cells was the same or slightly faster than the 129Sv MEF cell line. The rate of DSB repair in C57BL/6 cells was distinctly slower than that seen with 129Sv or CBA/H cells (**FIGURE 4.5 C,D**). In contrast to γ-rays, a significant level of DSBs persisted 24 h post-irradiation with α-particles (**FIGURE 4.5 C,D**), consistent with the concept of increased complexity of DNA damage induced by high LET α-particles compared to low LET γ-rays. Representative foci images following α-particle irradiation are presented in **FIGURE 4.4**.

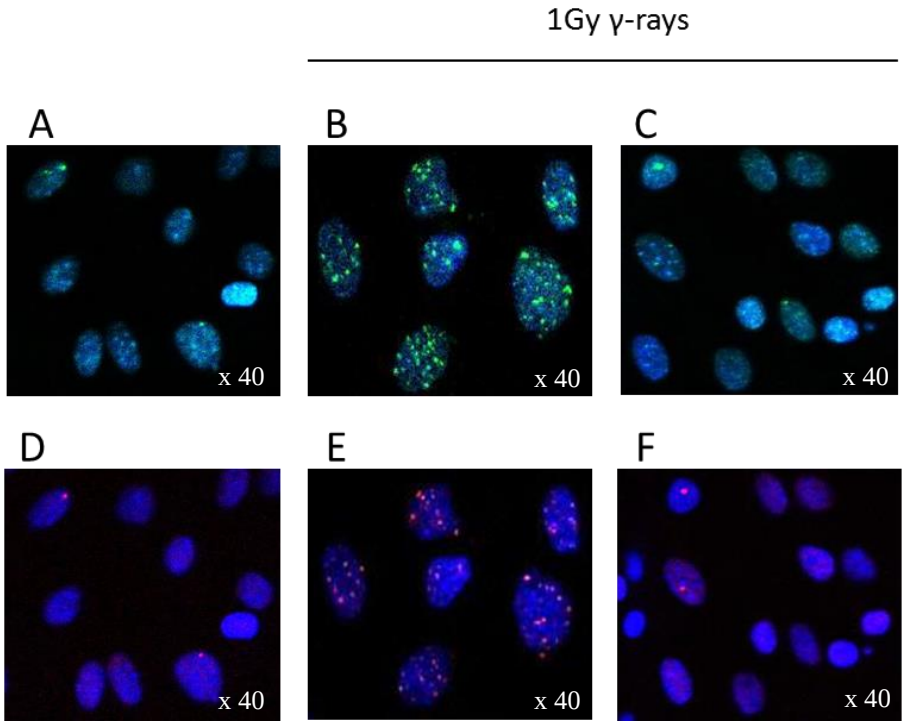


FIGURE 4.3 Representative images of γH2AX (A-C) and 53BP1 (D-F) foci in C57BL/6 MEF cell line after 1 Gy γ-ray radiation. A and D: control non-irradiated cells, B and E γH2AX and 53BP1 foci, respectively 30 min post-radiation, C and F γH2AX and 53BP1 foci, respectively 24 h post-radiation.

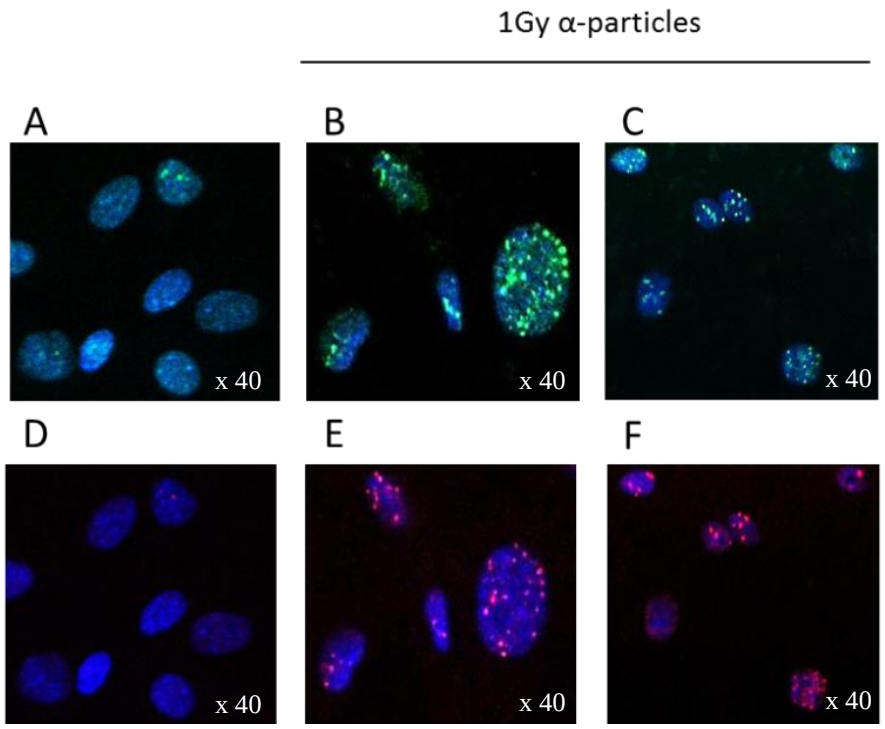


FIGURE 4.4 Representative images of γH2AX (A-C) and 53BP1 (D-F) foci in C57BL/6 MEF cell line after 1 Gy α-particles radiation. A and D: control non-irradiated cells, B and E γH2AX and 53BP1 foci, respectively 30 min post-radiation, C and F γH2AX and 53BP1 foci, respectively 24 h post-radiation.

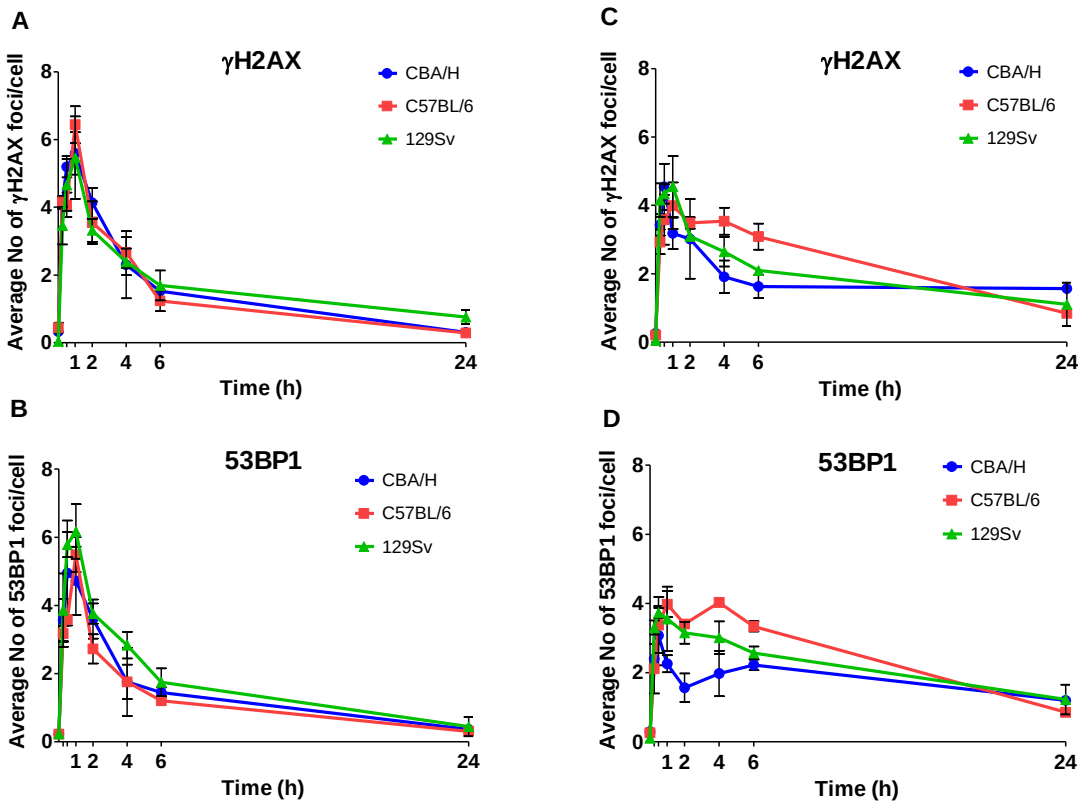


FIGURE 4.5 γH2AX and 53BP1 foci formation and loss in CBA/H, C57BL/6 and 129Sv MEFs after irradiation with 1 Gy γ-rays (A,B) and 1Gy α-particles (C,D). The number of γH2AX and 53BP1 foci peaked 0.5 h after irradiation with either γ-rays or α-particles. ~50 cells were counted per time point; n=3; error bars are SEM.

4.3.3 Homologous recombination repair of DSBs assessed by formation and loss of Rad51 and RPA foci induced in primary and immortal MEFs by γ-radiation

Rad51 and RPA (assayed using an antibody raised against the RPA32 subunit, section 2.7.2) were used as markers for HR. Initially, a dose response experiment was performed to ascertain the optimal radiation dose to be used in subsequent experiments. Representative images of C57BL/6 MEFs containing Rad51 and RPA foci (Rad51 and RPA positive/negative cell) 4 h post γ-irradiation with a dose of 10 Gy are presented in **FIGURE 4.6**. A cell was considered to be Rad51 or RPA positive if it contained >5 foci per cell. In **FIGURE 4.7** the dose dependent percentage of cells containing >5 Rad51 or RPA foci/cell is shown. The experiments show an increase in the number of positive cells with dose. The optimum dose of 10 Gy γ-rays was chosen to be used to examine any differences in the formation and loss of Rad51 and RPA foci with time in CBA/H, C57BL/6 and 129Sv primary MEFs (**FIGURE 4.8**). Some differences in the number of foci between the cell lines were seen with time. 129Sv showed fewer Rad51 or RPA positive cells, whereas more Rad51 or RPA positive cells were observed with C57BL/6. An alternative determination based on the average number of Rad51 foci per Rad51 positive cell is shown in **FIGURE 4.9A** whereas the average number of Rad51 foci per cell in the whole cell population is shown in **FIGURE 4.9B**. Similar trends were observed using these different presentations. In agreement with the differences observed in **FIGURE 4.8**, 129Sv cells showed the lowest number of Rad51 foci/Rad51 positive cell and similarly the lowest number of Rad51 foci/cell based on the whole population when compared to the numbers in CBA/H and C57BL/6 cells (**FIGURE 4.9**). These differences could indicate an impaired HR in 129Sv cell line relative to CBA/H and C57BL/6.

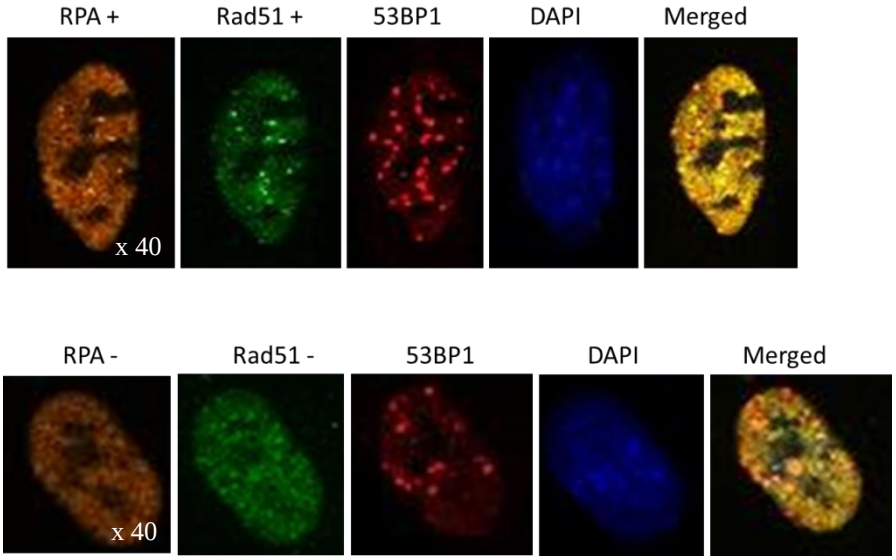


FIGURE 4.6 Representative images of Rad51 and RPA positive (Rad51+, RPA+) and Rad51and RPA negative (Rad51-, RPA-) C57BL/6 cells 4 h post 10 Gy γ-ray radiation.

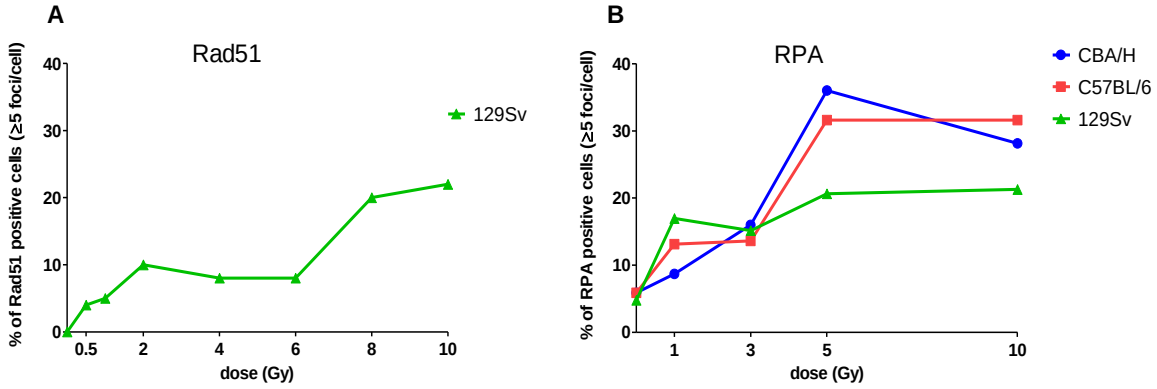


FIGURE 4.7 The effect of radiation dose on percentage of Rad51 (A) and RPA (B) positive cells in 129Sv and RPA positive cells (B) in CBA/H, C57BL/6 and 129Sv primary MEFs 2 h after exposure γ-radiation; n=1

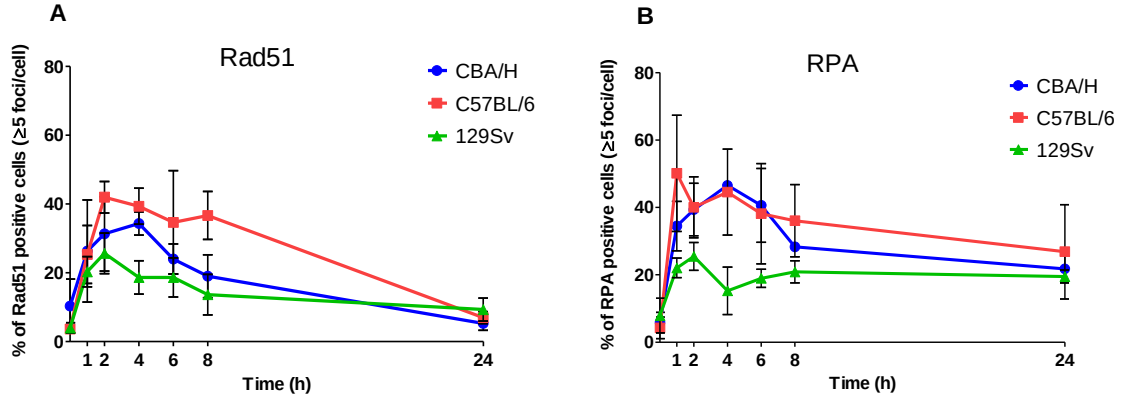


FIGURE 4.8 The percentage of Rad51 (A) and RPA (B) positive cells in CBA/H, C57BL/6 and 129Sv primary MEFs after irradiation with 10 Gy γ-rays and fixation at stated times; n=3; error bars are SEM.

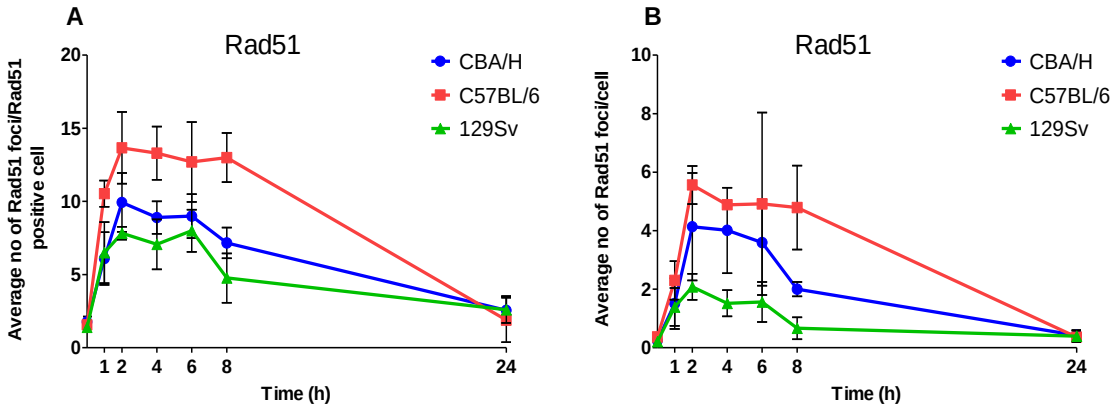


FIGURE 4.9: The number of Rad51 foci formation and loss in CBA/H, C57BL/6 and 129Sv primary MEFs after irradiation with 10 Gy γ-rays. Cells were fixed at stated time points. A: average number of foci per Rad51 positive cell, B: average number of foci per cell (based on whole population); n=3; error bars are SEM.

The number of Rad51 and RPA foci were also examined in immortalised MEFs following γ-irradiation with 10 Gy, to make sure that primary and immortal MEFs exhibit the same characteristics, as both were used in further experiments. **FIGURE 4.10** shows that as with primary MEFs (**FIGURE 4.8**), immortal CBA/H and C57BL/6 cells showed higher percentage of Rad51 and RPA positive cells than seen in the 129Sv cell line.

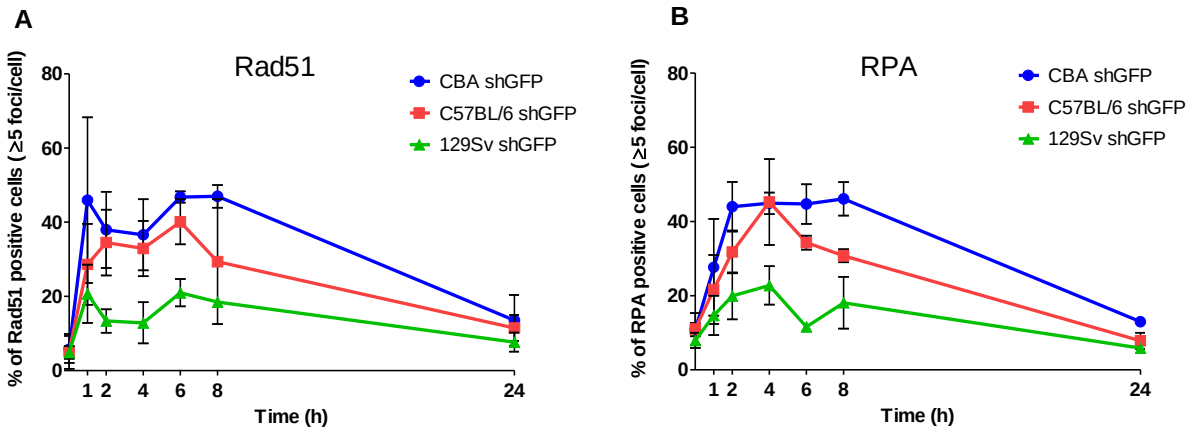


FIGURE 4.10 The percentage of Rad51 (A) or RPA (B) positive cells (>5 foci/cell) in CBA/H, C57BL/6 and 129Sv immortal MEFs after irradiation with 10 Gy γ-rays. Cells were fixed at stated time points; n=3; error bars are SEM.

4.3.4 Levels of CtIP and phospho-RPA32 in primary and immortal MEFs post-radiation or HU treatment

Since differences in the levels of radiation-induced Rad51 and RPA foci were reported in the previous section, the levels of CtIP were examined in the three cell lines CBA/H, C57BL/6 and 129Sv. CtIP is predominantly a nuclear protein and its level fluctuates significantly during cell cycle progression, with high levels in S and G2 phase and almost undetectable levels in G0 and G1 phase of the cell cycle [74]. It was therefore ensured that cells collected for western blot analysis were from exponentially growing cells. Extraction of cytoplasmic and nuclear proteins was performed with wild type CBA/H, C57BL/6 and 129Sv primary MEFs. The CtIP protein levels were found to be the same amongst the three cell lines with CtIP mainly present in the nuclear fraction (**FIGURE 4.11**).

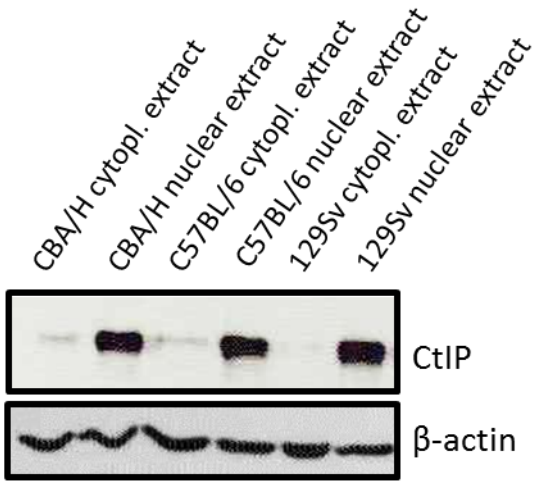


FIGURE 4.11 CtIP protein levels in cytoplasm and nuclear extracts of CBA/H, C57BL/6 and 129Sv MEF cell lines. β-actin was used as a loading control.

As previously reported, CtIP is essential for recruitment of RPA and ATR proteins to the DSB ends during HR [61, 221]. It was therefore important to check the levels of RPA32, phosphorylated RPA32 (pRPA32) and ATR post γ-radiation or post HU treatment. HU affects DNA synthesis by reversibly inhibiting ribonucleotide reductase, preventing the reduction of ribonucleotides to deoxyribonucleotides so that S-phase progression is impeded [44]. Similar levels of RPA32 protein expression were observed in control and 1-24 h post 10 Gy γ-irradiation in CBA/H, C57BL/6 and 129Sv primary MEFs, however pRPA32 was not detected. The times were chosen to correspond with the timescale for DSB repair by HR as discussed in Section 4.3.3. It has been reported that pRPA32 can be detected after very high doses of γ-radiation (50 Gy) [223], therefore immortal MEFs were treated with 10 Gy as well as 50 Gy γ-rays but pRPA32 was not detected 1-24 h following irradiation with either 10 or 50 Gy γ-rays (**FIGURE 4.13**).

Since DSBs formed from stalled or collapsed replication forks are predominantly repaired by HR [14, 224], it was decided to treat the cells with 1 mM of HU (which impedes S-phase progression) and probe for active RPA protein. pRPA32 was visible 6 and 24 h post HU treatment in CBA/H and C57BL/6 primary MEFs but not in 129Sv primary MEFs, whereas the total RPA levels remained unchanged in all three cell lines (**FIGURE 4.14**). Similarly with immortalised MEFs (**FIGURE 4.15**) pRPA32 was not seen in 129Sv MEFs.

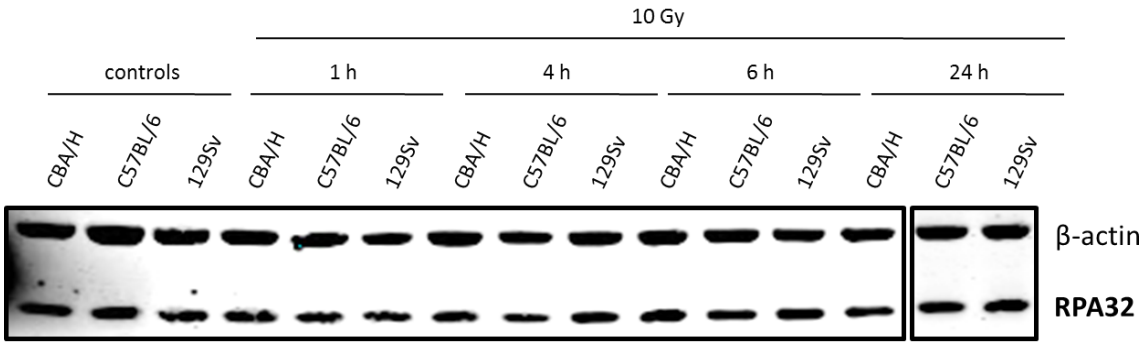


FIGURE 4.12 RPA32 protein expression in primary CBA/H, C57BL/6 and 129Sv MEFs post 10 Gy γ-radiation, β-actin was used as a loading control.

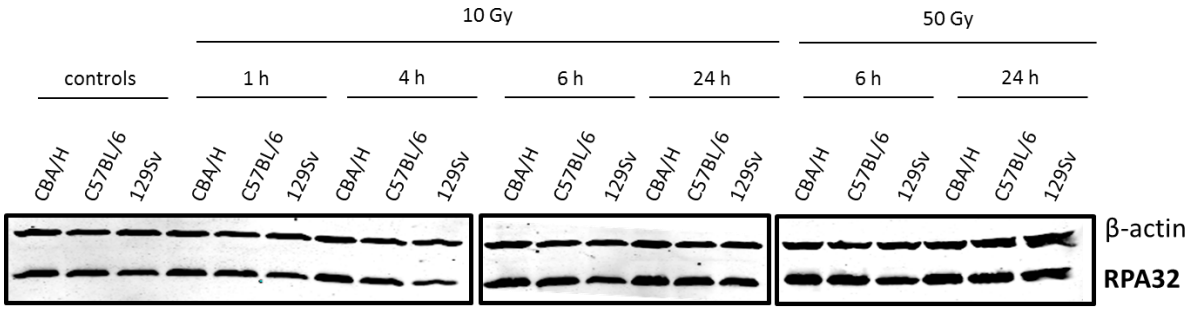


FIGURE 4.13 RPA32 protein expression in immortal CBA/H, C57BL/6 and 129Sv MEFs post 10 and 50 Gy γ-radiation, β-actin was used as a loading control.

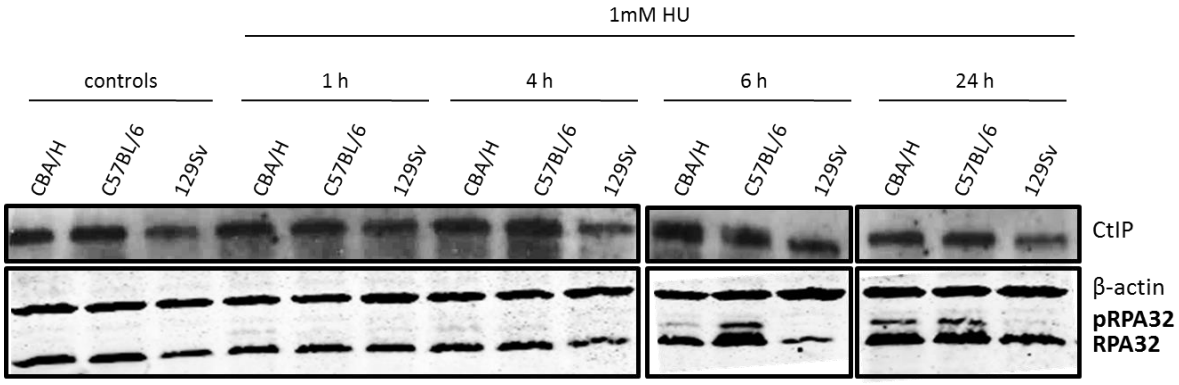


FIGURE 4.14 CtIP, RPA32 and pRPA32 protein expression in primary CBA/H, C57BL/6 and 129Sv MEFs post treatment with 1 mM HU, pRPA32 present in CBA/H and C57BL/6 6 and 24 h post HU treatment, β-actin was used as a loading control.

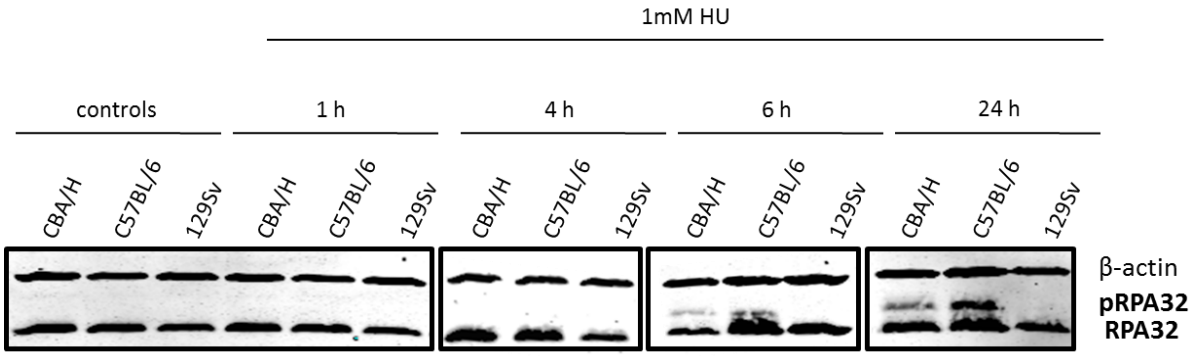


FIGURE 4.15 RPA32 and pRPA32 protein expression in immortal CBA/H, C57BL/6 and 129Sv MEFs post treatment with 1 mM HU, pRPA32 present in CBA/H and C57BL/6 6 and 24 h post HU treatment, β-actin was used as a loading control.

Since ATR recruitment to DSB ends is facilitated by CtIP, ATR protein expression was also examined in immortal CBA/H, C57BL/6 and 129Sv MEFs following treatment with 1 mM HU for 6 h. 129Sv cells exhibited much lower levels of ATR in comparison to CBA/H and C57BL/6 controls and HU treated immortal MEFs (**FIGURE 4.16**). This observation is consistent with the absence of pRPA32 in 129Sv MEFs and the reported role of active CtIP required to recruit RPA and ATR to DNA damage.

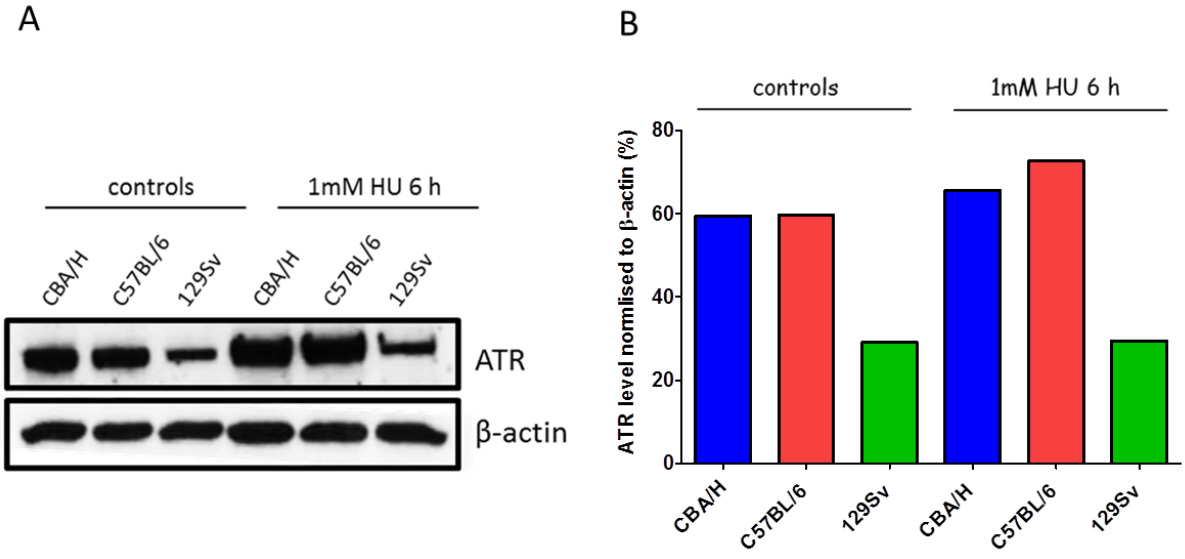


FIGURE 4.16 A: the level of ATR expression in CBA/H, C57BL/6 and 129Sv immortal MEFs. Cells were treated with 1 mM HU for 6 h or remained untreated, β-actin was used as a loading control. B: the quantification of the western blot, the ATR protein level of each sample was normalised to its β-actin control.

4.3.4.1 shRNA knock down of CtIP protein expression

shRNA has been used to knock down CtIP protein expression in order to examine the resultant effects on RPA recruitment and phosphorylation. Immortalised MEFs were used in this experiment to avoid senescence, which is a feature of primary MEFs, and to create cells stably expressing shRNA for prolonged CtIP knock down.

The CBA/H, C57BL/6 and 129Sv immortal MEFs were transfected with shRNA for CtIP knock down and shRNA for GFP as a control, in order to compare the level of pRPA32, as well as the number of RPA foci in control and CtIP knock down cells. The efficiency of CtIP knock down was high, as shown in **FIGURE 4.17**. The level of CtIP and RPA32 hyper-phosphorylated at serine 4 and 8 (RPA32 pS4/S8) in control (shGFP) and CtIP (shCtIP) knock down cells was evaluated 6 and 24 h post 10 Gy γ-radiation or during a 1 mM HU treatment. The level of CtIP was significantly lower in CtIP knock down cells (shCtIP) when compared to the controls (shGFP) in all cell lines. HU treatment induced phosphorylation of RPA32 pS4/S8, 6 and 24 h post HU treatment in CBA/H and C57BL/6 control MEFs (shGFP) but not in MEFs with CtIP knock down. In contrast, 129Sv shGFP MEFs showed no RPA32 pS4/S8 6 h post HU treatment and only low levels of phosphorylation at 24 h. Similarly to CBA/H and C57BL/6 cells with CtIP knock down, 129Sv shCtIP cells showed no RPA32 pS4/S8, 6 and 24 h post HU treatment. RPA32 pS4/S8 was not detected post 10 Gy radiation in CBA/H, C57BL/6 and 129Sv MEFs with or without CtIP knock down (**FIGURE 4.18**). These observations with CtIP knock down in the CBA/H, C57BL/6 and 129Sv cells are consistent with those seen in the 129Sv cells which contain the nsSNP in the CtIP gene.

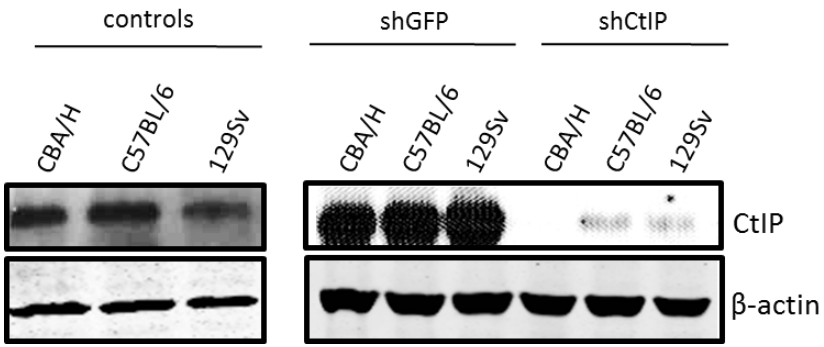


FIGURE 4.17 The level of CtIP protein in CBA/H, C57BL/6 and 129Sv transfected with shRNA for CtIP knock down (shCtIP), shRNA for GFP protein (shGFP) as a control, or untransfected (controls); The blot from untransfected cells was taken from Figure 3.14; β-actin was used as a loading control.

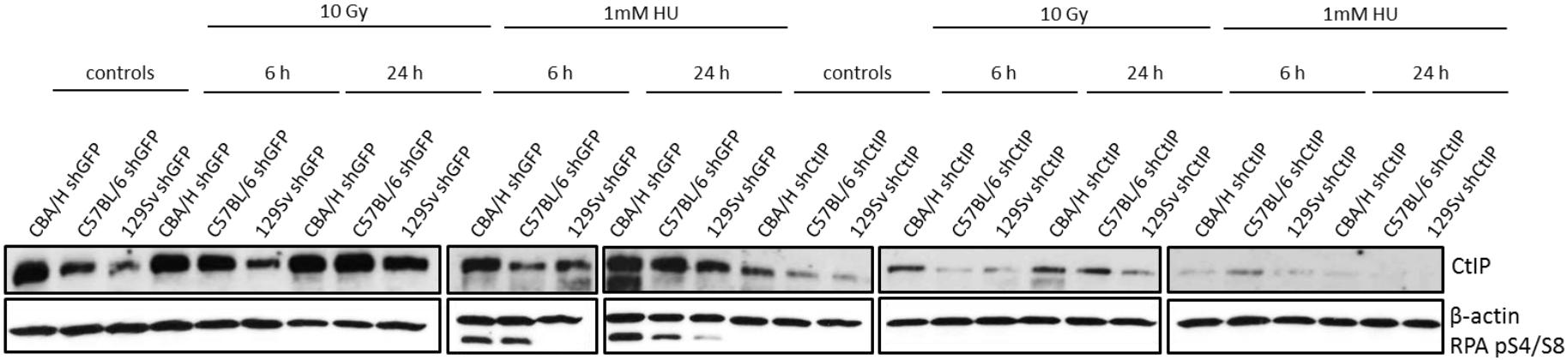


FIGURE 4.18 The level of CtIP and RPA32 pS4/S8 expression in CBA/H, C57BL/6 and 129Sv immortalised MEFs, control (shGFP) and CtIP knock down (shCtIP), determined 6 and 24 h post 10 Gy γ-radiation or 1 mM HU treatment; β-actin was used as a loading control.

4.3.4.2 The effect of CtIP knockdown on radiation-induced formation and loss of Rad51 and RPA foci in immortal MEFs

As described in section 4.3.3, immortal CBA/H and C57BL/6 cells showed higher percentages of cells containing >5 Rad51 or RPA foci than seen with 129Sv cell line following 10 Gy γ-irradiation. The numbers of Rad51 and RPA positive cells were evaluated using CBA/H, C57BL/6 and 129Sv cells in which CtIP had been knocked down, to gain further understanding of the effect of CtIP on Rad51 foci formation. CtIP depleted CBA/H and C57BL/6 cell lines showed much lower percentages of Rad51 and RPA positive cells at all times following 10 Gy γ-irradiation, except for the 24 h time point (**FIGURE 4.19 C,D)**, when compared with their respective controls (shGFP) (**FIGURE 4.19 A,B**). In contrast, the number of Rad51 and RPA positive cells in the CtIP depleted 129Sv cell line was similar to that seen in 129Sv cells expressing CtIP following 10 Gy γ-irradiation (**FIGURE 4.19**). In fact, the number of Rad51 and RPA positive cells in all the CtIP depleted MEFs were similar to 129Sv MEFs. These findings are consistent with 129Sv controls and CtIP knock down cells behaving similar to CBA/H and C57BL/6 shCtIP MEFs. These findings support the requirement of functional CtIP in recruitment of RPA and RAD51 to DSB ends during HR.

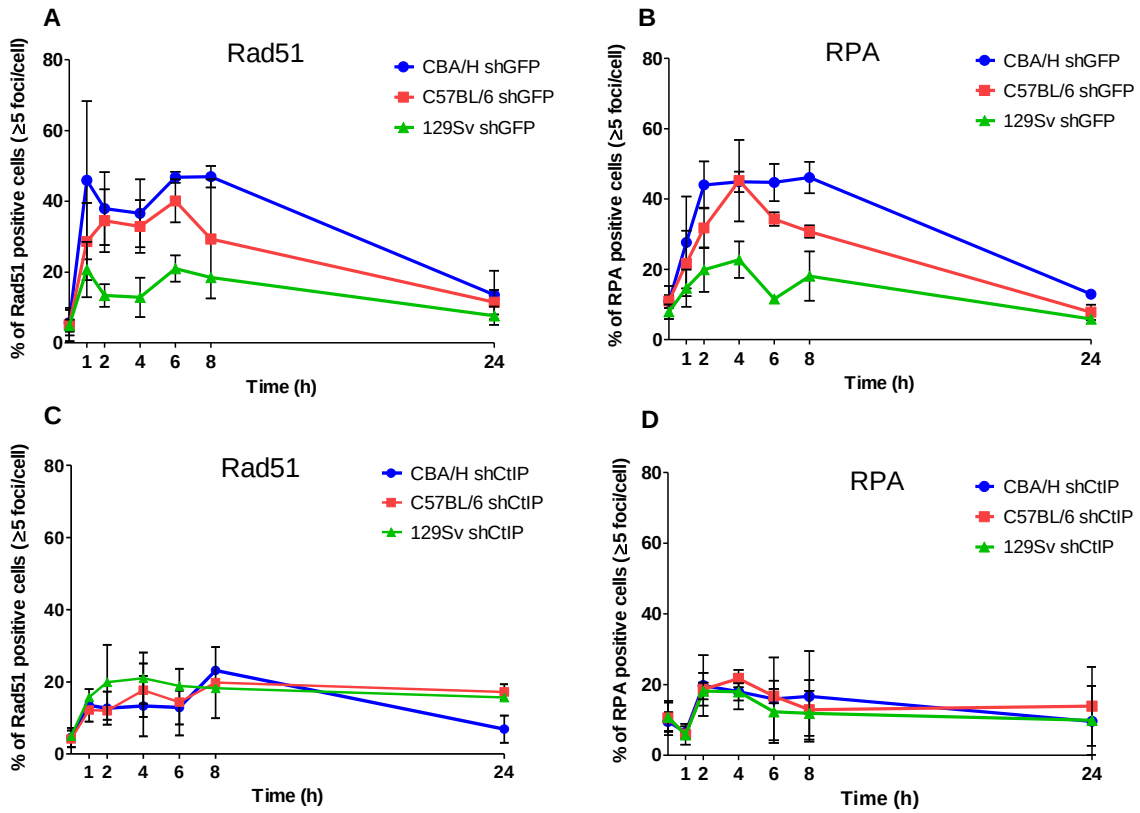


FIGURE 4.19 The percentage of Rad51 and RPA positive cells in CBA/H, C57BL/6 and 129Sv controls (A,B) and corresponding CtIP knock down cells (C,D) after irradiation with 10 Gy γ-rays. Cells were fixed at stated time points; n=3; error bars are SEM.

4.3.4.3 The effect of CtIP overexpression on the formation and loss of Rad51 and RPA foci post-irradiation in immortal MEFs

In order to confirm that the reduction in the percentage of Rad51 and RPA positive cells seen in 129Sv cells is due to dysfunctional CtIP, 129Sv cells were transfected with a plasmid containing full length mouse CtIP (section 2.2.3). As seen in **FIGURE 4.20**, this transfection resulted in overexpression of CtIP compared to control cells. CBA/H, C57BL/6, 129Sv and 129Sv overexpressing CtIP (129Sv + CtIP) were exposed to 10 Gy γ-rays, fixed at stated time points post-irradiation and the number of Rad51 and RPA positive cells (cells with >5 foci) were counted. Consistent with the findings described above, 129Sv cells showed lower percentages of Rad51 and RPA positive cells in comparison to CBA/H and C57BL/6 cells. The number of Rad51 and RPA positive cells observed in 129Sv + CtIP cells following 10 Gy γ-radiation was higher than the number seen in 129Sv cells and similar to the number seen in CBA/H and C57BL/6 cells which contain active CtIP. These findings confirm that Rad51 and RPA recruitment to the sites of DSBs is CtIP dependent and are consistent with the lower numbers of Rad51 and RPA foci in 129Sv wild type containing a nsSNP in CtIP gene (**FIGURE 4.21**).

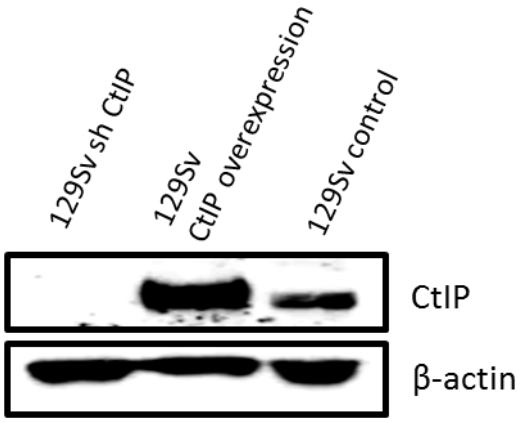


FIGURE 4.20 The level of CtIP in the 129Sv cell line with CtIP knock down (shCtIP), CtIP overexpression or control; β-actin was used as a loading control.

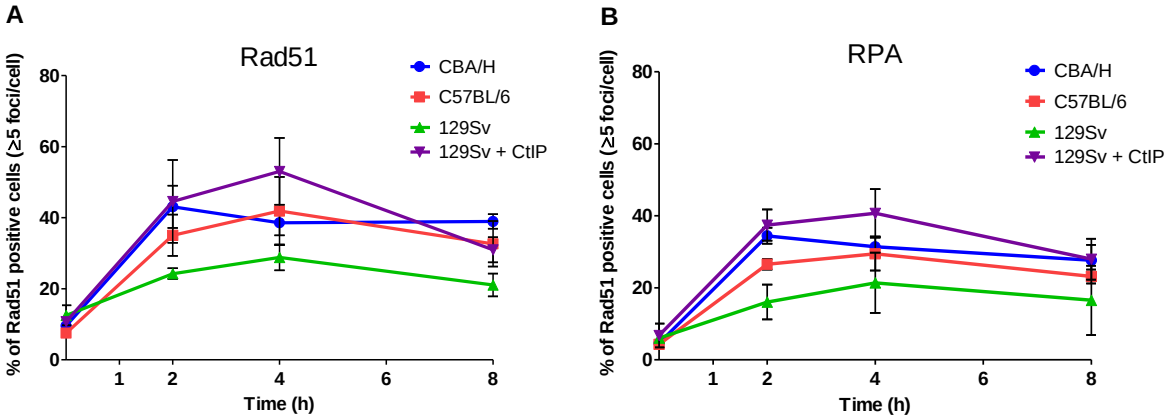


FIGURE 4.21 The percentage of Rad51 (A) and RPA (B) positive cells in CBA/H, C57BL/6, 129Sv and 129Sv + CtIP (129Sv overexpressing CtIP) post 10 Gy γ-ray radiation. Cells were fixed at stated time points; n=3; error bars are SEM.

4.3.5 CtIP and cell cycle

Due to the importance of cell cycle on the function of CtIP, the cell cycle distribution in primary and immortal MEFs was determined by flow cytometry as described in section 2.9.7. MEFs develop tetraploidy [225] even at very early passages. Although it was attempted to gate only the diploid population this could not be undertaken accurately as the S and G2 phase of the diploid population partly merge with the G1 and S phase of the tetraploid population. Diploid and tetraploid populations of primary MEFs are shown in **FIGURE 4.22**. For early passages (e.g. passage 2), tetraploidy contributes to only a small proportion to the total cell population, however after several divisions (e.g. passage 7), the tetraploid population significantly increases (visible on the right-hand side of the x-axis). Tetraploidy was also detected in immortal MEFs, the proportion was similar to that seen in later passages of primary MEFs. **FIGURE 4.23** shows cell cycle distribution in early passages of the three primary MEF cell lines CBA/H, C57BL/6 and 129Sv. The trend was similar for all the cell lines: increase in the G2 population 6 h post 5 and 10 Gy, slight increase in the G1 population 24 h post 1 Gy radiation and a much bigger increase in the G1 and G2 populations 24 h post 5 and 10 Gy radiation in comparison to the distributions seen with the non-irradiated cells (**FIGURE 4.23**). The S-phase population was slightly smaller in CBA/H cells, apart from in 24 h controls, when compared to C57BL/6 and 129Sv mice (**FIGURE 4.24**).

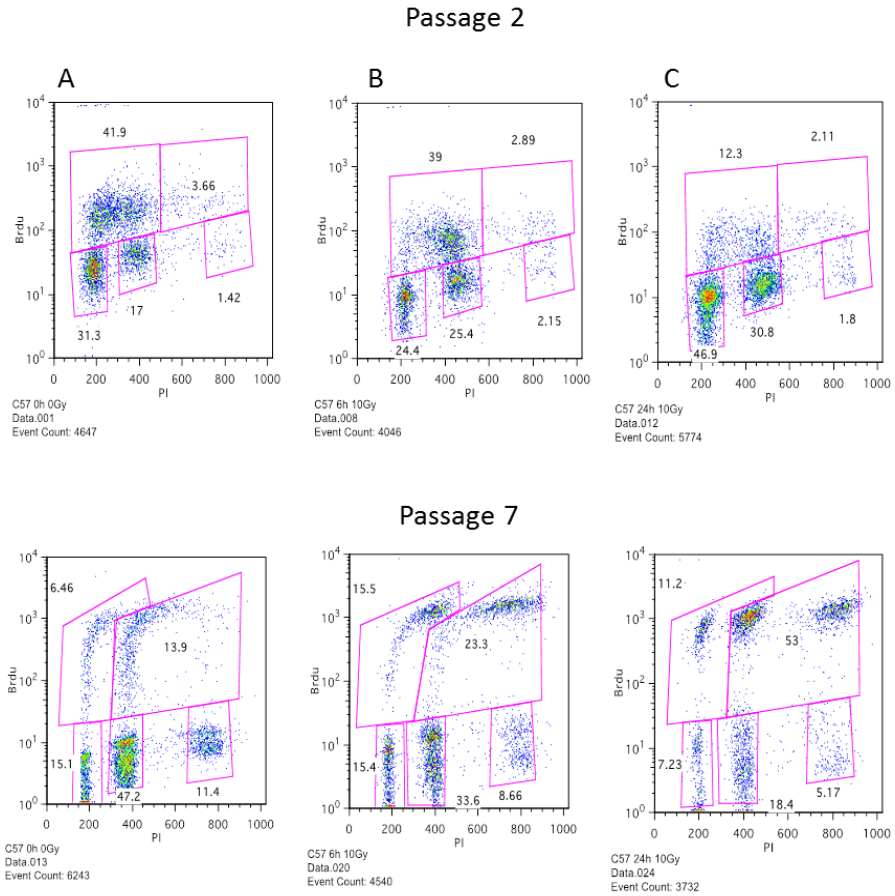


FIGURE 4.22 Representative data of the cell cycle distribution, showing diploid and tetraploid populations in passage 2 and passage 7 with C57BL/6 primary MEFs. Vertically: A- 0 h 0 Gy, B- 6 h 10 Gy, C- 24 h 10 Gy.

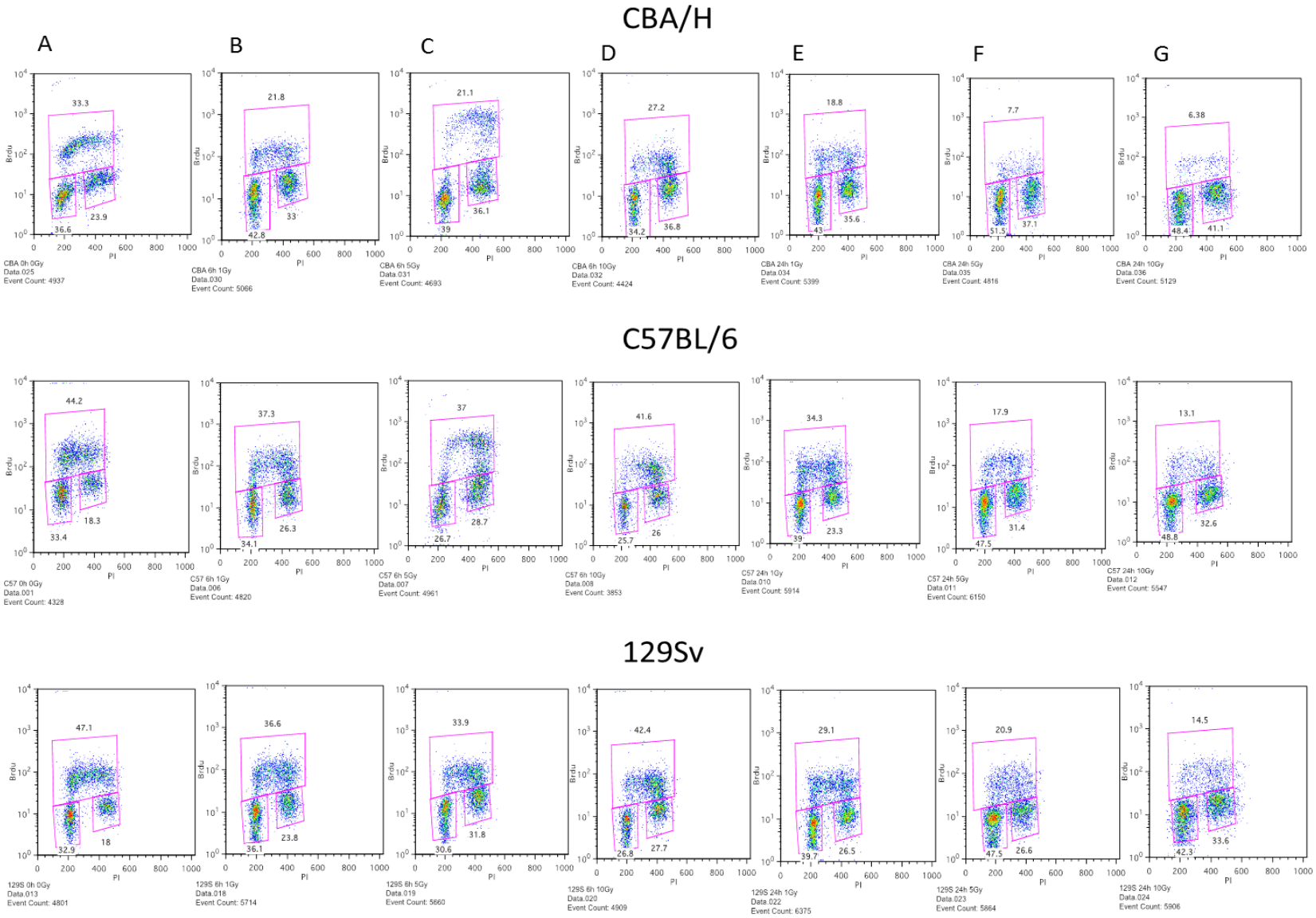


FIGURE 4.23 Representative data of cell cycle distribution of primary MEFs: CBA/H, C57BL/6 and 129Sv; Cells were irradiated with 0, 1, 5 or 10 Gy γ-rays and cell cycle distribution determined at 0, 6 or 24 h post-irradiation; Vertically: A- 0 h 0 Gy, B- 6 h 1 Gy, C- 6 h 5 Gy, D- 6 h 10 Gy, E-24 h 1Gy, F-24 h 5 Gy, G- 24 h 10 Gy; The diploid population was gated; n=3.

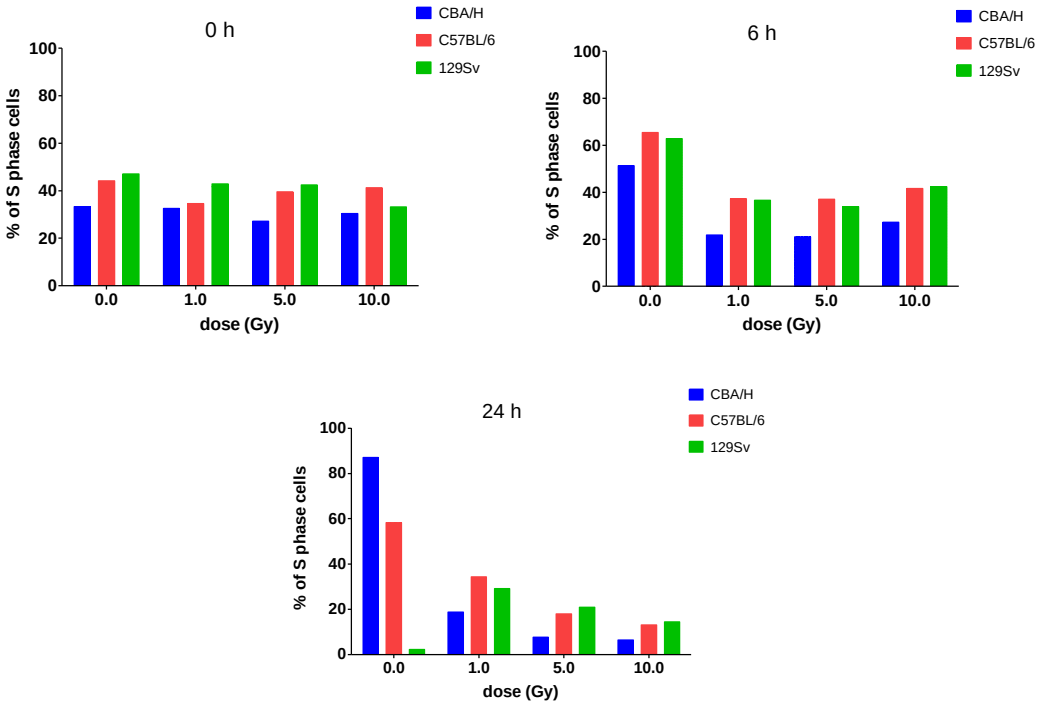


FIGURE 4.24 Percentage of S phase cells in primary CBA/H, C57BL/6 and 129Sv MEFs 0, 1, 5 and 10 Gy post γ-radiation at 0, 6 and 24 h time points. Data taken from the S phase population in Figure 3.23 complemented by 6 and 24 h controls.

Another approach to check the percentage of S-phase population in replicating CBA/H, C57BL/6 and 129Sv MEFs following exposure to IR was undertaken using an immunofluorescence assay. Cells were pulse labeled with EdU, an alternative to BrdU [21], prior to fixation. Cells were irradiated with 1 Gy γ-rays and fixed at stated time points post-irradiation. It has been reported that CtIP might be essential for progression from G1 to S [22] and G2 to M phase [68], therefore EdU labelling was performed with control immortal MEFs (shGFP transfected) as well as MEFs with CtIP knockdown (shCtIP). From the distributions observed with time, no large differences were seen in the percentage of EdU positive cells between the three shGFP transfected cell lines (**FIGURE 4.25 A**). With the CtIP knock down cells, CBA/H shCtIP MEFs exhibit lower percentage of EdU positive cells 1, 2 and 4 h post-irradiation (**FIGURE 4.25 B**) when compared to CBA/H shGFP MEFs 1, 2 and 4 h post-irradiation (**FIGURE 4.25 A**). The S-phase population was lower only 4 h post-radiation in C57BL/6 shCtIP MEFs comparing to 4 h with C57BL/6 shGFP cells. The 129Sv cell line showed a similar percentage of EdU positive cells in shGFP and shCtIP cells, which may indicate that CtIP knock down has less effect on cell cycle distribution in 129Sv MEFs.

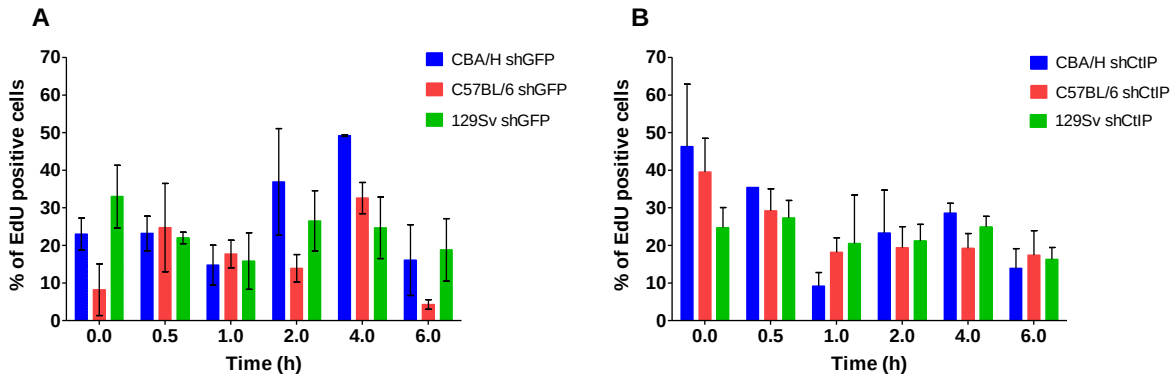


FIGURE 4.25 The percentage of S phase cells with CBA/H, C57BL/6 and 129Sv controls (A) and CtIP knock-down (B) immortal MEFs. Cells were fixed at indicated time points post 1 Gy γ-radiation; n=3; error bars are SEM

Control (shGFP) and CtIP knockdown immortal MEFs labelled with EdU were co-stained for 53BP1 in order to examine differences in DSB repair in the S-phase population of CBA/H, C57BL/6 and 129Sv MEFs. Representative images of EdU and 53BP1 staining post 1 Gy γ-irradiation are shown in **FIGURE 4.26.** Although CBA/H shGFP cells showed higher numbers of 53BP1 foci per EdU positive cell compared to the other cell lines 1 h post-irradiation, a definite difference in DSB repair was not seen between control MEFs (**FIGURE 4.27 A).** After CtIP knockdown in the three cell lines, the number of 53BP1 foci per EdU positive cell was slightly lower (by an average of 1-2 foci) for CBA/H and C57BL6 in comparison to controls but not with 129Sv cells where similar numbers were seen between control and CtIP knockdown cells (**FIGURE 4.27**). The trend was very similar when the number of 53BP1 foci per cell in the whole population was evaluated in shGFP and shCtIP MEFs. CBA/H and C57BL/6 shCtIP MEFs showed slightly lower number of 53BP1 foci per cell when compared to CBA/H and C57BL/6 controls. In contrast, the number of 53BP1 foci in 129Sv cells remained similar regardless of CtIP knock down (**FIGURE 4.28**). This result is consistent with the EdU data (**FIGURE 4.25**), where no differences between control and CtIP depleted 129Sv cells were observed.

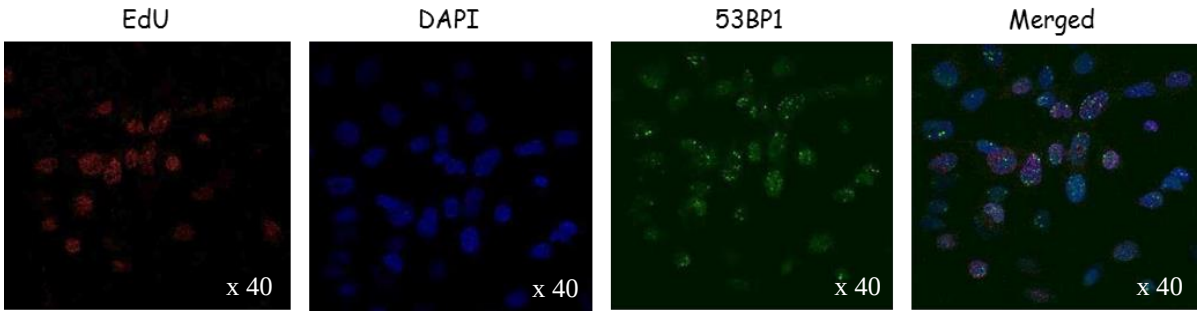


FIGURE 4.26 Representative images of EdU, DAPI and 53BP1 in C57BL/6 post 1 Gy γ-radiation.

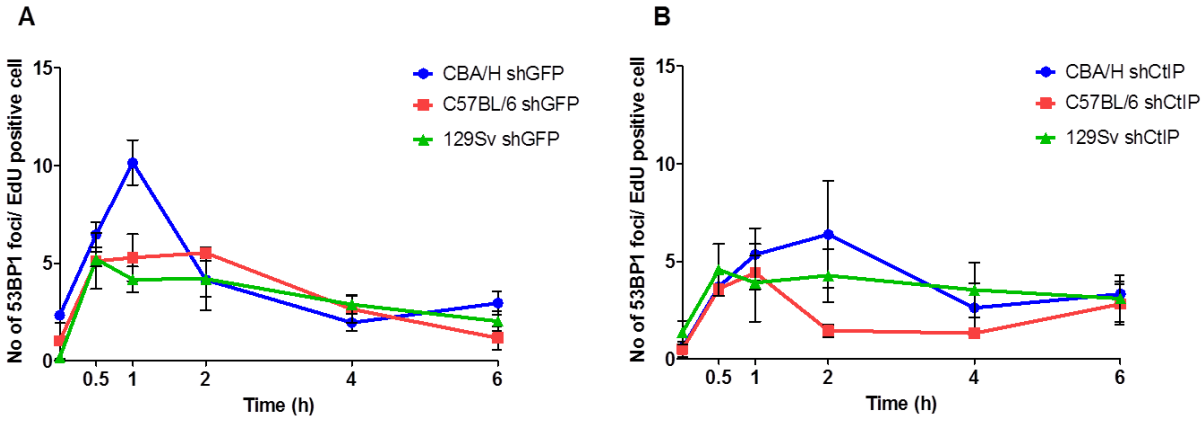


FIGURE 4.27 The number of 53BP1 foci per EdU positive cell in CBA/H, C57BL/6 and 129Sv immortal controls (A) and CtIP knockdown (B) MEFs after irradiation with 10 Gy γ-rays. Cells were fixed at stated times; n=3; error bars are SEM.

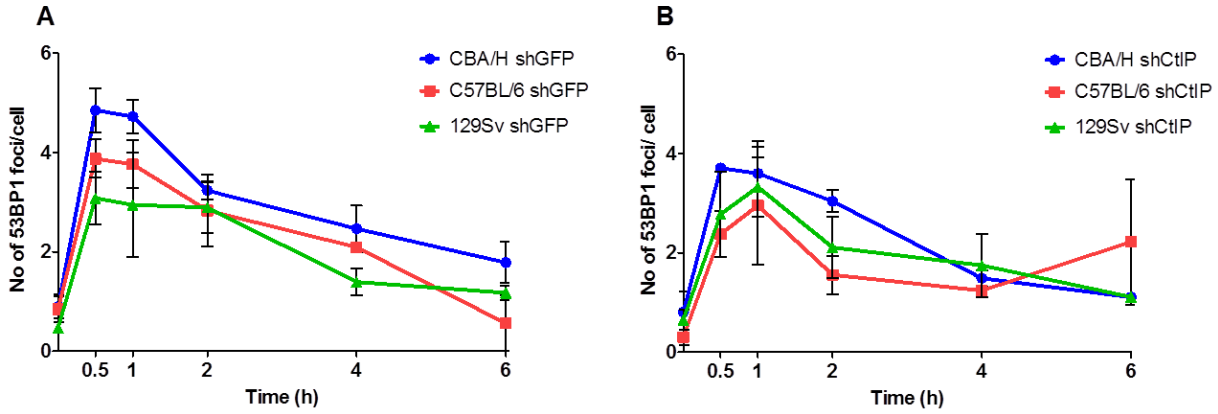


FIGURE 4.28 The number of 53BP1 foci per cell in the whole population in CBA/H, C57BL/6 and 129Sv immortal control (A) and CtIP knockdown (B) MEFs after irradiation with 10 Gy γ-rays. Cells were fixed at stated times; n=3; error bars are SEM.

4.4 Discussion

The reparability of γ-radiation-induced DSBs is similar between the CBA/H, C57BL/6 and 129Sv cell lines. However, up to 4 h post-irradiation with high LET radiation (α-particles), CBA/H and 129Sv cells showed a slightly faster repair rate of DSBs than C57BL/6 MEFs. An explanation could be that due to the nsSNP within the CtIP gene of the 129Sv cell line cells 'chose' the NHEJ repair pathway over HR in the absence of fully functional CtIP gene. Therefore, 129Sv cells could have repaired DSBs faster than C57BL/6 cells up to 4 h post α-particle irradiation. This explanation however cannot apply to CBA/H cells as a nsSNP was not detected in the CtIP gene. Using γH2AX and 53BP1 as markers of DSBs, a more likely explanation is that the small differences seen relate to the use of NHEJ to repair the majority of the DSB damage. The contribution of HR in DSB repair is minor in comparison to NHEJ, consistent with the high dose of γ-rays needed to observe Rad51 and RPA foci recruitment to the DNA damage sites. This is in contrast to γH2AX and 53BP1 foci which were visible after only 1 Gy of γ-radiation.

The decreased recruitment of the HR markers Rad51 and RPA in 129Sv cells, when compared to CBA/H and C57BL/6 cells after 10 Gy γ-irradiation, is consistent with reduced activity of the CtIP gene carrying Q418P nsSNP. Similarly, HU treatment induced phosphorylation of RPA32 in CBA/H and C57BL/6 cells but not in 129Sv would support the hypothesis that the nsSNP causes reduced activity of CtIP in the 129Sv cells. Protein expression of ATR was also significantly lower in 129Sv cells in comparison to the other two cell lines. This expression was independent of HU treatment. These findings would be consistent with defective DSB resection in 129Sv cells due to the presence of the nsSNP within the CtIP gene.

In order to verify that CtIP is essential for RPA32 phosphorylation (as shown by others [61,70,221]) and recruitment of Rad51 and RPA to DSB ends, CtIP protein expression was depleted using shRNA in the three immortalised MEF cell lines CBA/H, C57BL/6 and 129Sv. The percentage of radiation-induced Rad51 and RPA positive cells in CBA/H and C57BL/6 with CtIP knock-down dropped significantly (about 2 fold) in comparison to the irradiated controls (shGFP MEFs). The number of Rad51 and RPA positive cells observed in response to irradiation was lower in 129Sv cells compared with CBA/H and C57BL/6, and was unaffected by CtIP knock down. This data supports the proposal that the nsSNP present in 129Sv cells impairs CtIP function in DSB resection and therefore ssDNA formation, resulting in a low level of Rad51 and RPA recruitment to the CtIP-resected DSB ends. However, in order to confirm the importance of fully functional CtIP in DSB repair, active CtIP was overexpressed in 129Sv cell line to compensate for the defective nsSNP-carrying CtIP. The number of radiation-induced Rad51 and RPA positive cells was restored when full-length CtIP was overexpressed in 129Sv cells. This demonstrates the requirement for functional CtIP to recruit downstream proteins involved in HR.

C57BL/6 and 129Sv MEF cell lines showed similar cell cycle distribution, whereas CBA/H exhibited a slightly smaller S-phase population. This confirms that the lower percentage of Rad51 and RPA positive cells observed in 129Sv MEFs was not due to significant differences in the S-phase population between cell lines. There were no definite changes observed in the S-phase population of the three MEF cell lines following CtIP knock down. Differences in the reparability of DSBs in the S phase population of CBA/H, C57BL/6 and 129Sv MEFs were not seen. However, moderate differences were observed between the cell lines in the number of 53BP1 foci post CtIP knock down, with the level of 53BP1 foci being slightly lower (1-2 foci) in CBA/H and C57BL/6 shCtIP cells in

comparison to controls (shGFP MEFs). Whereas in 129Sv cells, CtIP knock down did not affect DNA reparability.

In summary, major differences between cell lines were observed in the efficiency of the HR pathway when CtIP was absent through knock down or defective as seen with the nsSNP in the CtIP gene of the 129Sv cell line. The results, including impaired recruitment of Rad51 and RPA to DSB ends in 129Sv cells, are consistent with the nsSNP in the CtIP of 129Sv cells having an influence on HR functionality. This impairment may lead to chromosomal aberrations.

5 The influence of the Q418P nsSNP in CtIP on homologous recombination and survival

5.1 Introduction

As has been described previously, CtIP is involved in HR by carrying out resection of DSBs. Sister chromatid exchange (SCE) is a direct effect of HR and is defined as symmetrical exchange between homologous portions of the chromosome, involving DNA breakage and re-union [88]. Spontaneous SCEs, occurring within different cell types with varying frequency, and are considered to be a product of normal DNA replication or endogenous DNA damage [226]. SCEs can be induced by several genotoxic agents, including mitomycin C (MMC) [187,227,228] or low [103,138,140] and high LET radiation [229, 230], suggesting that SCEs reflect DNA repair processes [139]. MMC, a DNA crosslinking agent [231] is a well-known inducer of sister chromatid exchanges [187]. It has been shown that spontaneous, MMC and radiation-induced numbers of SCEs are significantly reduced in HR-defective cells [137-140], as opposed to cells defective in NHEJ where SCE yields do not change in comparison to NHEJ proficient cells [140]. This substantiates HR as the main repair pathway associated with SCE [226,140]. High SCE incidence has been reported in patients with various types of cancer, including breast cancer, cutaneous malignant melanoma and lymphoma [232-234]. However, recently it has been shown that spontaneous SCE in uveal melanoma is decreased below normal baseline levels [235]. Therefore, the link between HR and SCE is complex, potentially involving

different proteins controlling spontaneous and induced SCEs as well as differences between species [226,138,140,236].

Cells defective in the HR pathway are much more sensitive to bifunctional alkylators (e.g MMC) [137], topoisomerase inhibitors (e.g Camptothecin) [61] or replication inhibitors (e.g HU) [14], than wild type (wt) cells, which was shown by reduction in cell survival [137,61,14] as well as the number of SCEs [137]. However, differences in cell survival were not observed when HR-defective and wt cells were exposed to low LET ionising radiation [14, 137], consistent with replication-associated DSBs being mainly repaired by HR [13].

5.2 Aim

The aim was to investigate the efficiency of HR in CBA/H, C57BL/6 and 129Sv (carrying the Q418P nsSNP within CtIP) MEF cell lines through spontaneous, radiation-induced or MMC-induced SCEs, and to examine any differences in cell survival following radiation or HU treatment.

5.3 Results

5.3.1 The differences between cell lines in spontaneous and induced SCE levels

HR plays a role in the repair of DSBs induced in S- and G2-phases of the cell cycle and the formation of SCEs, in part as a result of HR events at stalled or broken replication forks during attempted repair [226,140]. Therefore, the yields of SCEs following exposure to MMC or radiation were examined to determine whether there are differences in the involvement of HR between CBA/H, C57BL/6 and 129Sv immortal MEFs in the maintenance of genomic stability.

Cells were exposed to 0.5 µg/ml MMC, or were untreated (section 2.8.1). Representative images, showing the presence of SCEs in control and MMC treated cells, are shown in FIGURE 5.1. MMC induced around 15 and 18 SCEs in CBA/H and C57BL/6, respectively, representing a 3.8 and 2.5 fold increase in SCE formation in comparison to controls. In contrast, significantly lower numbers of SCEs were seen in either control or MMC treated 129Sv cells (TABLE 5.1 and FIGURE 5.2). Treatment with MMC did result in approximately a 2 fold increase when compared to control 129Sv cells, although the corresponding numbers of induced SCEs in MMC treated 129Sv cells are 3 and 3.6 fold lower than in CBA/H and C57BL/6 cells, respectively. Similarly, when spontaneous SCEs were compared between the three cell lines, 129Sv cells showed a 1.5 and approximately 3 fold decrease in comparison to CBA/H and C57BL/6 cells, respectively (TABLE 5.1FIGURE 5.1 and FIGURE 5.3). These findings are consistent with HR being impaired in 129Sv cells.

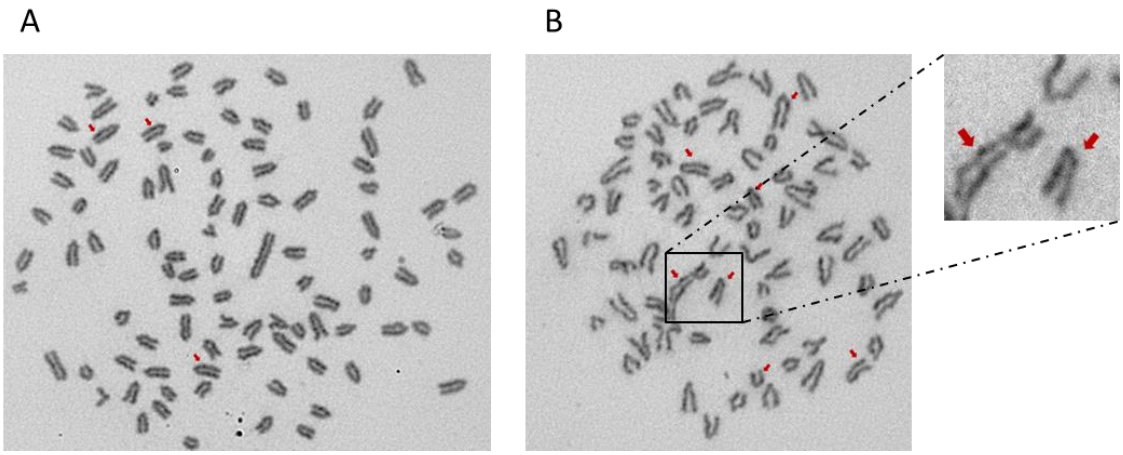


FIGURE 5.1 Representative images of SCEs in control (A) and MMC treated (B) C57BL/6 MEF cell line, red arrows indicate SCEs.

TABLE 5.1 The mean number of SCEs per metaphase in control and MMC treated (0.5 µg/ml) CBA/H, C57BL/6 and 129Sv cell lines.

Immortal MEF cell lines			
SCEs (mean)	CBA/H	C57BL/6	129Sv
control	4	7.4	2.6
MMC	15	18	5

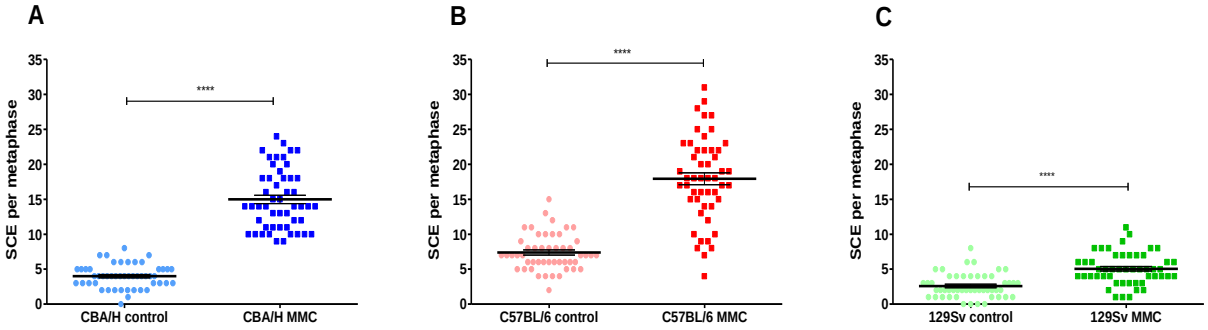


FIGURE 5.2 The frequency of SCEs in control and MMC treated (0.5 µg/ml) immortal MEF cell lines, CBA/H (A), C57BL/6 (B) and 129Sv (C); 50 metaphase spreads were scored per cell line (control and MMC treated); error bars are SEM: ****= p<0.0001

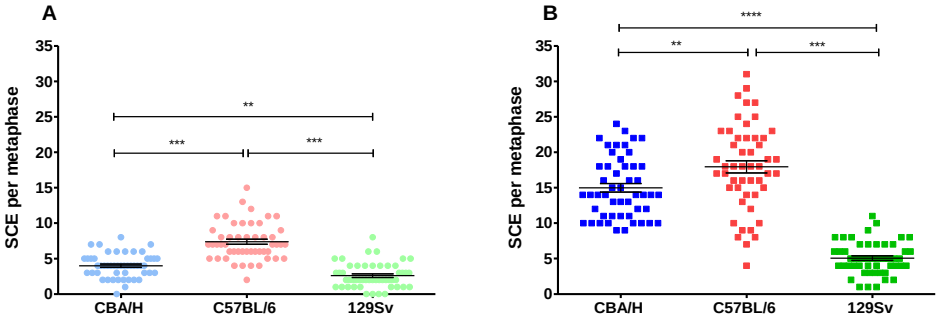


FIGURE 5.3 Comparison of spontaneous (A), and MMC induced (B) SCEs in CBA/H, C57BL/6 and 129Sv MEF cell lines; 50 metaphase spreads were scored per cell line; error bars are SEM; **=p<0.01; ***=p<0.001; ****=p<0.0001

Originally low LET radiation was shown to be inefficient in producing SCEs [237], in contrast to high LET radiation which leads to the formation of SCEs [229,230,238]. More recent publications however have reported an increase in SCE level post γ-radiation exposure of cells in the G2 phase of the cell cycle [39,103,239]. As exponentially growing cells were used and differences in DSB repair rate between the three MEF cell lines were previously observed post α-particle treatment (section 4.3.2) but not following γ-radiation, numbers of SCEs were examined following α-particle irradiation.

The three immortal MEF cell lines, CBA/H, C57BL/6 and 129Sv, were exposed under exponential growth conditions to 0.5 and 1 Gy α-particle radiation. In **TABLE 5.2** the mean numbers of SCEs are compared between control and irradiated MEF cell lines. The number of spontaneous SCEs was similar in CBA/H and C57BL/6 cells but approximately 1.5 fold lower in 129Sv MEFs (**FIGURE 5.4**). The mean number of spontaneous SCEs per metaphase varied between the experiments (**TABLE 5.1** and **TABLE 5.2**), which may reflect a lower number of metaphases counted (20 instead of 50) in the repeat experiment. The differences in the mean number of induced SCEs between the experiments occurred due to the fact that α-particles induce significantly less SCEs per metaphase in comparison to MMC [187, 230]. Irradiation with 0.5 Gy α-particles induced a 1.3 fold increase in the SCE level in all three cell lines when compared with the controls. A higher dose of α-particles (1 Gy) further increased the number of SCEs in CBA/H and C57BL/6 cell lines, resulting in around 1.7 fold increase compared to the controls. With 129Sv cells the number of SCEs observed was similar to that seen with 0.5 Gy (**TABLE 5.2** and **FIGURE 5.4C**). In **FIGURE 5.5**, the numbers of spontaneous and induced SCEs are compared in the three cell lines. 129Sv cells exhibit decreased numbers of SCEs post 0, 0.5 and 1 Gy α-particles irradiation compared to CBA/H and C57BL/6 cells, which reflects the trends seen with MMC treatment.

TABLE 5.2 The mean number of SCEs per metaphase in control and α-particles irradiated CBA/H, C57BL/6 and 129Sv cell lines.

Immortal MEF cell lines			
SCEs (mean)	CBA/H	C57BL/6	129Sv
control	2.5	2.7	1.7
α-particles 0.5 Gy	3.5	3.3	2.2
α-particles 1 Gy	4.3	4.5	2.4

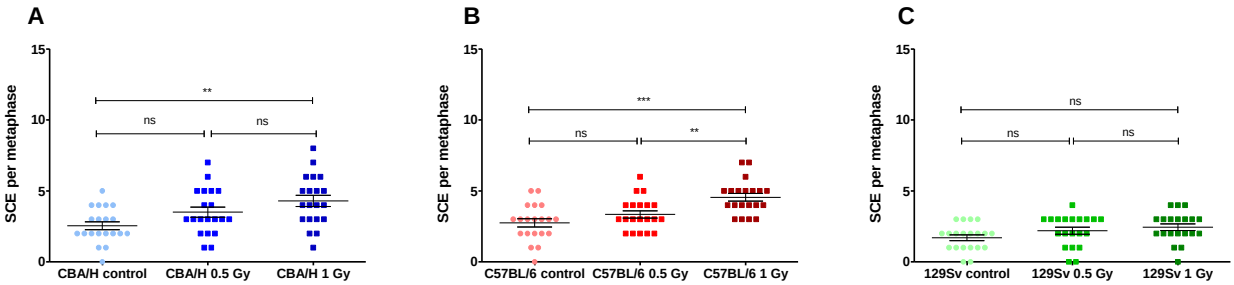


FIGURE 5.4 The frequency of SCEs in control and α-particles irradiated (0.5 and 1 Gy) immortal MEF cell cell lines, CBA/H (A), C57BL/6 (B) and 129Sv (C); 20 metaphase spreads were scored per cell line (control and α-particles irradiated); error bars are SEM; ns = non-significant *= p>0.05, **= p<0.01, ***= p<0.001

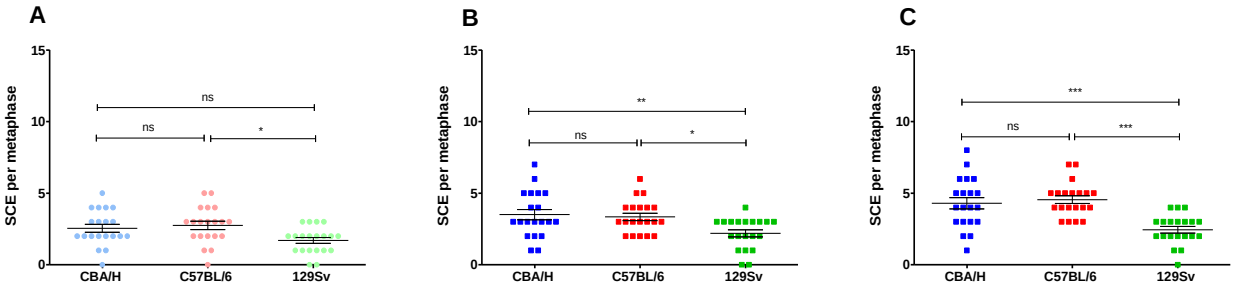


FIGURE 5.5 Comparison of the frequency of spontaneous (A), 0.5 Gy (B) and 1 Gy (C) α-particles induced SCEs in CBA/H, C57BL/6 and 129Sv immortal MEF cell lines; 20 metaphase spreads were scored per cell line; error bars are SEM; ns = non-significant, *= p>0.05, **= p<0.01; ***= p<0.001.

5.3.2 Sensitivity to radiation and HU in MEF cell lines

The clonogenic assay is the most widely used method to determine cell reproductive death after treatment with ionising radiation or other cytotoxic agents [114]. There were difficulties in obtaining sufficient plating efficiency with primary or immortal MEFs. A well-established type of clonogenic assay, called the dilution assay [188], can be used to obtain an estimate of the survival of cells which do not readily form colonies [189] (section 2.9.5.1). This method was initially used as a method to examine the radiosensitivity of CBA/H, C57BL/6 and 129Sv MEF cell lines. Control immortal MEFs (shGFP) as well as MEFs transfected with shRNA for CtIP knockdown were exposed to 0, 1, 5 and 10 Gy γ-radiation. The sensitivity to radiation was similar between the control or CtIP knockdown for all three cell lines except at the higher dose of 10 Gy where 129Sv shCtIP cells showed enhanced sensitivity in comparison to the CBA/H and C57BL/6 cell lines (**FIGURE 5.6**).

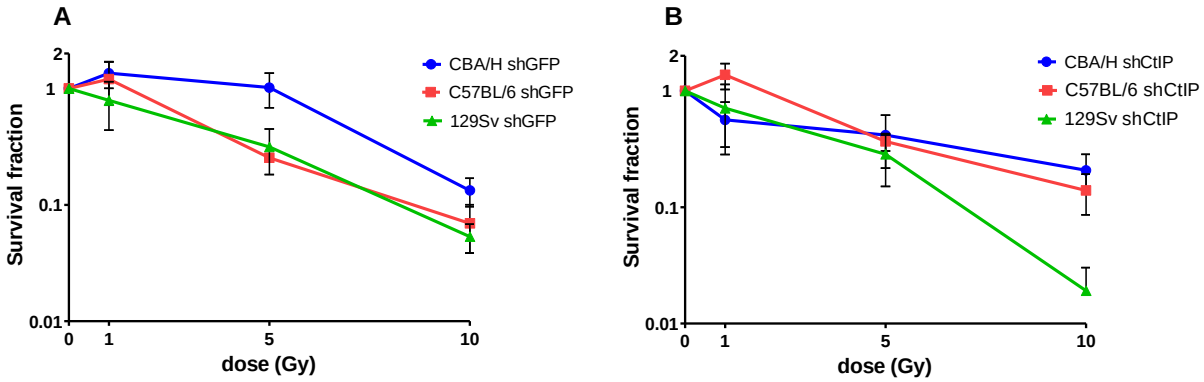


FIGURE 5.6 Dilution assay to determine dose dependence for cell survival with control (shGFP) (A) and CtIP KD (B) immortal MEFs: CBA/H, C57BL/6 and 129Sv, irradiated with γ-radiation; wells with no growth were counted after 7 days; n=3; error bars are SEM.

In order to use a standard colony forming assay [114] to measure cell survival, the low plating efficiency commonly observed with MEFs had to be overcome to enable comparison with the results obtained with the dilution assay. The clonogenic assay was therefore performed using large numbers of heavily irradiated (30 Gy) feeder cells, which

serve to condition the microenvironment of the much smaller number of cells to be tested for their colony formation [114, 240]. Based on the result obtained with the dilution assay, 129Sv shCtIP cells were included in the study to assess whether the CtIP gene containing the nsSNP influences not only DNA damage repair and SCE formation but also cellular inactivation as indicated from the dilution assay at 10 Gy γ-radiation.

As mentioned in the introduction of this chapter, cells defective in HR are much more sensitive to replication inhibitors, like HU which inhibits DNA synthesis [44], than wt cells. Differences in pRPA32 level post HU treatment were observed between the three different cell lines (section 4.3.4). Cell survival was therefore examined after exposure to ionising radiation (X- and γ-rays) or HU treatment. No differences were observed between immortal CBA/H, C57BL/6 and 129Sv MEF cell lines irradiated with 0, 1, 2, 3 and 4 Gy X-rays (**FIGURE 5.7**). The CtIP knockdown 129Sv cells also show the same radiosensitivity as the 129Sv control cells (**FIGURE 5.7**). Cells were also irradiated with 0, 1, 5 and the higher dose of 10 Gy γ-radiation to examine whether the differences between these three cell lines occur after exposure to higher doses of low LET radiation, as seen with the dilution assay with 129Sv cells. The radiosensitivity up to 10 Gy γ–rays was similar, with 129Sv cells being less radiosensitive and CBA/H cells more sensitive, although these differences were not statistically significant (**FIGURE 5.8**).

FIGURE 5.9 shows the survival of MEF cell lines after treatment with different concentrations of HU for a fixed time of 24 h. 129Sv and 129Sv shCtIP cells exhibited higher sensitivity than CBA/H and C57BL/6 to HU at concentrations of 2 and 5 mM. This observation is consistent with other published reports [14, 241] where cells defective in HR pathway were more sensitive to HU than control cells with no detected defect, such as CBA/H and C57BL/6 cells as used in these experiments.

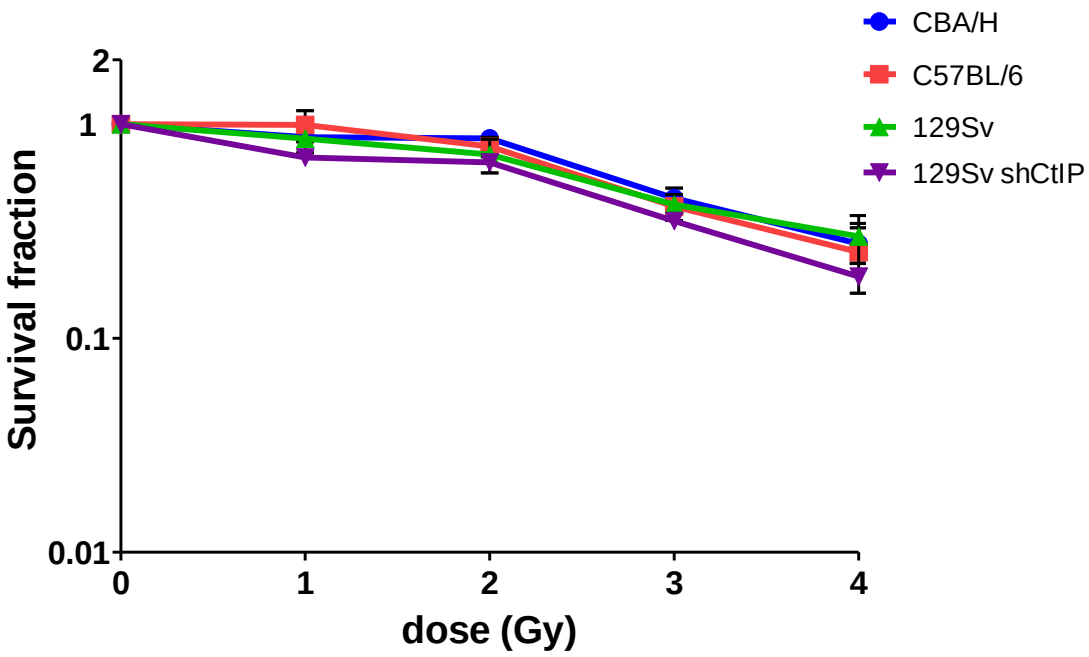


FIGURE 5.7 Clonogenic assay with immortal MEF cell lines: CBA/H, C57BL/6, 129Sv and 129Sv shCtIP, exposed to the stated doses of X-rays; colonies were counted after 7 days; n=3; error bars are SEM.

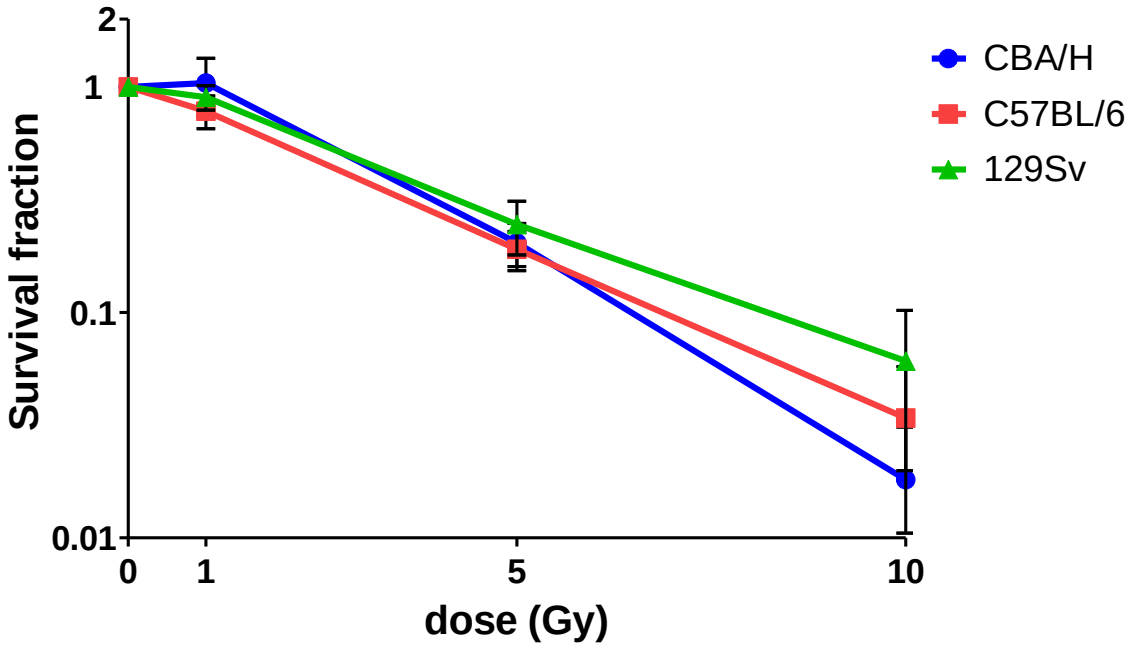


FIGURE 5.8 Clonogenic assay with immortal MEF cell lines: CBA/H, C57BL/6, 129Sv exposed to the stated doses of γ-radiation; colonies were counted after 7 days; n=3; error bars are SEM.

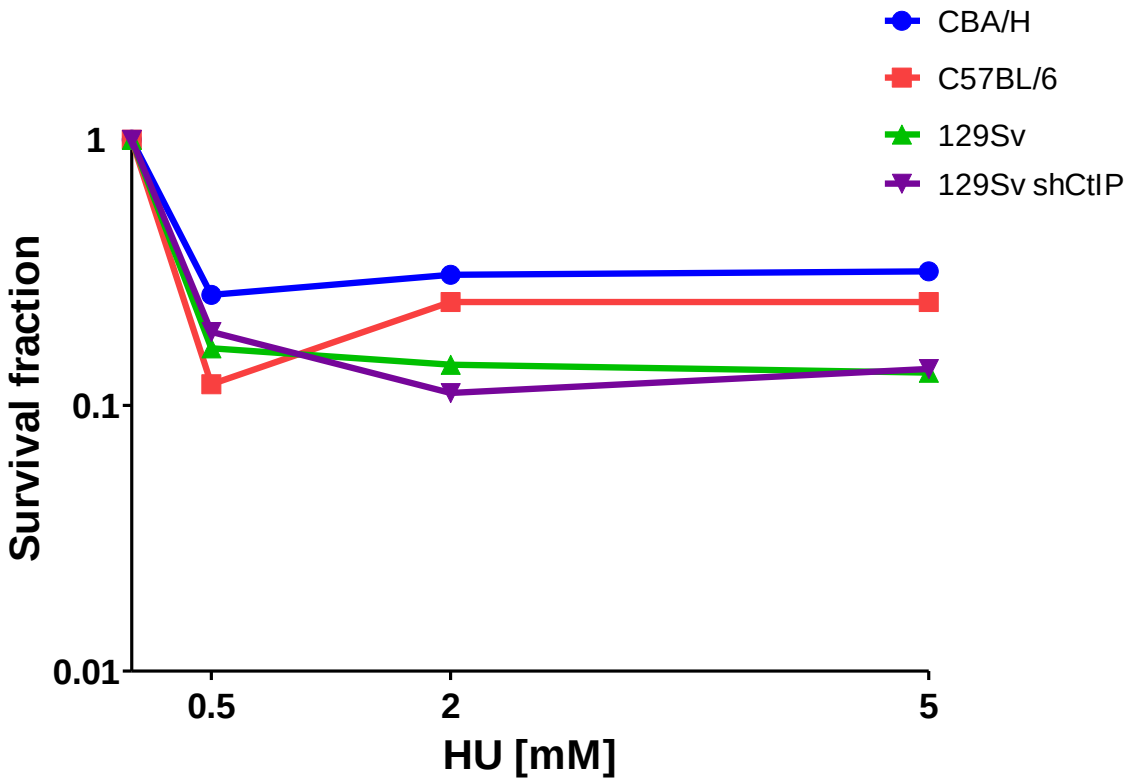


FIGURE 5.9 Clonogenic assay with immortal MEF cell lines: CBA/H, C57BL/6, 129Sv and 129Sv shCtIP, treated with the stated doses of HU for 24 h, medium was then changed and colonies were counted after 7 days; n=1.

The resazurin proliferation assay was also used to measure cell responses to ionising radiation, as it has been used as a reliable alternative method to clonogenic assays [191]. The resazurin assay (section 2.9.5.2) was performed with primary and immortal CBA/H, C57BL/6 and 129Sv MEF cell lines to measure cell proliferation after either γ-radiation or HU treatment. Large differences were not observed in the rate of proliferation between the three primary MEF cell lines 6 days post-irradiation. A small difference was seen in immortal CBA/H MEFs, which showed a somewhat higher proliferation rate than the other two cell lines (**FIGURE 5.10**). The differences between primary and immortal CBA/H cells could reflect that the proliferation assay with immortal MEFs was performed only once. After treatment with HU, the proliferation rate of 129Sv cells was much slower than that with C57BL/6 and slightly reduced compared to that seen with CBA/H (post 0.5 and 1 mM HU treatment) (**FIGURE 5.11A**). Immortal MEFs seemed to be affected even more by the treatment with increasing doses of HU than primary MEFs, although the experiment was only performed once. The trend between primary and immortal MEFs was similar in 129Sv cells, which demonstrated lower proliferation than the other two cell lines (**FIGURE 5.11**).

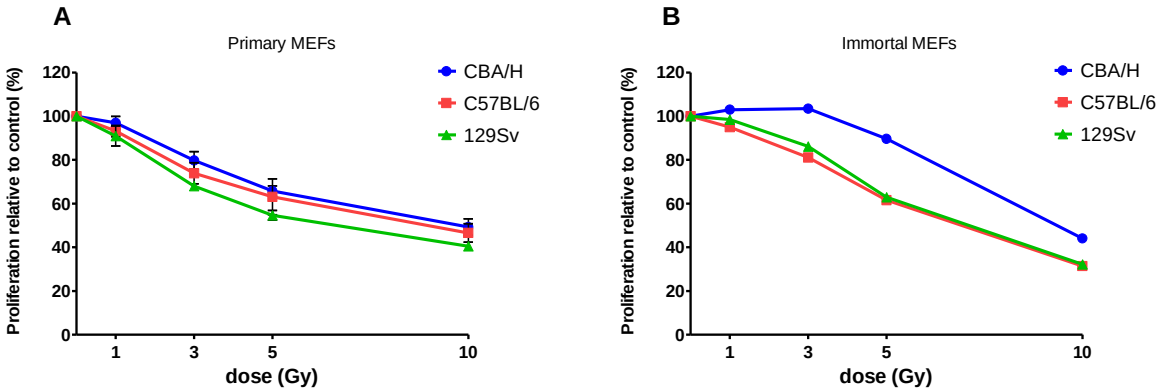


FIGURE 5.10 Resazurin proliferation assay with primary (A) and immortal (B) MEF cell lines: CBA/H, C57BL/6 and 129Sv. Cells were treated with stated doses of γ-radiation; absorbance was measured 6 days post treatment; n=3 (A), n=1 (B); error bars are SEM.

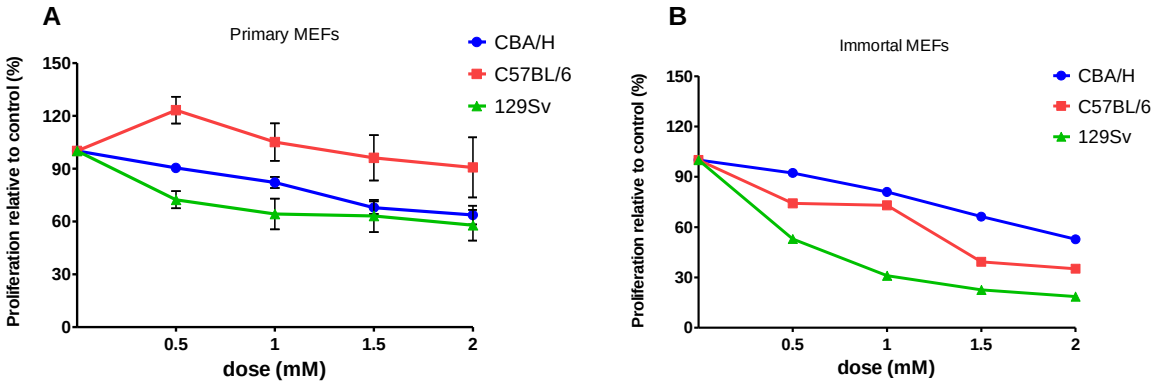


FIGURE 5.11 Resazurin proliferation assay with primary (A) and immortal (B) MEF cell lines: CBA/H, C57BL/6 and 129Sv. Cells were treated with stated doses of HU for 6 h, medium was then changed and absorbance was measured after 6 days; n=3 (A), n=1 (B); error bars are SEM.

5.4 Discussion

Previous reports have shown that cells defective in HR exhibit reduced numbers of spontaneous, MMC- or IR- induced SCE [137,139,39,138,140]. This includes cells depleted of CtIP, BRCA2 or Rad51 protein, which all showed a slight or significant decrease in spontaneous or 2 Gy X-ray-induced SCE yield when compared to CtIP, BRCA2 or Rad51 proficient cells [39, 138, 140]. 129Sv cells carrying the Q418P nsSNP within the CtIP gene, required for DSB resection during HR [22, 61], showed lower level of spontaneous, MMC or α-particle induced SCEs, compared to CBA/H and C57BL/6 cell lines. From the findings described in the literature as well as the finding showing lower level of SCEs in 129Sv cells, it is suggested that the nsSNP identified within the CtIP gene of the 129Sv cell line leads to impaired HR and as a consequence to reduced number of SCEs. Since CtIP is essential for DSB resection during HR, activation of proteins located downstream of CtIP, like RPA and Rad51 is CtIP dependent [61,221,70]. Therefore the finding that HR is impaired in 129Sv cells relative to CBA/H and C57BL/6 cell lines, is also consistent with the observation of reduced recruitment of Rad51 and RPA to the damage sites in 129Sv cells (section 4.3.3). The number of Rad51 and RPA positive cells in 129Sv cells was similar to CBA/H, C57BL/6 and 129Sv CtIP knock down cells, highlighting the level of HR impairment caused by the nsSNP.

Neither primary nor immortalised MEF cell lines, with the possible exception of 129Sv shCtIP, demonstrated any significant differences in sensitivity to ionising radiation, using dilution, clonogenic and resazurin proliferation assays. This lack of radiosensitivity is consistent with DSBs being repaired 24 h post γ-radiation, shown by a loss of γH2AX and 53BP1 foci (section 3.3.2). The 129Sv cell line with CtIP knock down may be more radiosensitive at 10 Gy radiation than the other two cell lines.

Small differences in survival with the replication inhibitor HU were observed between primary and immortal MEF cell lines by using proliferation and clonogenic assays. 129Sv cells were more sensitive to HU than CBA/H and C57BL/6 cells. This result is consistent with other studies, which have shown that cells defective in HR, Rad21 heterozygotes [137], RPA mutants [14] or CtIP knock down cells with added aphidicolin [61], are more sensitive to cytotoxic agents causing replication-associated DSBs, which require HR for repair [13].

A possible explanation for no differences in sensitivity to ionising radiation between the three cell lines could be back-up of impaired HR in 129Sv cells by NHEJ or SSA, although NHEJ is utilised to repair the majority of DSBs throughout the cell cycle. The DNA damage caused by cytotoxic agents like HU, however, results in replication DSBs which are mainly repaired by HR [14, 224] and possibly can not be repaired by a back-up pathway.

6 Discussion

Exposure to ionising radiation increases the risk of cancer, including AML, which is the most common myeloid leukaemia [154]. Using a surrogate assay of chromosomal radiosensitivity, CtIP has been identified as a potential candidate gene for susceptibility to radiation-induced AML [2], as well as a possible tumour suppressor [23]. In addition, homozygous inactivation of the CtIP gene causes very early embryonic lethality during mouse development [23] and CtIP heterozygote mice develop tumours, principally lymphomas. CtIP is also known to be required for resection during the repair of DSBs [22,61,51,52]. Therefore, the CtIP gene and its role in carcinogenesis, with particular respect to radiation-induced cancer, including rAML, is the focus of this thesis. The 129Sv mouse strain, was extensively studied during this project as its characteristic feature is the presence of a Q418P nsSNP within the CtIP gene. However, its sensitivity to rAML is unknown [180, 181]. The thesis therefore also examines whether the nsSNP influences CtIP function in DSB repair, cell cycle and survival upon induction of DNA damage.

6.1.1 The CtIP gene of 129Sv mouse strain contains disease-causing nsSNP

The Ensembl genome browser, used to check for the presence of nsSNPs within the mouse CtIP gene, identified seven nsSNPs, G7S, A16V, H338Y, Q418P, A498T and A882V which were checked by five algorithms (Panther, PhD-SNP, SIFT, SNAP and Meta-SNP) for disease prediction. Four nsSNPs (H338Y, Q418P, A498T, A882V) were predicted as disease-causing. The Q418P was the only one predicted by two out of the five algorithms as disease-causing, and additionally had a score very close to 0.5, the lower limit for

prediction of disease-causing, obtained with the PhD-SNP and Meta-SNP algorithms. Therefore, the Q418P is the most likely disease-causing missense variant of the seven CtIP nsSNPs assessed. The CBA/H, C57BL/6, and 129Sv strains of mice were tested for the presence of H338Y, Q418P, A498T and A882 nsSNPs and no nsSNPs were found in CBA/H and C57BL/6 strain. However the Q418P nsSNP was found in the 129Sv mouse strain (**TABLE 3.2**). The Q418P can be a strong disease-causing nsSNP, as it results in a change from acyclic amino acid (glutamine) into a cyclic one (proline), leading to a conformational change of a protein. This change can result in a disease-causing mutation [200, 211]. Two syndromes have been described as a consequence of nsSNPs present in the human CtIP gene [79]. Seckel and Jawad syndrome, which are recessively inherited dwarfism disorders, occur due to nsSNPs leading to premature stop codons in the CtIP transcript, and as a consequence lead to expression of a C-terminally truncated protein [79]. The Q418P nsSNP was identified as a potential modification at the protein level that could result in an impairment or reduction of CtIP function.

6.1.2 The CtIP nsSNP Q418P reduces the life span of 129Sv mice but not the survival of 129Sv MEF cell line following radiation and increases rAML development

Heterozygous inactivation of CtIP in mice results in tumour development, mainly lymphomas, indicating that CtIP functions as a tumour suppressor [22, 184]. Mouse models of radiation-induced AML have been developed to investigate the underlying processes of the disease, with the CBA/H strain being the most well studied [175]. CBA/H is a good model for rAML as spontaneous incidents of AML in this strain are very low- 0.1% [176]. C57BL/6 mouse strain is known to be resistant to rAML and therefore has been used in the past as well

as in this thesis as a control strain [176]. The 129Sv mouse strain, which was shown to have a nsSNP in CtIP gene, has an overall low incidence of spontaneous tumours, but its radiosensitivity to early onset of tumours including rAML was unknown [180, 181].

The three mouse strains, CBA/H, C57BL/6 and 129Sv, were exposed to a whole body, single, acute dose of 3 Gy X-rays in order to examine the differences in survival rate and cancer development. Irradiated CBA/H and 129Sv mice, in contrast to C57BL/6 strain, needed to be euthanised sooner in comparison to non-irradiated controls, indicating that radiation shortens their life span (**TABLE 3.3**). The finding in CBA/H mice is consistent with published data showing that the CBA/H strain is radio-sensitive relative to the known radio-resistant C57BL/6 strain [196]. The 129Sv strain showed a similar survival rate to CBA/H post-radiation (**TABLE 3.3** and **FIGURE 3.3**). This is in contrast to the earlier finding showing 129S/J to be radio-resistant [196]. This difference in radiosensitivity could be a result of genetic diversity between 129S2/SvHsd, used in this project (referred to as 129Sv), and the early work using the 129S/J strain. Alternatively, it could reflect the different experimental set ups. In the present study the mice were exposed to a single dose of 3 Gy X-rays whereas in the previous study [196] the mice were irradiated daily with 1 Gy X-rays until death.

The various indications of life-span shortening following irradiation were evaluated in 129Sv. The initial causes of death varied based on a variety of indirect indicators (Appendix B), however due to the prediction of a possible link between CtIP and rAML [2], the latter was examined in greater detail, and 11 % of irradiated 129Sv mice were diagnosed as possibly having rAML (Chapter 3). The number of suspected rAML cases, based on indirect markers, is lower than that seen in CBA/H mice (28 %), a strain well-known to develop rAML, but greater than the rAML resistant strain, C57BL/6, in which no suspected rAML cases were detected.

The differences in life span between the irradiated mouse strains did not correlate with the survival data obtained after irradiation of the MEF cell lines established from the three mouse strains. MEFs did not demonstrate any significant differences in radiosensitivity to low LET ionising radiation. However, small differences in survival with the replication inhibitor HU were observed between the three MEF cell lines. 129Sv and 129Sv, in which CtIP had been knocked down, were slightly more sensitive to HU than CBA/H and C57BL/6 cells (**FIGURE 5.9**). This is consistent with other reports which show no difference in radiosensitivity between wild type cells and cells defective in HR pathway, Rad21 heterozygotes [137] or RPA mutants [14]. However, differences in cell survival were observed in HR deficient cells (including CtIP knock down cells treated with aphidicolin [61]) after exposure to cytotoxic agents causing replication-associated DSBs (camptothecin, etoposide, HU, MMC) which require HR for repair [13,14,61,137].

A possible explanation could be that any impairment of HR in 129Sv cells is replaced by the NHEJ or SSA pathways, resulting in similar cell survival to CBA/H and C57BL/6 cells post-irradiation. A back-up pathway may not have been able to repair cellular DNA damage caused by HU, which depletes the nucleotide pool [44-46], as replication DSBs are mainly repaired by HR [14, 224] requiring a pool of nucleotides.

The mouse data suggests that the Q418P nsSNP, found only in the 129Sv mouse strain, may influence the life span as well as early onset of radiation-induced carcinogenesis, including rAML (11 %) and lung tumours (10 %), the second most common tumour identified in irradiated 129Sv mice (Appendix B).

As it has been established that the Q418 nsSNP does not affect radiosensitivity of MEF cells, the question arose whether it influences the efficiency of HR in the MEF cell lines.

6.1.3 The Q418P nsSNP impairs CtIP function

Upon DNA damage, CtIP plays a critical role in DSB resection, mainly in HR. It also carries out minimal resection of DNA broken ends in the alt-NHEJ repair pathway [22,61,51,52]. Therefore, impairment of CtIP function may affect the repair efficiency of radiation-induced DSBs, which may lead to genomic instability and cancer [50], but not significantly affect the cell's radiosensitivity.

CBA/H, C57BL/6 and 129Sv MEF cell lines were exposed to either low-LET γ-radiation or high-LET α-particles to assess DSB reparability and the effect of radiation quality using γH2AX and 53BP1 as markers of DSBs [62, 92]. With α-particles, some of the DSBs persisted for at least 24 h post-radiation, in contrast to γ-rays where the majority of the DSBs had been processed by 24 h. These observations are consistent with the concept of increased complexity of DNA damage induced by high LET α-particles compared with low LET γ-rays [37,62,92]. No difference was seen in the repair rate between the three MEF cell lines post 1 Gy γ-radiation, which might reflect that the majority of the radiation-induced DSBs were repaired by NHEJ. However, after 1 Gy α-particle irradiation a faster DSB repair was initially seen for a small fraction of DSBs in CBA/H and 129Sv cell lines, compared to C57BL/6. The small differences observed may be related to the use of the NHEJ pathway in the repair of the simpler DSBs caused by low LET radiation. CtIP may also play a role in alt-NHEJ, where minimal resection is needed [8], however, it is essential for DSB resection in HR [22, 61].

Due to the fact that γH2AX and 53BP1 are markers of DSBs repaired by NHEJ as well as HR, Rad51 and RPA were used as specific markers to look for any differences in the efficiency of HR repair in the three MEF lines. Lower recruitment of HR markers (Rad51 and RPA) to damage sites induced post-radiation or after treatment with HU or MMC,

were found in 129Sv MEF cells in comparison to CBA/H and C57BL/6 MEF cells (**FIGURE 6.1**). Similarly, phosphorylation of RPA32, induced by treatment with HU, was observed in CBA/H and C57BL/6 cells but not in 129Sv MEFs (**FIGURE 4.14** and **FIGURE 4.15**). Moreover, expression of ATR was significantly lower in 129Sv MEFs, independent of HU treatment, compared to the other two MEF cell lines (**FIGURE 4.16**). Data obtained using shRNA to knockdown CtIP in the three MEF lines (**FIGURE 4.18** and **FIGURE 4.19**) indicates that DSB resection is impaired due to reduced activity of CtIP. Therefore, it is proposed that the nsSNP within the CtIP gene of the 129Sv cell line causes reduced repair efficiency in HR. Taken together, these findings are consistent with previously published data, which shows that the activation of RPA [61, 71], Rad51 [70] and ATR [10], the key proteins involved in HR of DSB, is CtIP dependent [61,221,70].

Since the differences in efficiency of DSB repair by HR in MEF cell lines relate to the nsSNP in CtIP, the efficiency of HR was also examined using SCEs as a direct reflection of HR [88]. SCEs can occur spontaneously, as a product of normal DNA replication [226], through endogenous DNA damage [226], or can be induced by high LET [229, 230] and low LET radiation, as shown in G2 cells, [103,138,140]. Genotoxic agents, including MMC [187,227,228], also induce SCEs. In order to determine if any differences can be observed between CBA/H, C57BL/6 and 129Sv MEFs in the involvement of HR, the yield of SCEs following exposure to MMC and radiation were examined. 129Sv cells showed lower numbers of spontaneous, MMC and α-particles induced SCEs when compared to CBA/H and C57BL/6 cell lines (**TABLE 5.1** and **TABLE 5.2**). Lower SCE yield in 129Sv cells is consistent with several published reports showing that cells defective in HR (for example cells depleted of BRCA2 or Rad51) exhibit reduced numbers of SCEs [137,139,138,140].

In order to verify that reduced activity of CtIP in 129Sv cells is a consequence of the Q418P nsSNP, active CtIP was overexpressed in 129Sv cells, to compensate for the defect in CtIP. The number of radiation-induced Rad51 and RPA positive cells was restored when full-length CtIP was overexpressed in 129Sv cells, consistent with the proposal that the nsSNP impairs CtIP function and therefore recruitment of downstream proteins involved in HR, such as RPA.

The cell cycle distribution was determined in control and irradiated CBA/H, C57BL/6 and 129Sv MEFs to exclude the possibility that the number of Rad51 and RPA positive cells reflects differences in the S-phase population between the cell lines. The cell cycle distribution was very similar for C57BL/6 and 129Sv cell lines, whereas CBA/H exhibited a slightly smaller S-phase population (**FIGURE 4.24**). Therefore, the lower percentage of Rad51 and RPA positive cells observed in 129Sv MEFs is not due to significant differences in the S-phase population between the three cell lines.

The findings are consistent with the proposal that the Q418P nsSNP reduces CtIP's main function of DSB resection [22, 61] and as a consequence leads to impaired HR in 129Sv cells relative to CBA/H and C57BL/6 cell lines.

6.2 Conclusion

The CtIP gene and its role in carcinogenesis, including rAML, was the focus of this thesis. The Q418P, a strongly disease-causing nsSNP, identified within CtIP gene of 129Sv mouse strain has a strong influence on the efficiency of CtIP function in HR repair of DSBs and replication-induced DSBs. The impairment of HR appears to contribute to shortening of the life span of the mouse strain carrying this variant, and to increasing radiation-induced carcinogenesis, including rAML. New nsSNPs are constantly being

identified, therefore even though Q418P SNP has not yet been detected in humans, this or equivalent nsSNPs may be identified in the future.

An example of a disorder characterised by chromosomal instability, radiation sensitivity and enhanced cancer predisposition is Nijmegen breakage syndrome (NBS). This recessive genetic disorder has been linked to mutations within the NBS1 gene, involved in DSB repair, resulting in a truncated protein [242]. nsSNPs have been found in the NBS1 gene of patients diagnosed with hepatocellular carcinoma and intrahepatic cholangiocarcinoma [243]. Identification of nsSNPs and their impact on a specific gene could help further elucidate mechanisms of carcinogenesis and may help direct investigation into personalised (cancer) therapies.

7 Future Plans

The results described in this thesis are encouraging as they indicate increased carcinogenesis, including rAML, in irradiated 129Sv mice. The 129Sv mouse strain carries a nsSNP within the CtIP gene, which could be the cause of impaired HR and therefore susceptibility to cancer, as indicated by the described data. Further work is however needed in order to characterise tumours developed in 129Sv strain post radiation, as well as to confirm the presence of rAML in 9 out of the 78 irradiated 129Sv mice. The latter could be done by passaging the spleen cells from the 129Sv mice, diagnosed with possible rAML into recipient, non-irradiated 129Sv mice, in order to check for AML development.

The key feature of the rAML sensitive mouse strain (CBA/H) is the deletion of one copy of chromosome 2, following exposure to X-ray radiation. The deleted region includes the PU.1 gene, essential for the development of myeloid and lymphoid cell types. It would be of interest to determine, using comparative genomic hybridisation (CGH), whether deletion of chromosome 2 occurred in the 129Sv mice diagnosed with rAML.

Impaired HR can lead to chromosomal aberrations, including chromosomal rearrangements. Data presented in this thesis suggests impaired HR in 129Sv cell line, due to the nsSNP present in the CtIP gene of these cells. Therefore, it would be interesting to check for deletions or translocations in 129Sv MEF cells, using Multicolour-Fluorescence *In Situ* Hybridisation (M-FISH). Increased numbers of chromosomal rearrangements in the 129Sv cell line compared to CBA/H or C57BL/6 would further confirm the impairment of repair processes in 129Sv cells. However, in order to make sure that this impairment is due to the Q418P nsSNP within the CtIP gene, the nsSNP could be reversed using transcription

activator-like effector nucleases (TALENs). Higher HR levels in 129Sv cells with reversed nsSNP, compared to 129Sv carrying nsSNP would confirm the hypothesis.

The fidelity of HR in 129Sv cells could be defined using an HR assay, which includes the DR-GFP reporter and I-*Sce*I endonuclease. This assay could help explain why 129Sv cells showed no radiosensitivity in survival assays, and the number of DSBs (measured using γH2AX and 53BP1) returned to background 24 h post-irradiation, suggesting that DSBs have been repaired. However, Rad51 and RPA foci were lower at earlier times (up to 6 h) in 129Sv cells in comparison to CBA/H or C57BL/6. These results suggest that DSBs might be repaired incorrectly.

MMC is a DNA crosslinking agent, which causes replication-associated DSBs which require HR for repair. Data using SCEs as a marker of HR, presented in this thesis, showed lower level of SCEs in 129Sv cells compared with CBA/H or C57BL/6, and the biggest difference between the cell lines was seen post MMC treatment. Therefore MMC could be used as another method of demonstrating HR impairment, leading to a decrease in cell survival in 129Sv cells.

Further work is required to better understand how the Q418P nsSNP, located within the CtIP gene of the 129Sv mouse strain, affects carcinogenesis and impairment of DSB repair pathways, in particular HR.

Appendix A: References

1. Hall, E.J., *Radiobiology for the Radiologist 4th ed*. 1994, Philadelphia, USA: Lippincott Williams &Wilkins.
2. Darakhshan, F., et al., *Evidence for complex multigenic inheritance of radiation AML susceptibility in mice revealed using a surrogate phenotypic assay.* Carcinogenesis, 2006. **27**(2): p. 311-318.
3. Pouget, J.P. and S.J. Mather, *General aspects of the cellular response to low- and high-LET radiation.* Eur J Nucl Med, 2001. **28**(4): p. 541-61.
4. You, Z. and J.M. Bailis, *DNA damage and decisions: CtIP coordinates DNA repair and cell cycle checkpoints.* Trends Cell Biol, 2010. **20**(7): p. 402-9.
5. Peterson, S.E., et al., *Activation of DSB processing requires phosphorylation of CtIP by ATR.* Mol Cell, 2013. **49**(4): p. 657-67.
6. Buis, J., et al., *Mre11 regulates CtIP-dependent double-strand break repair by interaction with CDK2.* Nat Struct Mol Biol, 2012. **19**(2): p. 246-52.
7. Wang, H., et al., *CtIP protein dimerization is critical for its recruitment to chromosomal DNA double-stranded breaks.* J Biol Chem, 2012. **287**(25): p. 21471-80.
8. Yun, M.H. and K. Hiom, *CtIP-BRCA1 modulates the choice of DNA double-strand-break repair pathway throughout the cell cycle.* Nature, 2009. **459**(7245): p. 460-3.
9. Helleday, T., et al., *DNA double-strand break repair: from mechanistic understanding to cancer treatment.* DNA Repair (Amst), 2007. **6**(7): p. 923-35.
10. Sancar, A., et al., *Molecular mechanisms of mammalian DNA repair and the DNA damage checkpoints.* Annu Rev Biochem, 2004. **73**: p. 39-85.
11. Orr, B. and D.A. Compton, *A double-edged sword: how oncogenes and tumor suppressor genes can contribute to chromosomal instability.* Front Oncol, 2013. **3**: p. 164.
12. Stepanenko, A.A., Y.S. Vassetzky, and V.M. Kavsan, *Antagonistic functional duality of cancer genes.* Gene, 2013. **529**(2): p. 199-207.
13. Helleday, T., et al., *DNA repair pathways as targets for cancer therapy.* Nat Rev Cancer, 2008. **8**(3): p. 193-204.
14. Shi, W., et al., *The role of RPA2 phosphorylation in homologous recombination in response to replication arrest.* Carcinogenesis, 2010. **31**(6): p. 994-1002.
15. Parplys, A.C., et al., *DNA damage by X-rays and their impact on replication processes.* Radiother Oncol, 2012. **102**(3): p. 466-71.
16. Pouget, J.P., et al., *Formation of modified DNA bases in cells exposed either to gamma radiation or to high-LET particles.* Radiat Res, 2002. **157**(5): p. 589-95.
17. Harper, J.V., J.A. Anderson, and P. O'Neill, *Radiation induced DNA DSBs: Contribution from stalled replication forks?* DNA Repair (Amst), 2010. **9**(8): p. 907-13.
18. Kass, E.M. and M. Jasin, *Collaboration and competition between DNA double-strand break repair pathways.* FEBS Lett, 2010. **584**(17): p. 3703-8.
19. Lieber, M.R., *The mechanism of double-strand DNA break repair by the nonhomologous DNA end-joining pathway.* Annu Rev Biochem, 2010. **79**: p. 181-211.
20. Wang, H., et al., *The interaction of CtIP and Nbs1 connects CDK and ATM to regulate HR-mediated double-strand break repair.* PLoS Genet, 2013. **9**(2): p. e1003277.
21. Groth, P., et al., *Homologous recombination repairs secondary replication induced DNA double-strand breaks after ionizing radiation.* Nucleic Acids Res, 2012. **40**(14): p. 6585-94.
22. Liu, F. and W.H. Lee, *CtIP activates its own and cyclin D1 promoters via the E2F/RB pathway during G1/S progression.* Mol Cell Biol, 2006. **26**(8): p. 3124-34.

23. Chen, P.L., et al., *Inactivation of CtIP leads to early embryonic lethality mediated by G1 restraint and to tumorigenesis by haploid insufficiency.* Mol Cell Biol, 2005. **25**(9): p. 3535-42.
24. Hall, E.J., *Radiobiology for the Radiologist 5th ed*. 5th ed. 2000, Philadelphia, USA: Lippincott Williams & Williams.
25. Lehnert, S., *Biomolecular Action of Ionizing Radiation*, 2008, Taylor & Francis: New York, USA.
26. Roots, R., et al., *Characterization of hydroxyl radical-induced damage after sparsely and densely ionizing irradiation.* Int J Radiat Biol Relat Stud Phys Chem Med, 1985. **47**(2): p. 157-66.
27. Goodhead, D.T., *Initial events in the cellular effects of ionizing radiations: clustered damage in DNA.* Int J Radiat Biol, 1994. **65**(1): p. 7-17.
28. deLara, C.M., et al., *The effect of dimethyl sulfoxide on the induction of DNA double-strand breaks in V79-4 mammalian cells by alpha particles.* Radiat Res, 1995. **144**(1): p. 43-9.
29. Monson, R.R., Cleaver, J. E. & Abrams, H. L., *BEIR VII Phase 2: Health risks from exposure to low levels of ionising radiation.* 2006, Washington, D.C. USA: National Research Council, National Academies Press.
30. Dizdaroglu, M. and P. Jaruga, *Mechanisms of free radical-induced damage to DNA.* Free Radic Res, 2012. **46**(4): p. 382-419.
31. Wojewodzka, M., I. Buraczewska, and M. Kruszewski, *A modified neutral comet assay: elimination of lysis at high temperature and validation of the assay with anti-single-stranded DNA antibody.* Mutat Res, 2002. **518**(1): p. 9-20.
32. Lindahl, T., *Instability and decay of the primary structure of DNA.* Nature, 1993. **362**(6422): p. 709-15.
33. Harper, J.V., et al., *Induction of persistent double strand breaks following multiphoton irradiation of cycling and G1-arrested mammalian cells-replication-induced double strand breaks.* Photochem Photobiol, 2008. **84**(6): p. 1506-14.
34. Chan, W., et al., *Quantification of the 2-deoxyribonolactone and nucleoside 5'-aldehyde products of 2-deoxyribose oxidation in DNA and cells by isotope-dilution gas chromatography mass spectrometry: differential effects of gamma-radiation and Fe2+-EDTA.* J Am Chem Soc, 2010. **132**(17): p. 6145-53.
35. Nikjoo, H., et al., *Quantitative modelling of DNA damage using Monte Carlo track structure method.* Radiat Environ Biophys, 1999. **38**(1): p. 31-8.
36. Nikjoo, H., et al., *Track structure in radiation biology: theory and applications.* Int J Radiat Biol, 1998. **73**(4): p. 355-64.
37. Jenner, T.J., et al., *Induction and rejoining of DNA double-strand breaks in V79-4 mammalian cells following gamma- and alpha-irradiation.* Int J Radiat Biol, 1993. **64**(3): p. 265-73.
38. Riballo, E., et al., *A pathway of double-strand break rejoining dependent upon ATM, Artemis, and proteins locating to gamma-H2AX foci.* Mol Cell, 2004. **16**(5): p. 715-24.
39. Shibata, A., et al., *Factors determining DNA double-strand break repair pathway choice in G2 phase.* EMBO J, 2011. **30**(6): p. 1079-92.
40. Karlsson, K.H., et al., *Repair of radiation-induced heat-labile sites is independent of DNA-PKcs, XRCC1 and PARP.* Radiat Res, 2008. **169**(5): p. 506-12.
41. Dobbs, T.A., et al., *Interplay of two major repair pathways in the processing of complex double-strand DNA breaks.* DNA Repair (Amst), 2008. **7**(8): p. 1372-83.
42. Asaithamby, A., et al., *Repair of HZE-particle-induced DNA double-strand breaks in normal human fibroblasts.* Radiat Res, 2008. **169**(4): p. 437-46.
43. Jeggo, P.A. and M. Lobrich, *Artemis links ATM to double strand break rejoining.* Cell Cycle, 2005. **4**(3): p. 359-62.

44. Alvino, G.M., et al., *Replication in hydroxyurea: it's a matter of time.* Mol Cell Biol, 2007. **27**(18): p. 6396-406.
45. Lahkim Bennani-Belhaj, K., et al., *BLM Deficiency Is Not Associated with Sensitivity to Hydroxyurea-Induced Replication Stress.* J Nucleic Acids, 2010. **2010**.
46. Merrick, C.J., D. Jackson, and J.F. Diffley, *Visualization of altered replication dynamics after DNA damage in human cells.* J Biol Chem, 2004. **279**(19): p. 20067-75.
47. Deans, A.J. and S.C. West, *DNA interstrand crosslink repair and cancer.* Nat Rev Cancer, 2011. **11**(7): p. 467-480.
48. Keyes, S.R., et al., *Cytotoxicity and DNA crosslinks produced by mitomycin analogs in aerobic and hypoxic EMT6 cells.* Cancer Commun, 1991. **3**(10-11): p. 351-6.
49. Fujiwara, Y., Y. Kano, and Y. Yamamoto, *DNA interstrand cross-linking, repair, and SCE mechanism in human cells in special reference to Fanconi anemia.* Basic Life Sci, 1984. **29 Pt B**: p. 787-800.
50. Kocher, S., et al., *Radiation-induced double-strand breaks require ATM but not Artemis for homologous recombination during S-phase.* Nucleic Acids Res, 2012. **40**(17): p. 8336-47.
51. Escribano-Diaz, C., et al., *A cell cycle-dependent regulatory circuit composed of 53BP1-RIF1 and BRCA1-CtIP controls DNA repair pathway choice.* Mol Cell, 2013. **49**(5): p. 872-83.
52. Bennardo, N., et al., *Alternative-NHEJ is a mechanistically distinct pathway of mammalian chromosome break repair.* PLoS Genet, 2008. **4**(6): p. e1000110.
53. Truong, L.N., et al., *Microhomology-mediated End Joining and Homologous Recombination share the initial end resection step to repair DNA double-strand breaks in mammalian cells.* Proc Natl Acad Sci U S A, 2013. **110**(19): p. 7720-5.
54. Zhang, Y. and M. Jasin, *An essential role for CtIP in chromosomal translocation formation through an alternative end-joining pathway.* Nat Struct Mol Biol, 2011. **18**(1): p. 80-4.
55. Wang, M., et al., *PARP-1 and Ku compete for repair of DNA double strand breaks by distinct NHEJ pathways.* Nucleic Acids Res, 2006. **34**(21): p. 6170-82.
56. Mladenov, E. and G. Iliakis, *Induction and repair of DNA double strand breaks: the increasing spectrum of non-homologous end joining pathways.* Mutat Res, 2011. **711**(1-2): p. 61-72.
57. McVey, M. and S.E. Lee, *MMEJ repair of double-strand breaks (director's cut): deleted sequences and alternative endings.* Trends Genet, 2008. **24**(11): p. 529-38.
58. van Gent, D.C., J.H. Hoeijmakers, and R. Kanaar, *Chromosomal stability and the DNA double-stranded break connection.* Nat Rev Genet, 2001. **2**(3): p. 196-206.
59. Wang, H., et al., *Biochemical evidence for Ku-independent backup pathways of NHEJ.* Nucleic Acids Res, 2003. **31**(18): p. 5377-88.
60. Sugawara, N., G. Ira, and J.E. Haber, *DNA length dependence of the single-strand annealing pathway and the role of Saccharomyces cerevisiae RAD59 in double-strand break repair.* Mol Cell Biol, 2000. **20**(14): p. 5300-9.
61. Sartori, A.A., et al., *Human CtIP promotes DNA end resection.* Nature, 2007. **450**(7169): p. 509-14.
62. Yajima, H., et al., *The complexity of DNA double strand breaks is a critical factor enhancing end-resection.* DNA Repair (Amst), 2013.
63. Sung, P. and H. Klein, *Mechanism of homologous recombination: mediators and helicases take on regulatory functions.* Nat Rev Mol Cell Biol, 2006. **7**(10): p. 739-50.
64. Symington, L.S. and J. Gautier, *Double-strand break end resection and repair pathway choice.* Annu Rev Genet, 2011. **45**: p. 247-71.
65. Chinnadurai, G., *CtIP, a candidate tumor susceptibility gene is a team player with luminaries.* Biochim Biophys Acta, 2006. **1765**(1): p. 67-73.
66. Riches, L.C., A.M. Lynch, and N.J. Gooderham, *Early events in the mammalian response to DNA double-strand breaks.* Mutagenesis, 2008. **23**(5): p. 331-9.

67. Cortez, D., et al., *Requirement of ATM-dependent phosphorylation of brca1 in the DNA damage response to double-strand breaks.* Science, 1999. **286**(5442): p. 1162-6.
68. Yu, X. and J. Chen, *DNA damage-induced cell cycle checkpoint control requires CtIP, a phosphorylation-dependent binding partner of BRCA1 C-terminal domains.* Mol Cell Biol, 2004. **24**(21): p. 9478-86.
69. Huertas, P. and S.P. Jackson, *Human CtIP mediates cell cycle control of DNA end resection and double strand break repair.* J Biol Chem, 2009. **284**(14): p. 9558-65.
70. Simandlova, J., et al., *FBH1 disrupts RAD51 filaments in vitro and modulates homologous recombination in mammalian cells.* J Biol Chem, 2013.
71. Liaw, H., D. Lee, and K. Myung, *DNA-PK-dependent RPA2 hyperphosphorylation facilitates DNA repair and suppresses sister chromatid exchange.* PLoS One, 2011. **6**(6): p. e21424.
72. Liu, S., et al., *Distinct roles for DNA-PK, ATM and ATR in RPA phosphorylation and checkpoint activation in response to replication stress.* Nucleic Acids Res, 2012. **40**(21): p. 10780-94.
73. Stokes, P.H., et al., *Structural basis of the interaction of the breast cancer oncogene LMO4 with the tumour suppressor CtIP/RBBP8.* J Mol Biol, 2013. **425**(7): p. 1101-10.
74. Yu, X. and R. Baer, *Nuclear localization and cell cycle-specific expression of CtIP, a protein that associates with the BRCA1 tumor suppressor.* J Biol Chem, 2000. **275**(24): p. 18541-9.
75. Schaeper, U., et al., *Interaction between a cellular protein that binds to the C-terminal region of adenovirus E1A (CtBP) and a novel cellular protein is disrupted by E1A through a conserved PLDLS motif.* J Biol Chem, 1998. **273**(15): p. 8549-52.
76. Meloni, A.R., E.J. Smith, and J.R. Nevins, *A mechanism for Rb/p130-mediated transcription repression involving recruitment of the CtBP corepressor.* Proc Natl Acad Sci U S A, 1999. **96**(17): p. 9574-9.
77. Liu, V.F. and D.T. Weaver, *The ionizing radiation-induced replication protein A phosphorylation response differs between ataxia telangiectasia and normal human cells.* Mol Cell Biol, 1993. **13**(12): p. 7222-31.
78. Liu, B., et al., *CtIP is required for DNA damage-dependent induction of.* Cell Cycle, 2013. **13**(1).
79. Qvist, P., et al., *CtIP Mutations Cause Seckel and Jawad Syndromes.* PLoS Genet, 2011. **7**(10): p. e1002310.
80. Alderton, G.K., et al., *Seckel syndrome exhibits cellular features demonstrating defects in the ATR-signalling pathway.* Hum Mol Genet, 2004. **13**(24): p. 3127-38.
81. McIlwraith, M.J., et al., *Human DNA polymerase eta promotes DNA synthesis from strand invasion intermediates of homologous recombination.* Mol Cell, 2005. **20**(5): p. 783-92.
82. Bugreev, D.V., O.M. Mazina, and A.V. Mazin, *Rad54 protein promotes branch migration of Holliday junctions.* Nature, 2006. **442**(7102): p. 590-3.
83. Constantinou, A., et al., *Werner's syndrome protein (WRN) migrates Holliday junctions and co-localizes with RPA upon replication arrest.* EMBO Rep, 2000. **1**(1): p. 80-4.
84. Adair, G.M., et al., *Role of ERCC1 in removal of long non-homologous tails during targeted homologous recombination.* EMBO J, 2000. **19**(20): p. 5552-61.
85. Batty, D.P. and R.D. Wood, *Damage recognition in nucleotide excision repair of DNA.* Gene, 2000. **241**(2): p. 193-204.
86. Strumberg, D., et al., *Conversion of topoisomerase I cleavage complexes on the leading strand of ribosomal DNA into 5'-phosphorylated DNA double-strand breaks by replication runoff.* Mol Cell Biol, 2000. **20**(11): p. 3977-87.
87. Arnaudeau, C., C. Lundin, and T. Helleday, *DNA double-strand breaks associated with replication forks are predominantly repaired by homologous recombination involving an exchange mechanism in mammalian cells.* J Mol Biol, 2001. **307**(5): p. 1235-45.
88. Latt, S.A. and R.R. Schreck, *Sister chromatid exchange analysis.* Am J Hum Genet, 1980. **32**(3): p. 297-313.

89. Joshi, N. and S.G. Grant, *DNA double-strand break damage and repair assessed by pulsed-field gel electrophoresis.* Methods Mol Biol, 2005. **291**: p. 121-9.
90. Collins, A.R., *The comet assay for DNA damage and repair: principles, applications, and limitations.* Mol Biotechnol, 2004. **26**(3): p. 249-61.
91. Lobrich, M., et al., *gammaH2AX foci analysis for monitoring DNA double-strand break repair: strengths, limitations and optimization.* Cell Cycle, 2010. **9**(4): p. 662-9.
92. Leatherbarrow, E.L., et al., *Induction and quantification of gamma-H2AX foci following low and high LET-irradiation.* Int J Radiat Biol, 2006. **82**(2): p. 111-8.
93. Furuta, T., et al., *Phosphorylation of histone H2AX and activation of Mre11, Rad50, and Nbs1 in response to replication-dependent DNA double-strand breaks induced by mammalian DNA topoisomerase I cleavage complexes.* J Biol Chem, 2003. **278**(22): p. 20303-12.
94. Celeste, A., et al., *Histone H2AX phosphorylation is dispensable for the initial recognition of DNA breaks.* Nat Cell Biol, 2003. **5**(7): p. 675-9.
95. Rothkamm, K. and M. Lobrich, *Evidence for a lack of DNA double-strand break repair in human cells exposed to very low x-ray doses.* Proc Natl Acad Sci U S A, 2003. **100**(9): p. 5057-62.
96. Rogakou, E.P., et al., *Megabase chromatin domains involved in DNA double-strand breaks in vivo.* J Cell Biol, 1999. **146**(5): p. 905-16.
97. Stiff, T., et al., *ATM and DNA-PK function redundantly to phosphorylate H2AX after exposure to ionizing radiation.* Cancer Res, 2004. **64**(7): p. 2390-6.
98. Zhou, C., et al., *DNA damage evaluated by gammaH2AX foci formation by a selective group of chemical/physical stressors.* Mutat Res, 2006. **604**(1-2): p. 8-18.
99. Gulston, M., et al., *Processing of clustered DNA damage generates additional double-strand breaks in mammalian cells post-irradiation.* Nucleic Acids Res, 2004. **32**(4): p. 1602-9.
100. Lassmann, M., et al., *In vivo formation of gamma-H2AX and 53BP1 DNA repair foci in blood cells after radioiodine therapy of differentiated thyroid cancer.* J Nucl Med, 2010. **51**(8): p. 1318-25.
101. Schultz, L.B., et al., *p53 binding protein 1 (53BP1) is an early participant in the cellular response to DNA double-strand breaks.* J Cell Biol, 2000. **151**(7): p. 1381-90.
102. Celeste, A., et al., *Genomic instability in mice lacking histone H2AX.* Science, 2002. **296**(5569): p. 922-7.
103. Kakarougkas, A., et al., *Opposing roles for 53BP1 during homologous recombination.* Nucleic Acids Res, 2013.
104. Sedelnikova, O.A., et al., *Senescing human cells and ageing mice accumulate DNA lesions with unrepairable double-strand breaks.* Nat Cell Biol, 2004. **6**(2): p. 168-70.
105. Banath, J.P., S.H. Macphail, and P.L. Olive, *Radiation sensitivity, H2AX phosphorylation, and kinetics of repair of DNA strand breaks in irradiated cervical cancer cell lines.* Cancer Res, 2004. **64**(19): p. 7144-9.
106. Hitomi, K., S. Iwai, and J.A. Tainer, *The intricate structural chemistry of base excision repair machinery: implications for DNA damage recognition, removal, and repair.* DNA Repair (Amst), 2007. **6**(4): p. 410-28.
107. Hegde, M.L., T.K. Hazra, and S. Mitra, *Early steps in the DNA base excision/single-strand interruption repair pathway in mammalian cells.* Cell Res, 2008. **18**(1): p. 27-47.
108. Fortini, P. and E. Dogliotti, *Base damage and single-strand break repair: mechanisms and functional significance of short- and long-patch repair subpathways.* DNA Repair (Amst), 2007. **6**(4): p. 398-409.
109. Mantha, A.K., B. Sarkar, and G. Tell, *A short review on the implications of base excision repair pathway for neurons: Relevance to neurodegenerative diseases.* Mitochondrion, 2013.

110. Nikjoo, H., et al., *Computational approach for determining the spectrum of DNA damage induced by ionizing radiation.* Radiat Res, 2001. **156**(5 Pt 2): p. 577-83.
111. Pinto, M., K.M. Prise, and B.D. Michael, *Evidence for complexity at the nanometer scale of radiation-induced DNA DSBs as a determinant of rejoining kinetics.* Radiat Res, 2005. **164**(1): p. 73-85.
112. *Relative biological effectiveness (RBE), quality factor (Q), and radiation weighting factor (w(R)). A report of the International Commission on Radiological Protection.* Ann ICRP, 2003. **33**(4): p. 1-117.
113. Franken, N.A., et al., *Comparison of RBE values of high-LET alpha-particles for the induction of DNA-DSBs, chromosome aberrations and cell reproductive death.* Radiat Oncol, 2011. **6**: p. 64.
114. Franken, N.A., et al., *Clonogenic assay of cells in vitro.* Nat Protoc, 2006. **1**(5): p. 2315-9.
115. Weisenthal, L.M. and M.E. Lippman, *Clonogenic and nonclonogenic in vitro chemosensitivity assays.* Cancer Treat Rep, 1985. **69**(6): p. 615-32.
116. Yoshikawa, T., et al., *Phosphorylated H2AX foci in tumor cells have no correlation with their radiation sensitivities.* J Radiat Res, 2009. **50**(2): p. 151-60.
117. Barendsen, G.W., *The relationships between RBE and LET for different types of lethal damage in mammalian cells: biophysical and molecular mechanisms.* Radiat Res, 1994. **139**(3): p. 257-70.
118. Barendsen, G.W., *RBE-LET relationships for different types of lethal radiation damage in mammalian cells: comparison with DNA dsb and an interpretation of differences in radiosensitivity.* Int J Radiat Biol, 1994. **66**(5): p. 433-6.
119. Barendsen, G.W., *Sublethal damage and DNA double strand breaks have similar RBE-LET relationships: evidence and implications.* Int J Radiat Biol, 1993. **63**(3): p. 325-30.
120. Falk, M., E. Lukasova, and S. Kozubek, *Chromatin structure influences the sensitivity of DNA to gamma-radiation.* Biochim Biophys Acta, 2008. **1783**(12): p. 2398-414.
121. Magnander, K., et al., *Clustered DNA damage in irradiated human diploid fibroblasts: influence of chromatin organization.* Radiat Res, 2010. **173**(3): p. 272-82.
122. Goodarzi, A.A., et al., *ATM signaling facilitates repair of DNA double-strand breaks associated with heterochromatin.* Mol Cell, 2008. **31**(2): p. 167-77.
123. Goodarzi, A.A., A.T. Noon, and P.A. Jeggo, *The impact of heterochromatin on DSB repair.* Biochem Soc Trans, 2009. **37**(Pt 3): p. 569-76.
124. Guenther, M.G., et al., *A chromatin landmark and transcription initiation at most promoters in human cells.* Cell, 2007. **130**(1): p. 77-88.
125. Goodarzi, A.A., P. Jeggo, and M. Lobrich, *The influence of heterochromatin on DNA double strand break repair: Getting the strong, silent type to relax.* DNA Repair (Amst), 2010. **9**(12): p. 1273-82.
126. Goodarzi, A.A. and P.A. Jeggo, *The heterochromatic barrier to DNA double strand break repair: how to get the entry visa.* Int J Mol Sci, 2012. **13**(9): p. 11844-60.
127. Richmond, T.J., et al., *Structure of the nucleosome core particle at 7 A resolution.* Nature, 1984. **311**(5986): p. 532-7.
128. Kouzarides, T., *Chromatin modifications and their function.* Cell, 2007. **128**(4): p. 693-705.
129. Wang, H., et al., *Efficient rejoining of radiation-induced DNA double-strand breaks in vertebrate cells deficient in genes of the RAD52 epistasis group.* Oncogene, 2001. **20**(18): p. 2212-24.
130. Reynolds, P., et al., *The dynamics of Ku70/80 and DNA-PKcs at DSBs induced by ionizing radiation is dependent on the complexity of damage.* Nucleic Acids Res, 2012. **40**(21): p. 10821-31.
131. Rief, N. and M. Lobrich, *Efficient rejoining of radiation-induced DNA double-strand breaks in centromeric DNA of human cells.* J Biol Chem, 2002. **277**(23): p. 20572-82.

132. Chiolo, I., et al., *Double-strand breaks in heterochromatin move outside of a dynamic HP1a domain to complete recombinational repair.* Cell, 2011. **144**(5): p. 732-44.
133. Asaithamby, A., B. Hu, and D.J. Chen, *Unrepaired clustered DNA lesions induce chromosome breakage in human cells.* Proc Natl Acad Sci U S A, 2011. **108**(20): p. 8293-8.
134. Jakob, B., et al., *DNA double-strand breaks in heterochromatin elicit fast repair protein recruitment, histone H2AX phosphorylation and relocation to euchromatin.* Nucleic Acids Res, 2011. **39**(15): p. 6489-99.
135. Frankenberg-Schwager, M., et al., *Single-strand annealing, conservative homologous recombination, nonhomologous DNA end joining, and the cell cycle-dependent repair of DNA double-strand breaks induced by sparsely or densely ionizing radiation.* Radiat Res, 2009. **171**(3): p. 265-73.
136. Hill, M.A., et al., *Relative sensitivities of repair-deficient mammalian cells for clonogenic survival after alpha-particle irradiation.* Radiat Res, 2004. **162**(6): p. 667-76.
137. Xu, H., et al., *Rad21-cohesin haploinsufficiency impedes DNA repair and enhances gastrointestinal radiosensitivity in mice.* PLoS One, 2010. **5**(8): p. e12112.
138. Conrad, S., J. Kunzel, and M. Lobrich, *Sister chromatid exchanges occur in G2-irradiated cells.* Cell Cycle, 2011. **10**(2): p. 222-8.
139. Sonoda, E., et al., *Sister chromatid exchanges are mediated by homologous recombination in vertebrate cells.* Mol Cell Biol, 1999. **19**(7): p. 5166-9.
140. Beucher, A., et al., *ATM and Artemis promote homologous recombination of radiation-induced DNA double-strand breaks in G2.* EMBO J, 2009. **28**(21): p. 3413-27.
141. Radman, M., P. Jeggo, and R. Wagner, *Chromosomal rearrangement and carcinogenesis.* Mutat Res, 1982. **98**(3): p. 249-64.
142. Quesnel, B., et al., *Therapy-related acute myeloid leukemia with t(8;21), inv(16), and t(8;16): a report on 25 cases and review of the literature.* J Clin Oncol, 1993. **11**(12): p. 2370-9.
143. Zech, L., et al., *Characteristic chromosomal abnormalities in biopsies and lymphoid-cell lines from patients with Burkitt and non-Burkitt lymphomas.* Int J Cancer, 1976. **17**(1): p. 47-56.
144. Rowley, J.D. and H.J. Olney, *International workshop on the relationship of prior therapy to balanced chromosome aberrations in therapy-related myelodysplastic syndromes and acute leukemia: overview report.* Genes Chromosomes Cancer, 2002. **33**(4): p. 331-45.
145. Knudson, A.G., Jr., et al., *Chromosomal deletion and retinoblastoma.* N Engl J Med, 1976. **295**(20): p. 1120-3.
146. Hughes, J.S., et al., *Review of the radiation exposure of the UK population.* J Radiol Prot, 2005. **25**(4): p. 493-6.
147. Gilbert, E.S., *Ionising radiation and cancer risks: what have we learned from epidemiology?* Int J Radiat Biol, 2009. **85**(6): p. 467-82.
148. Sill, H., et al., *Therapy-related myeloid neoplasms: pathobiology and clinical characteristics.* Br J Pharmacol, 2011. **162**(4): p. 792-805.
149. Pierce, D.A., et al., *Studies of the mortality of atomic bomb survivors. Report 12, Part I. Cancer: 1950-1990.* Radiat Res, 1996. **146**(1): p. 1-27.
150. Nakanishi, M., et al., *Chromosomal instability in acute myelocytic leukemia and myelodysplastic syndrome patients among atomic bomb survivors.* J Radiat Res, 1999. **40**(2): p. 159-67.
151. Kamada, N., et al., *Cytogenetic and molecular changes in leukemia among atomic bomb survivors.* J Radiat Res, 1991. **32 Suppl 2**: p. 257-65.
152. Kogan, S.C., et al., *Bethesda proposals for classification of nonlymphoid hematopoietic neoplasms in mice.* Blood, 2002. **100**(1): p. 238-45.
153. Matutes, E., et al., *Definition of acute biphenotypic leukemia.* Haematologica, 1997. **82**(1): p. 64-6.

154. Estey, E. and H. Dohner, *Acute myeloid leukaemia.* Lancet, 2006. **368**(9550): p. 1894-907.
155. Grigoropoulos, N.F., et al., *Leukaemia update. Part 1: diagnosis and management.* BMJ, 2013. **346**: p. f1660.
156. Dohner, H., et al., *Diagnosis and management of acute myeloid leukemia in adults: recommendations from an international expert panel, on behalf of the European LeukemiaNet.* Blood, 2010. **115**(3): p. 453-74.
157. van der Loo, J.C., et al., *Identification of hematopoietic stem cell subsets on the basis of their primitiveness using antibody ER-MP12.* Blood, 1995. **85**(4): p. 952-62.
158. Spangrude, G.J., S. Heimfeld, and I.L. Weissman, *Purification and characterization of mouse hematopoietic stem cells.* Science, 1988. **241**(4861): p. 58-62.
159. Iwasaki, H. and K. Akashi, *Hematopoietic developmental pathways: on cellular basis.* Oncogene, 2007. **26**(47): p. 6687-96.
160. Dave, V.P., *Hierarchical role of CD3 chains in thymocyte development.* Immunol Rev, 2009. **232**(1): p. 22-33.
161. Hardy, R.R. and K. Hayakawa, *B cell development pathways.* Annu Rev Immunol, 2001. **19**: p. 595-621.
162. Leone, G., et al., *Therapy-related leukemia and myelodysplasia: susceptibility and incidence.* Haematologica, 2007. **92**(10): p. 1389-98.
163. Smith, S.M., et al., *Clinical-cytogenetic associations in 306 patients with therapy-related myelodysplasia and myeloid leukemia: the University of Chicago series.* Blood, 2003. **102**(1): p. 43-52.
164. Pedersen-Bjergaard, J., M.K. Andersen, and B. Johansson, *Balanced chromosome aberrations in leukemias following chemotherapy with DNA-topoisomerase II inhibitors.* J Clin Oncol, 1998. **16**(5): p. 1897-8.
165. Nakamori, Y., et al., *Therapy-related erythroleukemia caused by the administration of UFT and mitomycin C in a patient with colon cancer.* Int J Clin Oncol, 2003. **8**(1): p. 56-9.
166. Johansson, A.S., et al., *Structure-activity relationships and thermal stability of human glutathione transferase P1-1 governed by the H-site residue 105.* J Mol Biol, 1998. **278**(3): p. 687-98.
167. Sasai, Y., et al., *Genotype of glutathione S-transferase and other genetic configurations in myelodysplasia.* Leuk Res, 1999. **23**(11): p. 975-81.
168. Seedhouse, C., et al., *Polymorphisms in genes involved in homologous recombination repair interact to increase the risk of developing acute myeloid leukemia.* Clin Cancer Res, 2004. **10**(8): p. 2675-80.
169. Brusamolino, E., et al., *The risk of acute leukemia in patients treated for Hodgkin's disease is significantly higher aft [see bined modality programs than after chemotherapy alone and is correlated with the extent of radiotherapy and type and duration of chemotherapy: a case-control study.* Haematologica, 1998. **83**(9): p. 812-23.
170. Pui, C.H., et al., *Risk of adverse events after completion of therapy for childhood acute lymphoblastic leukemia.* J Clin Oncol, 2005. **23**(31): p. 7936-41.
171. Le Deley, M.C., et al., *Risk of secondary leukemia after a solid tumor in childhood according to the dose of epipodophyllotoxins and anthracyclines: a case-control study by the Societe Francaise d'Oncologie Pediatrique.* J Clin Oncol, 2003. **21**(6): p. 1074-81.
172. Bennett, J.M., et al., *Proposals for the classification of the acute leukaemias. French-American-British (FAB) co-operative group.* Br J Haematol, 1976. **33**(4): p. 451-8.
173. Vardiman, J.W., N.L. Harris, and R.D. Brunning, *The World Health Organization (WHO) classification of the myeloid neoplasms.* Blood, 2002. **100**(7): p. 2292-302.
174. Vardiman, J.W., et al., *The 2008 revision of the World Health Organization (WHO) classification of myeloid neoplasms and acute leukemia: rationale and important changes.* Blood, 2009. **114**(5): p. 937-51.

175. Mole, R.H., D.G. Papworth, and M.J. Corp, *The dose-response for x-ray induction of myeloid leukaemia in male CBA/H mice.* Br J Cancer, 1983. **47**(2): p. 285-91.
176. Boulton, E., et al., *Low-penetrance genetic susceptibility and resistance loci implicated in the relative risk for radiation-induced acute myeloid leukemia in mice.* Blood, 2003. **101**(6): p. 2349-54.
177. Dekkers, F., et al., *A two-mutation model of radiation-induced acute myeloid leukemia using historical mouse data.* Radiat Environ Biophys, 2011. **50**(1): p. 37-45.
178. Weil, M.M., et al., *Incidence of acute myeloid leukemia and hepatocellular carcinoma in mice irradiated with 1 GeV/nucleon (56)Fe ions.* Radiat Res, 2009. **172**(2): p. 213-9.
179. Suraweera, N., et al., *Mutations of the PU.1 Ets domain are specifically associated with murine radiation-induced, but not human therapy-related, acute myeloid leukaemia.* Oncogene, 2005. **24**(22): p. 3678-83.
180. Smith, G.S., R.L. Walford, and M.R. Mickey, *Lifespan and incidence of cancer and other diseases in selected long-lived inbred mice and their F 1 hybrids.* J Natl Cancer Inst, 1973. **50**(5): p. 1195-213.
181. Festing, M.F. and D.K. Blackmore, *Life span of specified-pathogen-free (MRC category 4) mice and rats.* Lab Anim, 1971. **5**(2): p. 179-92.
182. Bouffler, S.D., et al., *Chromosome 2 hypersensitivity and clonal development in murine radiation acute myeloid leukaemia.* Int J Radiat Biol, 1997. **72**(2): p. 181-9.
183. Wong, A.K., et al., *Characterization of a carboxy-terminal BRCA1 interacting protein.* Oncogene, 1998. **17**(18): p. 2279-85.
184. Gu, B. and P.L. Chen, *Expression of PCNA-binding domain of CtIP, a motif required for CtIP localization at DNA replication foci, causes DNA damage and activation of DNA damage checkpoint.* Cell Cycle, 2009. **8**(9): p. 1409-20.
185. Dirac, A.M. and R. Bernards, *Reversal of senescence in mouse fibroblasts through lentiviral suppression of p53.* J Biol Chem, 2003. **278**(14): p. 11731-4.
186. Bunting, S.F., et al., *53BP1 inhibits homologous recombination in Brca1-deficient cells by blocking resection of DNA breaks.* Cell, 2010. **141**(2): p. 243-54.
187. Moquet, J.E., et al., *Sister-chromatid exchanges induced by mitomycin C after exposure of human lymphocytes in G0 to a low dose of X-radiation.* Mutat Res, 1987. **176**(1): p. 143-6.
188. Hewitt, H.B. and C.W. Wilson, *A survival curve for mammalian leukaemia cells irradiated in vivo (implications for the treatment of mouse leukaemia by whole-body irradiation).* Br J Cancer, 1959. **13**(1): p. 69-75.
189. Grenman, R., et al., *Clonogenic cell assay for anchorage-dependent squamous carcinoma cell lines using limiting dilution.* Int J Cancer, 1989. **44**(1): p. 131-6.
190. Roberts, S.A., *Determination of cell dose-survival relationships from endpoint dilution assays.* Int J Radiat Biol, 1993. **64**(2): p. 251-5.
191. Anoopkumar-Dukie, S., et al., *Resazurin assay of radiation response in cultured cells.* Br J Radiol, 2005. **78**(934): p. 945-7.
192. Cook, W.D., et al., *PU.1 is a suppressor of myeloid leukemia, inactivated in mice by gene deletion and mutation of its DNA binding domain.* Blood, 2004. **104**(12): p. 3437-44.
193. Mueller, B.U., et al., *Heterozygous PU.1 mutations are associated with acute myeloid leukemia.* Blood, 2002. **100**(3): p. 998-1007.
194. Simpson, E.M., et al., *Genetic variation among 129 substrains and its importance for targeted mutagenesis in mice.* Nat Genet, 1997. **16**(1): p. 19-27.
195. Grahn, D., *Acute Radiation Response of Mice from a Cross between Radiosensitive and Radioresistant Strains.* Genetics, 1958. **43**(5): p. 835-43.
196. Roderick, T.H., *The response of twenty-seven inbred strains of mice to daily doses of whole-body X-irradiation.* Radiat Res, 1963. **20**: p. 631-9.
197. Henriquez-Hernandez, L.A., et al., *High-throughput genotyping system as a robust and useful tool in oncology: Experience from a single institution.* Biologicals, 2013.

198. Kumar, P., S. Henikoff, and P.C. Ng, *Predicting the effects of coding non-synonymous variants on protein function using the SIFT algorithm.* Nat Protoc, 2009. **4**(7): p. 1073-81.
199. Johansen, M.B., et al., *Prediction of disease causing non-synonymous SNPs by the Artificial Neural Network Predictor NetDiseaseSNP.* PLoS One, 2013. **8**(7): p. e68370.
200. Kundu, A., et al., *Leucine to proline substitution by SNP at position 197 in Caspase-9 gene expression leads to neuroblastoma: a bioinformatics analysis.* 3 Biotech, 2013. **3**(3): p. 225-34.
201. Abel, K.J., et al., *Mouse Brca1: localization sequence analysis and identification of evolutionarily conserved domains.* Hum Mol Genet, 1995. **4**(12): p. 2265-73.
202. Peng, M., et al., *Inactivating Mutations in GT198 in Familial and Early-Onset Breast and Ovarian Cancers.* Genes Cancer, 2013. **4**(1-2): p. 15-25.
203. Yin, Z.-B., et al., *Smoking and hOGG1 Ser326Cys polymorphism contribute to lung cancer risk: evidence from a meta-analysis.* Tumor Biology, 2013: p. 1-10.
204. Rubio-Moscardo, F., et al., *Rare Variants in Calcium Homeostasis Modulator 1 (CALHM1) Found in Early Onset Alzheimer's Disease Patients Alter Calcium Homeostasis.* PLoS One, 2013. **8**(9): p. e74203.
205. Capriotti, E., R. Calabrese, and R. Casadio, *Predicting the insurgence of human genetic diseases associated to single point protein mutations with support vector machines and evolutionary information.* Bioinformatics, 2006. **22**(22): p. 2729-34.
206. Gnad, F., et al., *Assessment of computational methods for predicting the effects of missense mutations in human cancers.* BMC Genomics, 2013. **14 Suppl 3**: p. S7.
207. Ng, P.C. and S. Henikoff, *Predicting deleterious amino acid substitutions.* Genome Res, 2001. **11**(5): p. 863-74.
208. Mi, H., et al., *PANTHER version 6: protein sequence and function evolution data with expanded representation of biological pathways.* Nucleic Acids Res, 2007. **35**(Database issue): p. D247-52.
209. Li, S., et al., *Snap: an integrated SNP annotation platform.* Nucleic Acids Res, 2007. **35**(Database issue): p. D707-10.
210. Capriotti, E., R.B. Altman, and Y. Bromberg, *Collective judgment predicts disease-associated single nucleotide variants.* BMC Genomics, 2013. **14 Suppl 3**: p. S2.
211. Chipev, C.C., et al., *A leucine----proline mutation in the H1 subdomain of keratin 1 causes epidermolytic hyperkeratosis.* Cell, 1992. **70**(5): p. 821-8.
212. Major, I.R. and R.H. Mole, *Myeloid leukaemia in x-ray irradiated CBA mice.* Nature, 1978. **272**(5652): p. 455-6.
213. Hestdal, K., et al., *Characterization and regulation of RB6-8C5 antigen expression on murine bone marrow cells.* J Immunol, 1991. **147**(1): p. 22-8.
214. Arnaout, M.A., *Structure and function of the leukocyte adhesion molecules CD11/CD18.* Blood, 1990. **75**(5): p. 1037-50.
215. Olme, C.H., et al., *Live cell detection of chromosome 2 deletion and Sfpi1/PU1 loss in radiation-induced mouse acute myeloid leukaemia.* Leuk Res, 2013. **37**(10): p. 1374-82.
216. Steger, M., et al., *Prolyl isomerase PIN1 regulates DNA double-strand break repair by counteracting DNA end resection.* Mol Cell, 2013. **50**(3): p. 333-43.
217. Balajee, A.S. and C.R. Geard, *Replication protein A and gamma-H2AX foci assembly is triggered by cellular response to DNA double-strand breaks.* Exp Cell Res, 2004. **300**(2): p. 320-34.
218. Syljuasen, R.G., et al., *Inhibition of human Chk1 causes increased initiation of DNA replication, phosphorylation of ATR targets, and DNA breakage.* Mol Cell Biol, 2005. **25**(9): p. 3553-62.
219. Brown, E.J. and D. Baltimore, *Essential and dispensable roles of ATR in cell cycle arrest and genome maintenance.* Genes Dev, 2003. **17**(5): p. 615-28.

220. Branzei, D. and M. Foiani, *Maintaining genome stability at the replication fork.* Nat Rev Mol Cell Biol, 2010. **11**(3): p. 208-19.
221. Zou, L. and S.J. Elledge, *Sensing DNA damage through ATRIP recognition of RPA-ssDNA complexes.* Science, 2003. **300**(5625): p. 1542-8.
222. Parrinello, S., et al., *Oxygen sensitivity severely limits the replicative lifespan of murine fibroblasts.* Nat Cell Biol, 2003. **5**(8): p. 741-7.
223. Cheng, X., et al., *Ionizing radiation-induced phosphorylation of RPA p34 is deficient in ataxia telangiectasia and reduced in aged normal fibroblasts.* Radiother Oncol, 1996. **39**(1): p. 43-52.
224. Heller, R.C. and K.J. Marians, *Replisome assembly and the direct restart of stalled replication forks.* Nat Rev Mol Cell Biol, 2006. **7**(12): p. 932-43.
225. Ichijima, Y., et al., *DNA Lesions Induced by Replication Stress Trigger Mitotic Aberration and Tetraploidy Development.* PLoS ONE, 2010. **5**(1): p. e8821.
226. Gravells, P., et al., *Reduced FANCD2 influences spontaneous SCE and RAD51 foci formation in uveal melanoma and Fanconi anaemia.* Oncogene, 2013. **32**(46): p. 5338-46.
227. Sharma, N.K., *Modulation of radiation-induced and mitomycin C-induced chromosome damage by apigenin in human lymphocytes in vitro.* J Radiat Res, 2013. **54**(5): p. 789-97.
228. Wojcik, A., et al., *Rad51C-deficient CL-V4B cells exhibit normal levels of mitomycin C-induced SCEs but reduced levels of UVC-induced SCEs.* Biochem Biophys Res Commun, 2005. **326**(4): p. 805-10.
229. Aghamohammadi, S.Z., D.T. Goodhead, and J.R. Savage, *Induction of sister chromatid exchanges (SCE) in G0 lymphocytes by plutonium-238 alpha-particles.* Int J Radiat Biol Relat Stud Phys Chem Med, 1988. **53**(6): p. 909-15.
230. Schmid, E. and H. Roos, *Dose dependent of sister chromatid exchanges in humans lymphocytes induced by in vitro alpha-particle irradiation.* Radiat Environ Biophys, 1996. **35**(4): p. 311-4.
231. Speit, G., et al., *Insensitivity of the in vitro cytokinesis-block micronucleus assay with human lymphocytes for the detection of DNA damage present at the start of the cell culture.* Mutagenesis, 2012. **27**(6): p. 743-7.
232. Privitera, E., et al., *Sister chromatid exchange and proliferation pattern in stimulated lymphocytes of cutaneous malignant melanoma patients.* Cancer Genet Cytogenet, 1985. **15**(1-2): p. 37-45.
233. De Braekeleer, E., et al., *Double Inv(3)(q21q26), a rare but recurrent chromosomal abnormality in myeloid hemopathies.* Anticancer Res, 2013. **33**(2): p. 639-42.
234. Slavutsky, I., et al., *Sister chromatid exchange in malignant lymphomas.* Cancer Genet Cytogenet, 1984. **13**(2): p. 153-8.
235. Hoh, L., et al., *Atypically low spontaneous sister chromatid exchange formation in uveal melanoma.* Genes Chromosomes Cancer, 2011. **50**(1): p. 34-42.
236. Nagasawa, H., et al., *Low doses of alpha particles do not induce sister chromatid exchanges in bystander Chinese hamster cells defective in homologous recombination.* DNA Repair (Amst), 2008. **7**(3): p. 515-22.
237. Littlefield, L.G., et al., *Sister chromatid exchanges in human lymphocytes exposed to ionizing radiation during G0.* Radiat Res, 1979. **78**(3): p. 514-21.
238. Lehnert, B.E., E.H. Goodwin, and A. Deshpande, *Extracellular factor(s) following exposure to alpha particles can cause sister chromatid exchanges in normal human cells.* Cancer Res, 1997. **57**(11): p. 2164-71.
239. Raderschall, E., et al., *Formation of higher-order nuclear Rad51 structures is functionally linked to p21 expression and protection from DNA damage-induced apoptosis.* J Cell Sci, 2002. **115**(Pt 1): p. 153-64.
240. Lin, S. and P. Talbot, *Methods for culturing mouse and human embryonic stem cells.* Methods Mol Biol, 2011. **690**: p. 31-56.

241. Ouyang, K.J., et al., *SUMO modification regulates BLM and RAD51 interaction at damaged replication forks.* PLoS Biol, 2009. **7**(12): p. e1000252.
242. Tauchi, H., et al., *Nijmegen breakage syndrome gene, NBS1, and molecular links to factors for genome stability.* Oncogene, 2002. **21**(58): p. 8967-80.
243. Wang, Y., et al., *Mutation Inactivation of Nijmegen Breakage Syndrome Gene (NBS1) in Hepatocellular Carcinoma and Intrahepatic Cholangiocarcinoma.* PLoS One, 2013. **8**(12): p. e82426.

Appendix B

Sequencing of DNA from three mouse strains for the presence of H388Y, Q418P, A498T, A882V nsSNPs found in the CtIP gene

<u>129Sv cell line</u>

H388Y Reverse

AGGGGGAGAAACTTGTATTCAAACCCAAAT**G**AGCTTTCACAGTAGAGGTAGC
TCCAAATACCGGANANNACGCCA

Q418P Forward

ACTTACAATAAAACTGTAAGTGACTCTGTAGATGAAC**C**GTGCAGTGCTGACCA
CATGAATACTACTGTTGCTGATAAATATTTGGTGCCTTTGAAATCCCTGGGAGG

A498T Forward

NNTCTGNNNNTGTCAGATCGGTTTGCA**G**CTACTCAGCGGCAAGAGAAGAACC
ACGGAAACGAGACTTCTAAAAACAAACTTAAGCAAGCCACTATTTACGAGGCT

A882V Forward (Sequencing not successful)

NNNNNNNGNNNTTNNNNNNNNNGNNNNNNNNNNNGNNTGNCCNANNNGTTT
GGTGGTTTTNNNCGGNNAAGAANNNNNNGNNANGAAACTTCTANNANACANN
TAANATCCCGCTATNTNNTTGNGGTTTGGANGNTNNTNCCNGGNNNCCNNNNC
NAGGGCTTTTTCCTCTGAAACCGGCCTGGGGGCACNTTACNCNNNGNTCACTG
GCCGCCTCATCCTTCATGCTTTTGGATGCGTTGCGTACCAGNGATNCGTNNCCC

Appendix B:

CNCCTCCTANNGTTCGGATTNAAACCTCTTTCTCCCCTCCAANGATCTCGTNNA
CATAACCCTCATAACACCNCCNNCTCGGGGGGTGAAAATNNGTTTAAACCCCA
CNTCCCGCCCCCTGGTGTTATCAATTCCCTTCTNCTGTTCGNGCCGGGGCTTNA
AATT

A882V Reverse (Sequencing not successful)

NNNNNNGNNNNNNNNNNNNNNNNNNNNNNGGNNNNCNNNNNNNNNNNG
NGGTTNCTCCNGGAAAAAGAAAACNTGGGANNCAGNCTTCTNNAAANNATTT
TGGGNCATTTTTNNAAGGTTTGGAGGCCCNTTNNAGGGNNNANTAANAGGNC
ATTGTCCTNATCGAAAGGGGGCTGGGGGCCTTTTTGNATGTTCAGGATGTNCT
AATCCTCTTCCNNNTGGATGTNNNGAACAACAGGGATGCTCCCACCTCACNCT
ACTACTGATTCAAAACAATGTTTGGTGCCTTTGAAATCCCNGTGAGGTAAACA
TCCAGAANCAACANCACTGAGGGGNAAAAGAAGCATGGANTACAGCNCCCCC
CGCCTGTTTTTTCCAAATCACATGCCCCCTTCTTNNCCGGGGGATNATNNNTTC
TCCNTCCAGGGACNCTTTCTGATATATATCCCTNTGCAGCTATCGAAACCNTTT
ATANGNCTNNGNATCTNTTANCNNNCNGN

C57BL/6 cell line

H388Y Reverse

AGAGAGAGGGGGAGAAACTTGTATTCAAACCCAAAT**G**AGCTTTCACAGTAGA
GGTAGCTCCAAATACCGGNNANNACGCCA

Q418P Forward

CTTACAATAAAACTGTAAGTGACTCTGTAGATGAAC**A**GTGCAGTGCTGACCAC
ATGAATACTACTGTTGCTGATAAATATTTGGTGCCTTTGAAATCCC

A498T Forward

GGANAACCTCTGGACCTGTCAGATCGGTTTGCA**G**CTACTCAGCGGCAAGAGA
AGAACCACGGAAACGAGACTTCTAAAAACAAACTTAAGCAAGCCACTATTTA

Appendix B:

A882V Reverse

CTCTCCTGCTTTCACGCCAGTGTCTAGGTCCTCTGTTCTTTGCCTTTTGGAGAAA
AGACC**G**CGTTGTAAGGCTGCCGTCTTTTGNNNNGAGGACACNNCTGNGNGAT
GNNNNNNNNNGNNNACNNGAAGGGNGGTTAAGCTGATAGCANAATNTCTG

CBA/H cell line

H388Y Reverse

AGGGGGAGAAACTTGTATTCAAACCCAAAT**G**AGCTTTCACAGTAGAGGTAGC
TCCAAATACCGNNNANNNACGNN

Q418P Forward

GNTACTTACAATAANCTGTAAGTGACTCTGTAGATGAAC**A**GTGCAGTGCTGAC
CACATGAATACTACTGTTGCTGATAAATATTTGGTGCCTTTGAAATCCCTGGGA

A498T Forward

NNNNNNNNNNGNNNNNNTCTGGACCTGTCAGATCGGTTTGCA**G**CTACTCAGC
GGCAAGAGAAGAACCACGGAAACGAGACTTCTAAAAACAAACTTAA

A882V Reverse

ACGCCAGTGTCTAGGTCCTCTGTTCTTTGCCTTTTGGAGAAAAGACC**G**CGTTG
TAAGGCTGCCGTCTTTTGNNNNGAGGACAAA

Appendix B:

Tumours (other than rAML) found in irradiated and non-irradiated 129Sv mice

TABLE B.1 Tumours found in irradiated 129Sv mice.

Tumour	No of mice	% from the irradiated population (78)
Lung	8	10
Liver	5	6
Harderian gland	4	5
Mammary	2	3
Vertebral	5	6
Stomach	3	4
Testicular	1	1
Uterine	1	1

TABLE B.2 Tumours found in non-irradiated 129Sv mice
.

Tumour	No of mice	% from the non-irradiated population (20)
Liver	1	10
Mammary	1	5
Thymic lymphoma	2	5
Uterine	1	5

SPRINGER LICENSE
TERMS AND CONDITIONS

Mar 09, 2014

This is a License Agreement between Agata Nasilowska ("You") and Springer ("Springer") provided by Copyright Clearance Center ("CCC"). The license consists of your order details, the terms and conditions provided by Springer, and the payment terms and conditions.

All payments must be made in full to CCC. For payment instructions, please see information listed at the bottom of this form.

License Number	3344911152061
License date	Mar 09, 2014
Licensed content publisher	Springer
Licensed content publication	European Journal of Nuclear Medicine
Licensed content title	General aspects of the cellular response to low- and high-LET radiation
Licensed content author	Jean-Pierre Pouget
Licensed content date	Jan 1, 2001
Volume number	28
Issue number	4
Type of Use	Thesis/Dissertation
Portion	Figures
Author of this Springer article	No
Order reference number	
Original figure numbers	4
Title of your thesis / dissertation	The role of CtIP gene as genetic susceptibility factor for radiation leukaemogenesis
Expected completion date	Jun 2014
Estimated size(pages)	200
Total	0.00 GBP
Terms and Conditions	

Introduction

The publisher for this copyrighted material is Springer Science + Business Media. By clicking "accept" in connection with completing this licensing transaction, you agree that the following terms and conditions apply to this transaction (along with the Billing and Payment terms and conditions established by Copyright Clearance Center, Inc. ("CCC"), at the time that you opened your Rightslink account and that are available at any time at http://myaccount.copyright.com).

Limited License

With reference to your request to reprint in your thesis material on which Springer Science and

Business Media control the copyright, permission is granted, free of charge, for the use indicated in your enquiry.

Licenses are for one-time use only with a maximum distribution equal to the number that you identified in the licensing process.

This License includes use in an electronic form, provided its password protected or on the university's intranet or repository, including UMI (according to the definition at the Sherpa website: http://www.sherpa.ac.uk/romeo/). For any other electronic use, please contact Springer at (permissions.dordrecht@springer.com or permissions.heidelberg@springer.com).

The material can only be used for the purpose of defending your thesis, and with a maximum of 100 extra copies in paper.

Although Springer holds copyright to the material and is entitled to negotiate on rights, this license is only valid, subject to a courtesy information to the author (address is given with the article/chapter) and provided it concerns original material which does not carry references to other sources (if material in question appears with credit to another source, authorization from that source is required as well).

Permission free of charge on this occasion does not prejudice any rights we might have to charge for reproduction of our copyrighted material in the future.

Altering/Modifying Material: Not Permitted
You may not alter or modify the material in any manner. Abbreviations, additions, deletions and/or any other alterations shall be made only with prior written authorization of the author(s) and/or Springer Science + Business Media. (Please contact Springer at (permissions.dordrecht@springer.com or permissions.heidelberg@springer.com)

Reservation of Rights
Springer Science + Business Media reserves all rights not specifically granted in the combination of (i) the license details provided by you and accepted in the course of this licensing transaction, (ii) these terms and conditions and (iii) CCC's Billing and Payment terms and conditions.

Copyright Notice:Disclaimer
You must include the following copyright and permission notice in connection with any reproduction of the licensed material: "Springer and the original publisher /journal title, volume, year of publication, page, chapter/article title, name(s) of author(s), figure number(s), original copyright notice) is given to the publication in which the material was originally published, by adding; with kind permission from Springer Science and Business Media"

Warranties: None

Example 1: Springer Science + Business Media makes no representations or warranties with respect to the licensed material.

Example 2: Springer Science + Business Media makes no representations or warranties with respect to the licensed material and adopts on its own behalf the limitations and disclaimers established by CCC on its behalf in its Billing and Payment terms and conditions for this licensing transaction.

Indemnity
You hereby indemnify and agree to hold harmless Springer Science + Business Media and CCC, and their respective officers, directors, employees and agents, from and against any and all claims arising out of your use of the licensed material other than as specifically authorized pursuant to this license.

No Transfer of License
This license is personal to you and may not be sublicensed, assigned, or transferred by you to any other person without Springer Science + Business Media's written permission.

No Amendment Except in Writing
This license may not be amended except in a writing signed by both parties (or, in the case of Springer Science + Business Media, by CCC on Springer Science + Business Media's behalf).

Objection to Contrary Terms
Springer Science + Business Media hereby objects to any terms contained in any purchase order, acknowledgment, check endorsement or other writing prepared by you, which terms are inconsistent with these terms and conditions or CCC's Billing and Payment terms and conditions. These terms and conditions, together with CCC's Billing and Payment terms and conditions (which are incorporated herein), comprise the entire agreement between you and Springer Science + Business Media (and CCC) concerning this licensing transaction. In the event of any conflict between your obligations established by these terms and conditions and those established by CCC's Billing and Payment terms and conditions, these terms and conditions shall control.

Jurisdiction
All disputes that may arise in connection with this present License, or the breach thereof, shall be settled exclusively by arbitration, to be held in The Netherlands, in accordance with Dutch law, and to be conducted under the Rules of the 'Netherlands Arbitrage Instituut' (Netherlands Institute of Arbitration).***OR:***

All disputes that may arise in connection with this present License, or the breach thereof, shall be settled exclusively by arbitration, to be held in the Federal Republic of Germany, in accordance with German law.

Other terms and conditions:

v1.3

If you would like to pay for this license now, please remit this license along with your payment made payable to "COPYRIGHT CLEARANCE CENTER" otherwise you will be invoiced within 48 hours of the license date. Payment should be in the form of a check or money order referencing your account number and this invoice number RLNK501245986. Once you receive your invoice for this order, you may pay your invoice by credit card. Please follow instructions provided at that time.

Make Payment To:
Copyright Clearance Center
Dept 001
P.O. Box 843006
Boston, MA 02284-3006

For suggestions or comments regarding this order, contact RightsLink Customer Support: customercare@copyright.com or +1-877-622-5543 (toll free in the US) or +1-978-646-2777.

Gratis licenses (referencing $0 in the Total field) are free. Please retain this printable

license for your reference. No payment is required.

ELSEVIER LICENSE
TERMS AND CONDITIONS

Mar 09, 2014

This is a License Agreement between Agata Nasilowska ("You") and Elsevier ("Elsevier") provided by Copyright Clearance Center ("CCC"). The license consists of your order details, the terms and conditions provided by Elsevier, and the payment terms and conditions.

All payments must be made in full to CCC. For payment instructions, please see information listed at the bottom of this form.

Supplier	Elsevier Limited The Boulevard,Langford Lane Kidlington,Oxford,OX5 1GB,UK
Registered Company Number	1982084
Customer name	Agata Nasilowska
Customer address	Old Road Campus Research Building Oxford, OX3 7DQ
License number	3344891235269
License date	Mar 09, 2014
Licensed content publisher	Elsevier
Licensed content publication	DNA Repair
Licensed content title	DNA double-strand break repair: From mechanistic understanding to cancer treatment
Licensed content author	Thomas Helleday,Justin Lo,Dik C. van Gent,Bevin P. Engelward
Licensed content date	1 July 2007
Licensed content volume number	6
Licensed content issue number	7
Number of pages	13
Start Page	923
End Page	935
Type of Use	reuse in a thesis/dissertation
Portion	figures/tables/illustrations
Number of figures/tables/illustrations	5
Format	both print and electronic
Are you the author of this Elsevier article?	No
Will you be translating?	No
Title of your thesis/dissertation	The role of CtIP gene as genetic susceptibility factor for radiation leukaemogenesis

Expected completion date	Jun 2014
Estimated size (number of pages)	200
Elsevier VAT number	GB 494 6272 12
Permissions price	0.00 GBP
VAT/Local Sales Tax	0.00 GBP / 0.00 GBP
Total	0.00 GBP

Terms and Conditions

INTRODUCTION

1. The publisher for this copyrighted material is Elsevier. Byclicking "accept" in connection with completing this licensingtransaction, you agree that the following terms and conditions apply to thistransaction (along with the Billing and Payment terms and conditionsestablished by Copyright Clearance Center, Inc. ("CCC"), at the timethat you opened your Rightslink account and that are available at any time at http://myaccount.copyright.com).

GENERAL TERMS

2. Elsevier hereby grants you permission to reproduce the aforementionedmaterial subject to the terms and conditions indicated.

3. Acknowledgement: If any part of the material to be used (for example,figures) has appeared in our publication with credit or acknowledgement toanother source, permission must also be sought from that source. If suchpermission is not obtained then that material may not be included in yourpublication/copies. Suitable acknowledgement to the source must be made, eitheras a footnote or in a reference list at the end of your publication, asfollows:

"Reprinted from Publication title, Vol /edition number, Author(s), Title ofarticle / title of chapter, Pages No., Copyright (Year), with permission fromElsevier [OR APPLICABLE SOCIETY COPYRIGHT OWNER]." Also Lancet special credit -"Reprinted from The Lancet, Vol. number, Author(s), Title of article, PagesNo., Copyright (Year), with permission from Elsevier."

4. Reproduction of this material is confined to the purpose and/or media forwhich permission is hereby given.

5. Altering/Modifying Material: Not Permitted. However figures andillustrations may be altered/adapted minimally to serve your work. Any otherabbreviations, additions, deletions and/or any other alterations shall be madeonly with prior written authorization of Elsevier Ltd. (Please contact Elsevierat permissions@elsevier.com)

6. If the permission fee for the requested use of our material is waived inthis instance, please be advised that your future requests for Elseviermaterials may attract a fee.

7. Reservation of Rights: Publisher reserves all rights not specificallygranted in the combination of (i) the license details provided by you andaccepted in the course of this licensing transaction, (ii) these terms andconditions and (iii) CCC's Billing and Payment terms and conditions.

8. License Contingent Upon Payment: While you may exercise the rightslicensed immediately upon issuance of the license at the end of the licensingprocess for the transaction, provided that you have

disclosed complete andaccurate details of your proposed use, no license is finally effective unlessand until full payment is received from you (either by publisher or by CCC) asprovided in CCC's Billing and Payment terms and conditions. If fullpayment is not received on a timely basis, then any license preliminarilygranted shall be deemed automatically revoked and shall be void as if nevergranted. Further, in the event that you breach any of these terms andconditions or any of CCC's Billing and Payment terms and conditions, thelicense is automatically revoked and shall be void as if never granted. Use of materials as described in a revoked license, as well as any use of thematerials beyond the scope of an unrevoked license, may constitute copyrightinfringement and publisher reserves the right to take any and all action toprotect its copyright in the materials.

9. Warranties: Publisher makes no representations or warranties with respectto the licensed material.

10. Indemnity: You hereby indemnify and agree to hold harmless publisher andCCC, and their respective officers, directors, employees and agents, from andagainst any and all claims arising out of your use of the licensed materialother than as specifically authorized pursuant to this license.

11. No Transfer of License: This license is personal to you and may not besublicensed, assigned, or transferred by you to any other person withoutpublisher's written permission.

12. No Amendment Except in Writing: This license may not be amended exceptin a writing signed by both parties (or, in the case of publisher, by CCC onpublisher's behalf).

13. Objection to Contrary Terms: Publisher hereby objects to any termscontained in any purchase order, acknowledgment, check endorsement or otherwriting prepared by you, which terms are inconsistent with these terms andconditions or CCC's Billing and Payment terms and conditions. These termsand conditions, together with CCC's Billing and Payment terms and conditions(which are incorporated herein), comprise the entire agreement between you andpublisher (and CCC) concerning this licensing transaction. In the eventof any conflict between your obligations established by these terms andconditions and those established by CCC's Billing and Payment terms andconditions, these terms and conditions shall control.

14. Revocation: Elsevier or Copyright Clearance Center may deny thepermissions described in this License at their sole discretion, for any reasonor no reason, with a full refund payable to you. Notice of such denialwill be made using the contact information provided by you. Failure toreceive such notice will not alter or invalidate the denial. In no eventwill Elsevier or Copyright Clearance Center be responsible or liable for anycosts, expenses or damage incurred by you as a result of a denial of yourpermission request, other than a refund of the amount(s) paid by you toElsevier and/or Copyright Clearance Center for denied permissions.

LIMITED LICENSE

The following terms and conditions apply only to specific license types:

15. **Translation**: This permission is granted fornon-exclusive world **English** rights only unless yourlicense was granted for translation rights. If you licensed translation rightsyou may only translate this content into the languages you requested. Aprofessional translator must perform all translations and reproduce the contentword for word preserving the integrity of the article. If this license is tore-use 1 or 2 figures then permission is granted for non-exclusive world rightsin all languages.

16. **Posting licensed content on any Website**: The followingterms and conditions apply as

follows: Licensing material from an Elsevierjournal: All content posted to the web site must maintain the copyright informationline on the bottom of each image; A hyper-text must be included to the Homepageof the journal from which you are licensing at http://www.sciencedirect.com/science/journal/xxxxx orthe Elsevier homepage for books at http://www.elsevier.com; CentralStorage: This license does not include permission for a scanned version of thematerial to be stored in a central repository such as that provided byHeron/XanEdu.

Licensing material from an Elsevier book: A hyper-text link must be includedto the Elsevier homepage at http://www.elsevier.com . Allcontent posted to the web site must maintain the copyright information line onthe bottom of each image.

Posting licensed content on Electronic reserve: In addition to the above the following clausesare applicable: The web site must be password-protected and made available onlyto bona fide students registered on a relevant course. This permission isgranted for 1 year only. You may obtain a new license for future websiteposting.

For journal authors: the following clauses are applicable inaddition to the above: Permission granted is limited to the author acceptedmanuscript version* of your paper.

***Accepted Author Manuscript (AAM) Definition:** An accepted authormanuscript (AAM) is the author's version of the manuscript of an article thathas been accepted for publication and which may include any author-incorporatedchanges suggested through the processes of submission processing, peer review,and editor-author communications. AAMs do not include other publishervalue-added contributions such as copy-editing, formatting, technicalenhancements and (if relevant) pagination.

You are not allowed to download and post the published journal article (whetherPDF or HTML, proof or final version), nor may you scan the printed edition tocreate an electronic version. A hyper-text must be included to the Homepage ofthe journal from which you are licensing at http://www.sciencedirect.com/science/journal/xxxxx. As part of our normal production process, you will receive an e-mail noticewhen your article appears on Elsevier's online service ScienceDirect(www.sciencedirect.com). That e-mail will include the article's Digital ObjectIdentifier (DOI). This number provides the electronic link to the publishedarticle and should be included in the posting of your personal version. We askthat you wait until you receive this e-mail and have the DOI to do any posting.

Posting to a repository: Authorsmay post their AAM immediately to their employer's institutional repository forinternal use only and may make their manuscript publically available after thejournal-specific embargo period has ended.

Please also refer to Elsevier'sArticle Posting Policy for further information.

18. **For book authors** the following clauses are applicable in addition tothe above: Authors are permitted to place a briefsummary of their work online only.. You are notallowed to download and post the published electronic version of your chapter,nor may you scan the printed edition to create an electronic version. Posting to a repository: Authors arepermitted to post a summary of their chapter only in their institution'srepository.

20. **Thesis/Dissertation**: If your license is for use in athesis/dissertation your thesis may be submitted to your institution in eitherprint or electronic form. Should your thesis be published commercially, pleasereapply for permission. These requirements include permission for the

Libraryand Archives of Canada to supply single copies, on demand, of the completethesis and include permission for UMI to supply single copies, on demand, ofthe complete thesis. Should your thesis be published commercially, pleasereapply for permission.

Elsevier Open Access Terms andConditions

Elsevier publishes Open Access articles in both its Open Access journals andvia its Open Access articles option in subscription journals.

Authors publishing in an Open Access journal or who choose to make theirarticle Open Access in an Elsevier subscription journal select one of thefollowing Creative Commons user licenses, which define how a reader may reusetheir work: Creative Commons Attribution License (CC BY), Creative CommonsAttribution – Non Commercial - ShareAlike (CC BY NCSA) and Creative Commons Attribution – Non Commercial – No Derivatives (CC BYNC ND)

Terms & Conditions applicable toall Elsevier Open Access articles:

Any reuse of the article must not represent the author as endorsing theadaptation of the article nor should the article be modified in such a way asto damage the author's honour or reputation.

The author(s) must be appropriately credited.

If any part of the material to be used (for example, figures) has appearedin our publication with credit or acknowledgement to another source it is theresponsibility of the user to ensure their reuse complies with the terms andconditions determined by the rights holder.

Additional Terms & Conditionsapplicable to each Creative Commons user license:

CC BY: You may distribute andcopy the article, create extracts, abstracts, and other revised versions,adaptations or derivative works of or from an article (such as a translation),to include in a collective work (such as an anthology), to text or data minethe article, including for commercial purposes without permission from Elsevier

CC BY NC SA: For non-commercialpurposes you may distribute and copy the article, create extracts, abstractsand other revised versions, adaptations or derivative works of or from anarticle (such as a translation), to include in a collective work (such as ananthology), to text and data mine the article and license new adaptations or creationsunder identical terms without permission from Elsevier

CC BY NC ND: For non-commercialpurposes you may distribute and copy the article and include it in a collectivework (such as an anthology), provided you do not alter or modify the article,without permission from Elsevier

Any commercial reuse of Open Access articles published with a CC BY NC SA or CC BY NC NDlicense requires permission from Elsevier and will be subject to a fee.

Commercial reuse includes:

- Promotional purposes (advertising or marketing)

- Commercial exploitation (e.g. a product forsale or loan)
- Systematic distribution (for a fee or free ofcharge)

Please refer to Elsevier'sOpen Access Policy for further information.

21. **Other Conditions**:

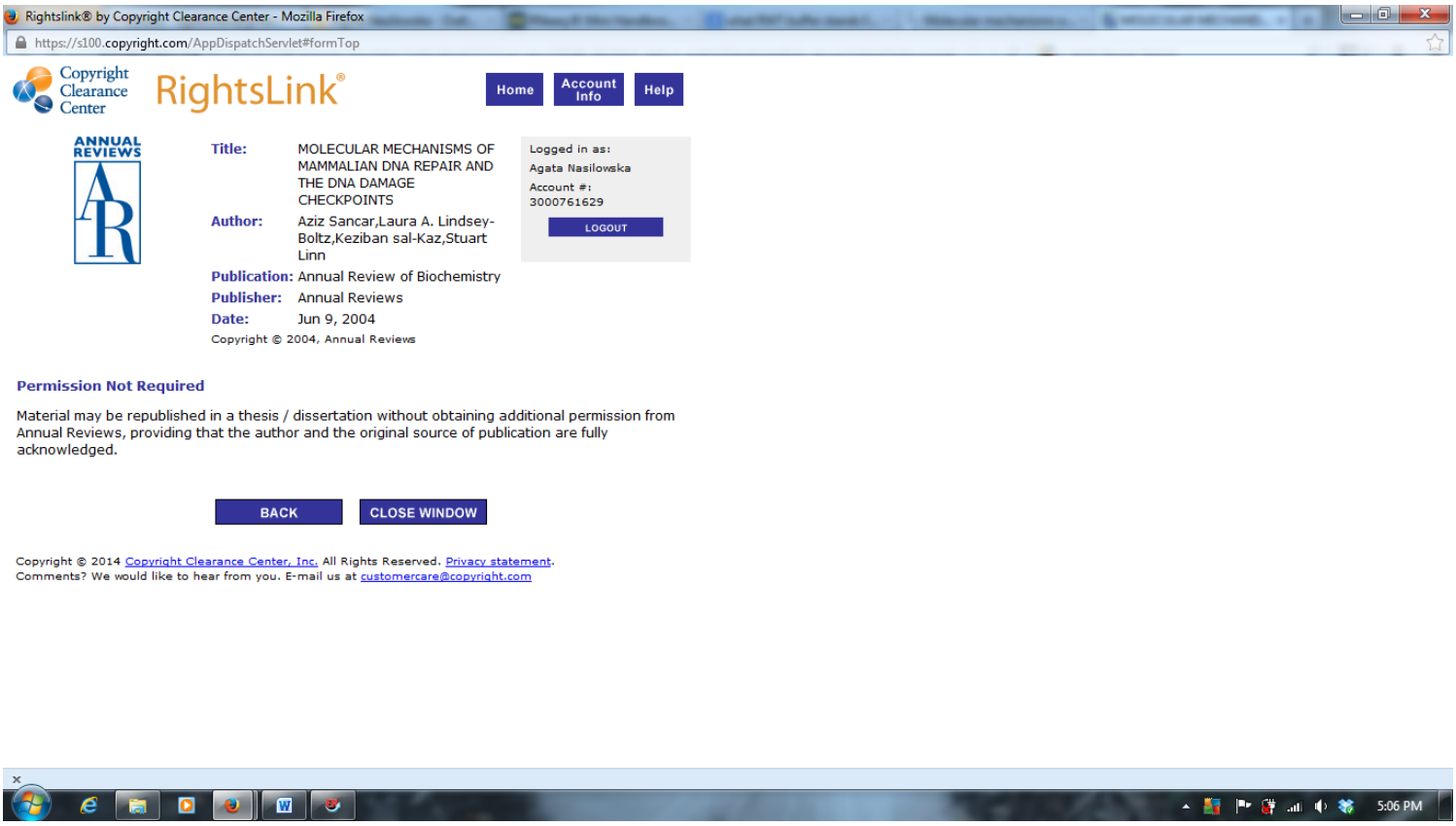
v1.7

If you would like to pay for this license now, please remit this license along with your payment made payable to "COPYRIGHT CLEARANCE CENTER" otherwise you will be invoiced within 48 hours of the license date. Payment should be in the form of a check or money order referencing your account number and this invoice number RLNK501245966. Once you receive your invoice for this order, you may pay your invoice by credit card. Please follow instructions provided at that time.

Make Payment To:
Copyright Clearance Center
Dept 001
P.O. Box 843006
Boston, MA 02284-3006

For suggestions or comments regarding this order, contact RightsLink Customer Support: customercare@copyright.com or +1-877-622-5543 (toll free in the US) or +1-978-646-2777.

Gratis licenses (referencing $0 in the Total field) are free. Please retain this printable license for your reference. No payment is required.


Rightslink® by Copyright Clearance Center - Mozilla Firefox
https://s100.copyright.com/AppDispatchServlet#formTop
Copyright Clearance Center
RightsLink®
Home
Account Info
Help
ANNUAL REVIEWS
Title: MOLECULAR MECHANISMS OF MAMMALIAN DNA REPAIR AND THE DNA DAMAGE CHECKPOINTS
Author: Aziz Sancar,Laura A. Lindsey-Boltz,Keziban sal-Kaz,Stuart Linn
Publication: Annual Review of Biochemistry
Publisher: Annual Reviews
Date: Jun 9, 2004
Copyright © 2004, Annual Reviews
Logged in as:
Agata Nasilowska
Account #:
3000761629
LOGOUT
Permission Not Required
Material may be republished in a thesis / dissertation without obtaining additional permission from Annual Reviews, providing that the author and the original source of publication are fully acknowledged.
BACK
CLOSE WINDOW
Copyright © 2014 Copyright Clearance Center, Inc. All Rights Reserved. Privacy statement.
Comments? We would like to hear from you. E-mail us at customercare@copyright.com
5:06 PM